2008

Synthesis of disubstituted amino acids and peptide inhibitors of amyloid beta aggregation

Gregory Todd McCandless
Louisiana State University and Agricultural and Mechanical College, gmccand@lsu.edu

SYNTHESIS OF DISUBSTITUTED AMINO ACIDS AND PEPTIDE INHIBITORS OF AMYLOID BETA AGGREGATION

A Thesis

Submitted to the Graduate Faculty of the
Louisiana State University and
Agricultural and Mechanical College
in partial fulfillment of the
requirements for the degree of
Master of Science

in

The Department of Chemistry

by
Gregory T. McCandless
B.S., Louisiana State University, 1999
December 2008

ACKNOWLEDGEMENTS

During the course of my research, there have been several individuals who helped me along the way. In this section, I would like to acknowledge a few of them.

I want to thank my advisor, Professor Robert Hammer, who guided my research efforts, provided me with solutions to overcome synthetic barriers and gave me the latitude to try my own ideas. I am indebted to Professors George Stanley, William Crowe and Fareed Aboul-ela for sharing their knowledge with me as well as being sources of encouragement. I would like to thank my group members, especially Cyrus Bett, who provided assistance and discussions on my project, and Sibel Erdem, who was my closest friend in the lab. I also benefited indirectly by the opportunities I had assisting two undergraduates, Sarah Curtis and Amber Scroggs, on their research projects. A special acknowledgement is due to Dr. Frank Fronczek (X-ray facility director) and Ms. Martha Juban (former protein facility director) for providing the time to discuss results and explain important instrumentation details.

In closing, I want to thank my very supportive wife, Julia. Without her by my side, none of this would have been possible.

TABLE OF CONTENTS

ABSTRACT

The aggregation process of amyloid beta from monomeric peptide to oligomers and fibrils is believed to be connected with the neurological disorder Alzheimer's disease. The focus of this research is the synthesis of alpha, alpha-disubstituted amino acids and peptide inhibitors of amyloid beta aggregation. The inhibitors are designed to interrupt (or alter) this process by binding to amyloid beta's central hydrophobic core region (residues 17-20, Leucine-Valine-Phenylalanine-Phenylalanine). Target specificity is achieved via self recognition by basing the inhibitors on the sequence in this region. The inclusion of disubstituted amino acids in the sequence of the inhibitors will provide a blocking face (or side) to prevent further disease linked aggregation. This thesis describes the experimental investigations that were conducted to evaluate design elements that can be added to enhance inhibitor designs and methods for improving the synthesis of disubstituted amino acids.

CHAPTER 1

ALZHEIMER'S DISEASE – A PEPTIDE AGGREGATION PREDICAMENT

A few of the major human disorders, such as Alzheimer's disease, Type II diabetes, Parkinson's disease and Huntington's disease, have been linked to a peptide or protein aggregation process.[1] The identification of the peptide or protein responsible for each these disorders has been key to understanding how to prevent, slow down or even reverse the aggregation. Amyloid beta peptide, which can vary from 39 to 43 amino acid residues in length, is believed to be the initiator of the neurological disorder in Alzheimer's disease. It is produced in the central nervous system, primarily in the brain, by a succession of two proteolytic cleavages of the amyloid precursor protein (APP) and has no known biological role. Interestingly, the manufacturing of this amyloid beta appears to be a normal process that occurs in individuals that do not exhibit the symptoms associated with Alzheimer's disease.[2] Why is this peptide, which appears to be useless, being created, how is production of it being physiologically regulated and what do we do about the disease-linked aggregation? These are just some of the complexities to the problem associated with amyloid beta. The riddle behind the creation and regulation of amyloid beta has yet to be solved. However, researchers have made some headway into developing methods to deal with the aggregation.[3]

Ideally, preventing the production of amyloid beta would be the best remedy to the situation. The responsible parties, β- and γ-secretase, have been identified for the cleavage from the precursor, APP (see **Figure 1.1**). If we can prevent the *N*-terminus cleavage associated with β-secretase, the production of amyloid beta would not occur. However, this might lead to trading one problem for another by increasing probability for the formation of another disease-linked peptide. That peptide, known as "p3", is a short fragment created by the cleavages of APP with α- and γ-secretase. It has a role in formation of nonfibrillar deposits or lesions associated with

Down's syndrome, another neurological disorder that progresses at a faster rate than Alzheimer's disease.[4] The trouble with inhibiting the γ-secretase associated with the *C*-terminus cleavage is a possible adverse affect on the roles it is playing elsewhere. One of the known roles of γ-secretase is the proteolysis of the notch protein.[5, 6] The notch protein is instrumental in the cellular signaling essential to cell development.[2] Therefore, if preventing the creation of amyloid beta is too difficult without creating other problems, what shall we do?

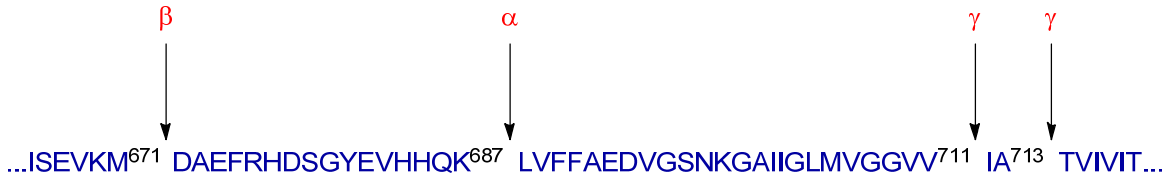

Figure 1.1. Cleavage sites of α-, β- and γ-secretase within the APP protein sequence which result in the formation of either amyloid beta or p3 peptides.[2]

This is where the design of short peptide inhibitors that bind to amyloid beta and prevent the aggregation process comes in. Using the same self-recognition that assists the assembly of peptide aggregates into oligomers and fibrils (see **Figure 1.2**), researchers have been able to design inhibitors that bind to a specific region within amyloid beta's sequence and disrupt the propensity for further aggregation.[7] The approach we have used in our inhibitors is to incorporate disubstituted amino acids in alternating positions which will target the hydrophobic core of the amyloid beta peptide sequence (See **Figure 1.3**). The alternating approach will allow the inhibitor to have a binding face consisting of natural amino acids identical to the target and a blocking face that will consist of disubstituted amino acids (See **Figure 1.4**).

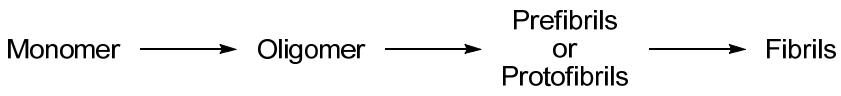

Figure 1.2. The aggregation process of amyloid beta peptide from monomers to fibrils.

^{1}DAEFRHDSGYEVHHQK^{16} LVFF^{20} AEDVGSNKGAIIGLMVGGVV^{40} IA^{42}

Figure 1.3. The hydrophobic core (residues 17-20, LVFF) of amyloid beta peptide.

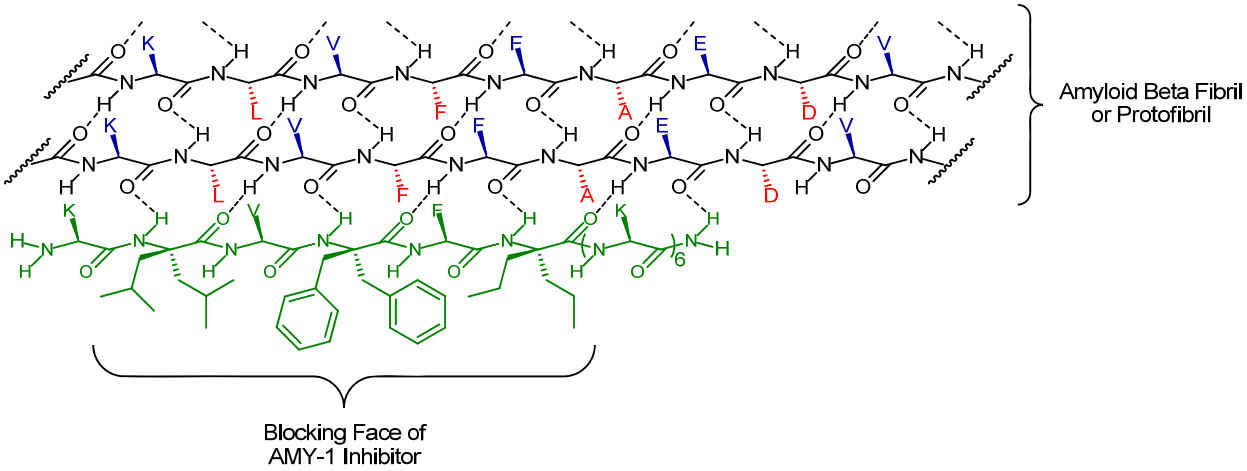

Figure 1.4. Illustration of inhibitor (AMY-1) binding to the hydrophobic core of amyloid beta on one face while blocking on the opposite face with disubstituted amino acids (adapted from figure in reference 8).

This thesis will report the synthesis of α,α-disubstituted amino acids and peptide inhibitors as well as the important factors that influence peptide aggregation and inhibitor designs. Also included in this document are preliminary investigations using surface plasmon resonance instrument to measure inhibitor binding affinities and future directions for this project.

1.1 References

1. Glabe, C. G., Common Mechanisms of Amyloid Oligomer Pathogenesis in Degenerative Disease. *Neurobiol. Aging* **2006**, 27, 570-575.

2. Selkoe, D. J., Alzheimer's disease: Genes, proteins, and therapy. *Physiol. Rev.* **2001**, 81, 741-766.

3. Haass, C.; Selkoe, D. J., Soluble Protein Oligomers in Neurodegeneration: Lessons from the Alzheimer's Amyloid β-Peptide. *Nat. Rev. Mol. Cell Biol.* **2007**, 8, 101-112.

4. Lalowski, M.; Golabek, A.; Lemere, C. A.; Selkoe, D. J.; Wisniewski, H. M.; Beavis, R. C.; Frangione, B.; Wisniewski, T., The "Nonamyloidogenic" p3 Fragment (Amyloid β17-42) is a Major Constituent of Down's Syndrome Cerebellar Preamyloid. *J. Biol. Chem.* **1996**, 271, 33623-33631.

5. Kimberly, W. T.; LaVoie, M. J.; Ostaszewski, B. L.; Ye, W. J.; Wolfe, M. S.; Selkoe, D. J., γ-Secretase is a Membrane Protein Complex Comprised of Presenilin, Nicastrin, Aph-1, and Pen-2. *Proc. Natl. Acad. Sci. U. S. A.* **2003**, 100, 6382-6387.

6. Weihofen, A.; Binns, K.; Lemberg, M. K.; Ashman, K.; Martoglio, B., Identification of Signal Peptide Peptidase, a Presenilin-Type Aspartic Protease. *Science* **2002**, 296, 2215-2218.

7. Stains, C. I.; Mondal, K.; Ghosh, I., Molecules that Target beta-Amyloid. *ChemMedChem* **2007**, 2, 1674-1692.

8. Etienne, M. A.; Aucoin, J. P.; Fu, Y. W.; McCarley, R. L.; Hammer, R. P., Stoichiometric Inhibition of Amyloid β-Protein Aggregation with Peptides Containing Alternating α,α-Disubstituted Amino Acids. *J. Am. Chem. Soc.* **2006**, 128, 3522-3523.

CHAPTER 2

THE INFLUENCE OF AROMATIC RESIDUES IN PEPTIDE AGGREGATION AND A SYNTHETIC STRATEGY TO MANIPULATE π-STACKING

2.1 Introduction

What is the major factor contributing to a peptide's propensity to aggregate into amyloid fibrils? Is it aromaticity or hydrophobicity? The experts, who have clearly expressed their bias by downplaying one over the other, are in disagreement.

The significance and role of π-stacking of aromatic rings in peptide and protein self assembly have been reviewed.[1] It was demonstrated that the aggregation of a peptide fragment (residues 22 to 29, H-Asn-**Phe**-Gly-Ala-Ile-Leu-Ser-Ser-OH) from the sequence for islet amyloid polypeptide (IAPP), which forms morphologically similar fibrils as the full sequence, can be altered to only producing non-fibrillic amorphous aggregates by the simple replacement of phenylalanine (indicated in **red**) with alanine. The aggregates were determined to be non-fibrillic as shown by the absence of gold-green birefringence, or double refraction, when stained with the dye Congo Red under polarized light which is an established method for detecting amyloid fibrils. The author also points out that there is at least one aromatic residue within most of the identified regions that are critical to aggregation within amyloid disease-linked peptides. Aromatic amino acids are also present in the shortest peptide fragments based on the sequences of amyloid related peptides that still aggregate into fibrils.[2] Gazit hypothesized that the aromatic rings are the major molecular recognition elements that hastens the transition of the peptide to a beta sheet secondary structure. X-ray diffraction shows that the structure of amyloid fibrils is ordered which suggests that the aggregation could not be simply due to nonspecific hydrophobic interactions.[1, 2] The importance in molecular recognition may also explain why several inhibitors

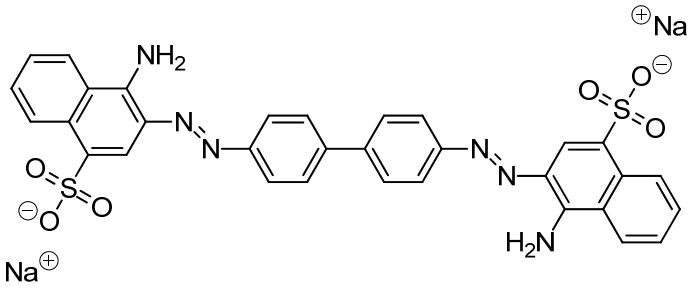

Figure 2.1. The aromatic structure of Congo Red, a dye which is widely used in the detection of amyloid fibrils.

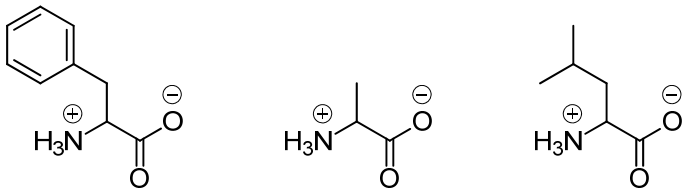

Phe (0.88) Ala (0.74) Leu (0.85)

Figure 2.2. Zwitterionic form of phenylalanine, alanine and leucine with respective hydrophobic values[3] (higher values indicate an increase in hydrophobicity).

of peptide aggregation (including Congo Red, see **Figure 2.1** for structure) contain at least one aromatic ring.[4]

Another hypothesis on what controls peptide/protein fibrillogenesis is local hydrophobicity. Advocates of this belief would argue that the phenylalanine to alanine mutation is a large change in hydrophobic surface area and thus is an "illegal substitution". Therefore, the conclusions made by Gazit are misleading. Tracz et al. demonstrated that making the substitution with leucine, a more conservative non-aromatic replacement (see **Figure 2.2**) in side chain size and hydrophobicity, results in the formation of fibrils which were confirmed to be fibrillic using Congo Red.[5]

Another contradicting study by Raleigh and co-workers using the entire islet amyloid polypeptide sequence (H-Lys-Cys-Asn-Thr-Ala-Thr-Cys-Ala-Thr-Gln-Arg-Leu-Ala-Asn-**Phe**-Leu-Val-His-Ser-Ser-Asn-Asn-**Phe**-Gly-Ala-Ile-Leu-Ser-Ser-Thr-Asn-Val-Gly-Ser-Asn-Thr-**Tyr**-NH_2) replaced all three aromatic amino acids (indicated in **red**) with leucine to study the role that intramolecular aromatic interactions may play in the aggregation process. Based on the conclusions drawn from thioflavin-T fluorescence assays, circular dichroism (CD), transmission electron microscopy (TEM) and atomic force microscopy (AFM), the authors found that aromatic residues are not needed to form amyloid fibrils. However, the rate of fibrillogenesis is five times slower.[6] This aggregation slow-down was also observed by Chiti and co-workers in their systematic replacement of aromatic residues within the 98 residue sequence for human muscle acylphosphatase (see **Figure 2.3** for sequence). All of their substitutions lead to decreased aggregation rate. But what is most interesting to note about their kinetic data is that their substitutions of phenylalanine or tyrosine with leucine resulted in slower rates of aggregation than the corresponding substitutions with the less hydrophobic alanine. Despite the conflicting results, they still champion the hydrophobicity over aromaticity.[7]

H-Ser-Thr-Ala-Gln-Ser-Leu-Lys-Ser-Val-Asp-**Tyr**-Glu-Val-**Phe**-
Gly-Arg-Val-Gln-Gly-Val-Cys-**Phe**-Arg-Met-**Tyr**-Thr-Glu-Asp-
Glu-Ala-Arg-Lys-Ile-Gly-Val-Val-Gly-**Trp**-Val-Lys-Asn-Thr-Ser-
Lys-Gly-Thr-Val-Thr-Gly-Gln-Val-Gln-Gly-Pro-Glu-Asp-Lys-
Val-Asn-Ser-Met-Lys-Ser-Trp-Leu-Ser-Lys-Val-Gly-Ser-Pro-Ser-
Ser-Arg-Ile-Asp-Arg-Thr-Asn-**Phe**-Ser-Asn-Glu-Lys-Thr-Ile-Ser-
Lys-Leu-Glu-**Tyr**-Ser-Asn-**Phe**-Ser-Ile-Arg-**Tyr**-NH_2

Figure 2.3. Full sequence of human muscle acylphosphatase (aromatic residues indicated in **red**).

Gazit and co-workers made this timing observation by alluding to the huntingtin protein associated with Huntington's disease.[8] The normal version of this protein is 3,144 amino acids in length and contains a long sequence of glutamines starting at the 18th residue from the *N*-terminus. Through mutation, the repetition of glutamine residues gets longer and longer. These increases in length of a hydrophilic domain correlates directly with a higher probability and earlier onset of the disease, and a higher propensity for the protein to aggregate into fibrils.[9] However, the aggregation process is longer by orders of magnitude.[8]

If that is not convincing enough, Gazit's group also published work demonstrating fibril formation from hydrophilic peptide fragments (such as H-Asp-**Phe**-Asn-Lys-**Phe**-OH) of the human calcitonin hormone. The hydrophobicity of this short peptide, which was increased by the addition of two phenylalanines, is lost by the inclusion of three hydrophilic residues; aspartate, asparagine and lysine (see **Figure 2.4**). The full length hormone sequence is useful in calcium homeostasis in its native peptide structure, but harmful when it aggregates into fibrils linked to medullary thyroid carcinoma. This study concludes that there is no correlation between hydrophobicity and the formation of amyloid fibrils.[10]

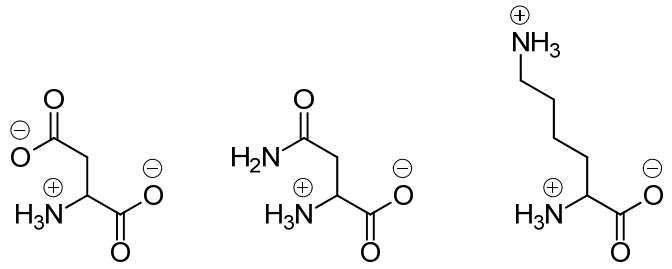

Figure 2.4. Zwitterionic form of aspartate, asparagine and lysine with respective hydrophobic values[3] (higher values indicate an increase in hydrophobicity).

Based on these findings, we decided it would be prudent to spend more time working on the synthesis of aromatic disubstituted amino acid. Previous work (published[11] and unpublished) has shown that the difficulty lies in the dibenzylation step of ethyl nitroacetate (see **Figure 2.5**). Efforts were made to determine how to improve this process. We had also previously demonstrated the dialkylation of a few benzyl halides that containing electron withdrawing groups (nitro, cyano and methylcarboxy) in the *para* position.[11] We thought it would be interesting to see if benzyl halides with *para* electron donating groups (methylthio and methoxy) could also be used in the dibenzylation step. Our reasoning behind this interest is to see if *para* substituents can influence any π-stacking or hydrophobic interactions that may be essential for the interaction of peptide based inhibitors and the amyloid beta peptide containing aromatic amino acids. Based on previous theoretical calculations and experimental results, this can be done by manipulating the electron density of the π system of the aromatic ring via substituent effects regardless of the exact π-π orientation (i.e. face-face stacked, offset stacked, or edge-face as shown in **Figure 2.6**).[12-14]

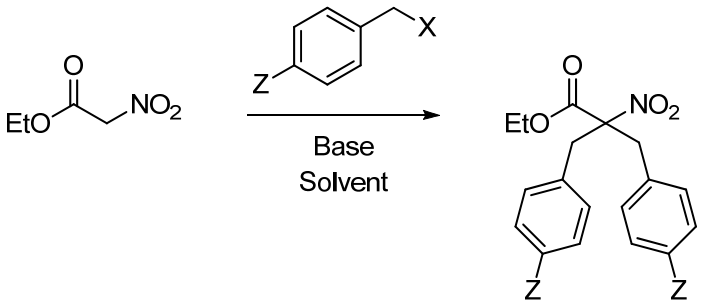

Figure 2.5. General scheme of the dibenzylation of ethyl nitroacetate with a benzyl halide.

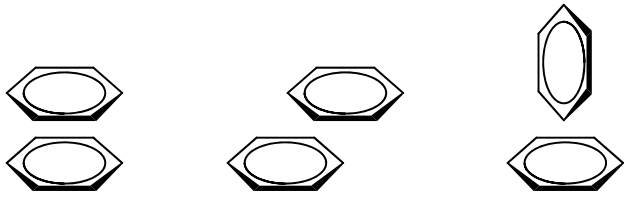

Figure 2.6. Representation of face-face stacked, offset stacked, or edge-face orientations.

2.2 Results and Discussion

Based on well-established literature precedent, the use of electron donating groups in the *para* position of benzyl bromide should promote a nucleophilic attack on the benzyl carbon atom by an ethyl nitroacetate anion, which was formed by deprotonation at the alpha carbon with N,N-diisopropylethylamine (see **Figure 2.7** for mechanism). If this was true, the dialkylation with 4-(methylthio)benzyl bromide followed by cleavage of the methylthio groups could help overcome the moderate yields of 63 % when using benzyl bromide. But much to my chagrin, the yields using 4-(methylthio)benzyl bromide, 24 to 29 % (Entry 1, **Table 2.1** and **Figures 2.8**, **2.9**), were about half the amount reported for benzyl bromide under the same conditions.[11] Alterations to reagent equivalents and reaction temperature led to similar results (Entry 2-4, **Table 2.1**). The methylthio groups also proved to be resistant to removal under hydrogenation conditions with Raney nickel or reduction conditions with zinc dust and acetic acid. Efforts using 4-methoxybenzyl bromide as the benzyl halide were also in vain as no desired dibenzylated product was formed (Entry 12 & 13, **Table 2.1**). This was very puzzling since it had been reported by Baker that the rate of the reaction when using *p*-methoxy substituted benzyl halides was so high that it could not be measured (via the Volhard titration method of determining the concentration of chlorides and bromides with silver nitrate and ammonium thiocyanate).[15] This contrary result suggested perhaps that this reaction was not going by the proposed S_N2 mechanism.

Trying to sort out these disappointing yields, I proceeded to experiment with benzyl bromide and found that, in my hands, only 26 to 32 % yields could be obtained (Entry 5, **Table 2.1** and **Figures 2.10, 2.11**). I tried changing the order of addition of reagents as done in one of our previous publications[11] with no avail (data not shown). Increasing the amount of electrophile and base from 2.1 to 2.5 equivalents did not help the cause (Entry 6, **Table 2.1**). Nor did the

substitution of N,N-diisopropylethylamine (pKa 11.4) with N,N,N′,N′-tetramethyl-1,8-naphthalenediamine (pKa 12.3), which is also known as Proton Sponge, make matters better (Entry 7, **Table 2.1**). One of the named reactions, the Finkelstein reaction, proved to be quite handy in improving my yields. The classic example of this reaction converts alkyl bromides and chlorides to iodides using either potassium or sodium iodide, which are both soluble in acetone. The insoluble salt product that is formed precipitates out of solution and shifts the reaction towards completion by following Le Châtelier's principle.[16, 17] However, this halogen exchange

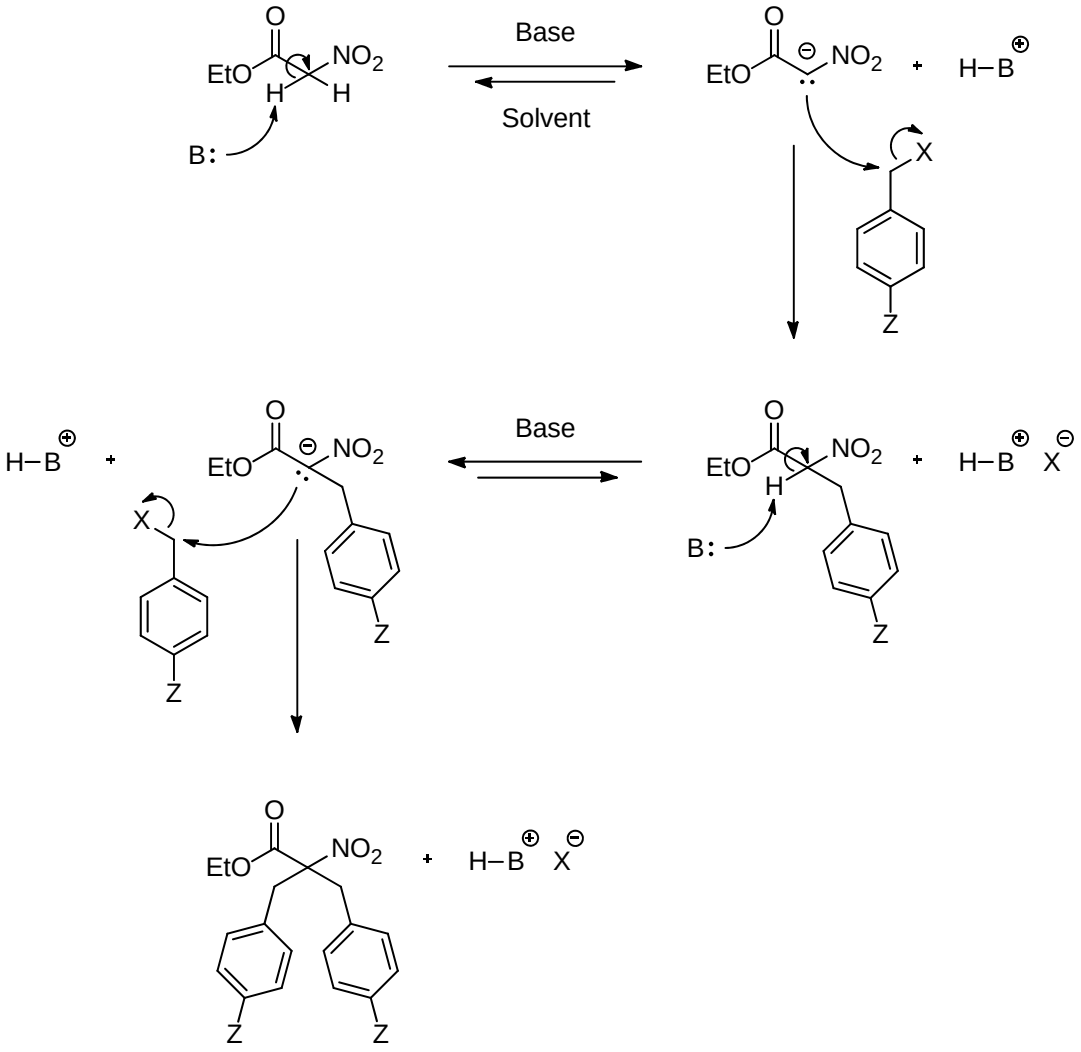

Figure 2.7. General mechanism of the dibenzylation of ethyl nitroacetate with a benzyl halide.

Table 2.1. Dialkylation of ethyl nitroacetate under various experimental conditions

Entry	Electrophile	Method	T (°C)	Yield %*
1	*p*-CH_3SPhCH_2Br	A	0-25	24-29
2	*p*-CH_3SPhCH_2Br	B	50	24
3	*p*-CH_3SPhCH_2Br	B	70	23
4	*p*-CH_3SPhCH_2Br	C	25	27
5	$PhCH_2Br$	C	25	26-32
6	$PhCH_2Br$	D	25	32
7	$PhCH_2Br$	E	25	26
8	$PhCH_2I$	F	25	19-28
9	$PhCH_2Br$	G	25	39
10	$PhCH_2Br$	H	25	34
11	$PhCH_2Cl$	G	25	29
12	*p*-CH_3OPhCH_2Br	A	0-25	0
13	*p*-CH_3OPhCH_2Br	I	60	0
14	*p*-CH_3OPhCH_2I	F	25	0
15	*p*-CH_3OPhCH_2Br	G	25	0
16	*p*-CH_3OPhCH_2Br	H	25	15
17	*p*-CH_3OPhCH_2Cl	H	25	15

* Yields are based on product obtained after recrystallization

Method A: Electrophile (2.05 eq.), Bu_4NBr (0.1 eq.) and DIEA (2.05 eq.) in DMF
Method B: Electrophile (2.25 eq.), Bu_4NBr (0.1 eq.) and DIEA (2.25 eq.) in DMF
Method C: Electrophile (2.1 eq.), Bu_4NBr (0.1 eq.) and DIEA (2.1 eq.) in DMF
Method D: Electrophile (2.5 eq.), Bu_4NBr (0.1 eq.) and DIEA (2.5 eq.) in DMF
Method E: Electrophile (2.5 eq.), Bu_4NBr (0.1 eq.) and **Proton Sponge** (2.1 eq.) in DMF
Method F: Electrophile (2.5 eq.) and DIEA (2.5 eq.) in DMF
Method G: Electrophile (2.5 eq.), **KI** (3.2 eq.) and DIEA (2.5 eq.) in DMF
Method H: Electrophile (2.5 eq.), **KI** (3.2 eq.) and DIEA (2.5 eq.) in **Acetonitrile**
Method I: Electrophile (3.7 eq.), Bu_4NBr (0.1 eq.) and DIEA (2.05 eq.) in DMF

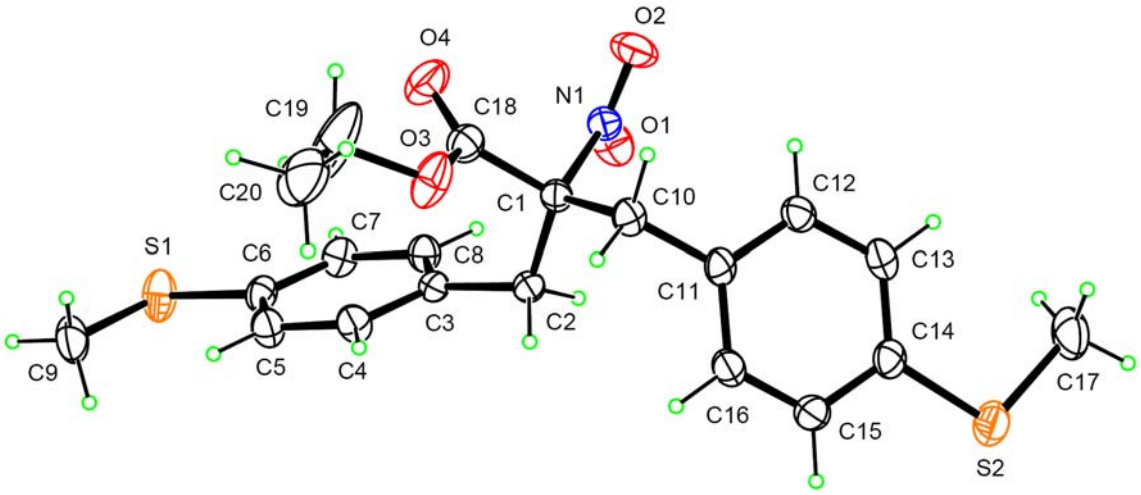

Figure 2.8. ORTEP representation (ellipsoids 50 %) of ethyl 2-(4-(methylthio)benzyl)-3-(4-(methylthio)phenyl)-2-nitropropanoate (**2.4.2)**.

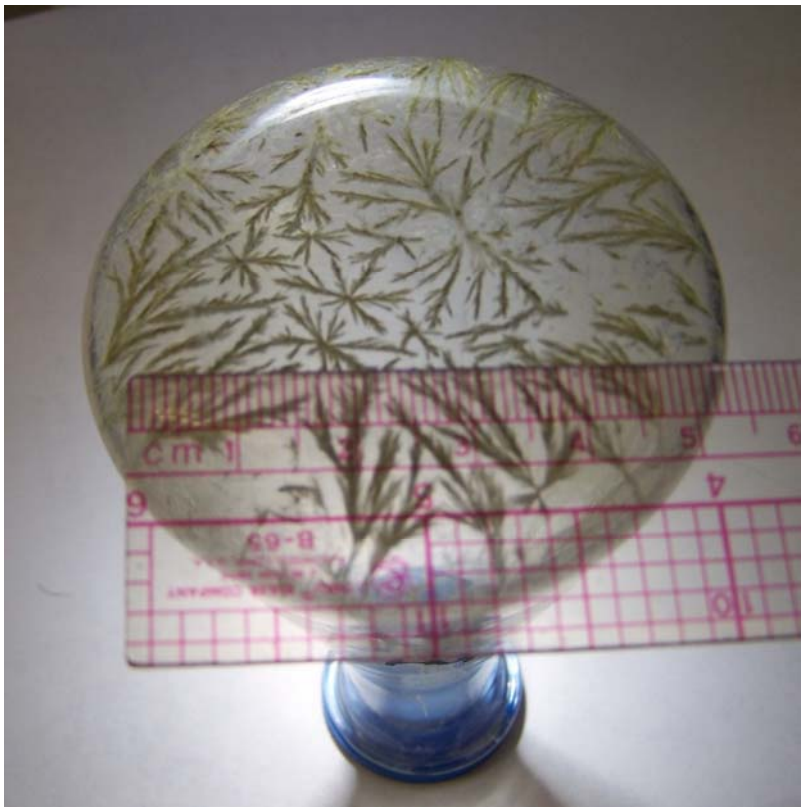

Figure 2.9. Dendritic crystals of ethyl 2-(4-(methylthio)benzyl)-3-(4-(methylthio)phenyl)-2-nitropropanoate (**2.4.2)**.

Figure 2.10. Ethyl 2-benzyl-2-nitro-3-phenylpropanoate crystals (**2.4.1)**.

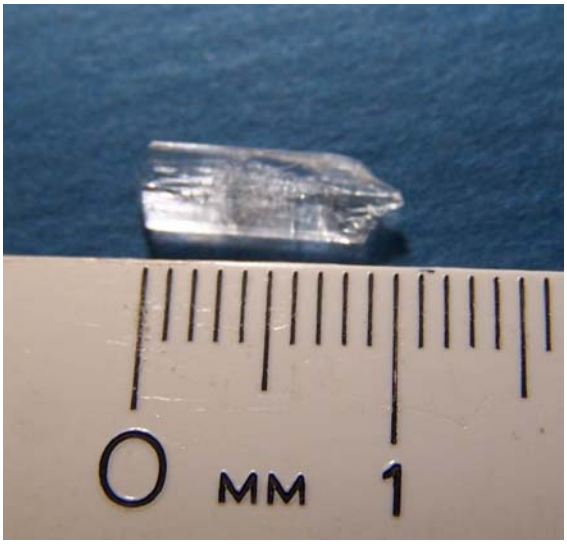

Figure 2.11. Size of ethyl 2-benzyl-2-nitro-3-phenylpropanoate crystal (**2.4.1)**.

could be capitalized on during the dibenzylation step in a different solvent, N,N-dimethylformamide. Yields under these conditions rose as high as 55 % after purification with a silica gel column and 39 % post-crystallization in ethanol (Entry 9, **Table 2.1**). **Note:** I have a preference in reporting the crystalline yields since I have greater confidence in the purity of the product.

The previously unreactive 4-(methylthio)benzyl bromide was reevaluated to see if halogen exchange could remedy the situation. Unfortunately, the result was still the same (Entry 14 & 15, **Table 2.1**). However, success was made when the solvent was changed to acetonitrile, resulting in a 15 % yield of crystalline disubstituted product (Entry 16, **Table 2.1** and **Figures 2.12, 2.13**). Similar results were obtained when using *p*-methylthiobenzyl chloride (Entry 17, **Table 2.1**).

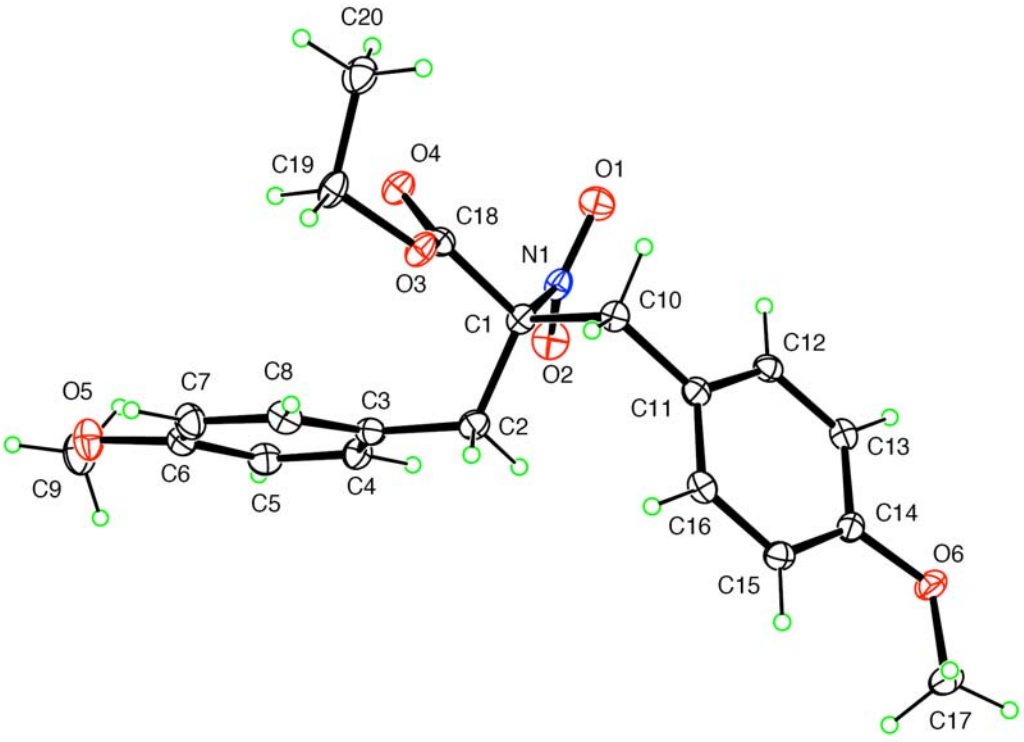

Figure 2.12. ORTEP representation (ellipsoids 50 %) of ethyl 2-(4-methoxybenzyl)-3-(4-methoxyphenyl)-2-nitropropanoate (**2.4.3**).

Figure 2.13. Crystals of ethyl 2-(4-methoxybenzyl)-3-(4-methoxyphenyl)-2-nitropropanoate (**2.4.3**).

2.3 Conclusions

It was demonstrated that benzyl halides containing electron donating substituents in the *para* position could be successfully dialkylated onto the α-carbon of ethyl nitroacetate albeit with more difficulty than previously anticipated. There was also progress made on improving the yields by halogen exchange à la Finkelstein type reaction. However, the conversion to iodides is not always a good thing for dibenzylation as will be shown in **Chapter 3** with *para* electron withdrawing groups. Optimized protocols for preparing ethyl 2-benzyl-2-nitro-3-phenylpropanoate, ethyl 2-(4-(methylthio)benzyl)-3-(4-(methylthio)phenyl)-2-nitropropanoate and ethyl 2-(4-methoxybenzyl)-3-(4-methoxyphenyl)-2-nitropropanoate provided in the following experimental section, **2.4**.

2.4 Experimental

2.4.1 Ethyl 2-benzyl-2-nitro-3-phenylpropanoate

The reaction was carried out under argon at room temperature and monitored by thin-layer chromatography. Ethyl nitroacetate (1.0 g, 7.51 mmol), potassium iodide (4.0 g, 24.1

mmol) and benzyl bromide (3.2 g, 18.8 mmol) were added to a round-bottom flask containing anhydrous N,N-dimethylformamide (5 mL). Then N,N-diisopropylethylamine (2.4 g, 18.8 mmol) was added slowly to the reaction mixture (without cooling) while stirring. After diluting in diethyl ether (100mL), impurities were extracted by washing with 1N HCl (2 x 40 mL), saturated sodium carbonate solution (2 x 40 mL), and water (5 x 20 mL) in a separatory funnel. Magnesium sulfate was used to dry the organic layer and later removed by paper filtration. The filtrate was then concentrated on a rotary evaporator and the desired product was isolated using a silica gel column (hexanes-ethyl acetate, 90:10). Recrystallization in hot ethanol followed by slow cooling resulted in colorless crystals. Yield, 0.91 g (39%); mp 81 – 83 °C; ^{1}H-NMR (250 MHz, $CDCl_3$) δ 7.32 – 7.16 (m, 10H), 4.12 (q, J=7.2 Hz, 2H), 3.49 (s, 4H), 1.13 (t, J=7.2 Hz, 3H); ^{13}C-NMR (250 MHz, $CDCl_3$) δ 166.2, 133.1, 130.0, 128.5, 127.7, 97.1, 62.6, 40.0, 13.4; MS (ESI) calculated for $C_{18}H_{19}NO_4$ $[M + H]^+$ 314.1, found 314.1; Crystal data (Mo *Kα* radiation) for $C_{18}H_{19}NO_4$ confirmed match by performing lattice check of reported literature values.[18]

2.4.2 Ethyl 2-(4-(methylthio)benzyl)-3-(4-(methylthio)phenyl)-2-nitropropanoate

This compound was synthesized with 4-(methylthio)benzyl bromide (4.1 g, 18.8 mmol) as the benzyl halide and tetrabutylammonium bromide (0.24 g, 0.75 mmol), instead of potassium iodide. The same basic procedure was followed as written in previous section (**2.4.1**). Yield, 0.82 g (24%); mp 99 – 101 °C; ^{1}H-NMR (250 MHz, $CDCl_3$) δ 7.18 (d, J=8.2 Hz, 4H), 7.07 (d, J=8.3 Hz, 4H), 4.14 (q, J=7.1 Hz, 2H), 3.42 (s, 4H), 2.47 (s, 6H), 1.15 (t, J=7.1 Hz, 3H); ^{13}C-NMR (250 MHz, $CDCl_3$) δ 166.1, 138.3, 130.4, 129.6, 126.4, 96.9, 62.7, 39.5, 15.5, 13.5; MS (ESI) calculated for $C_{20}H_{23}NO_4S_2$ $[M + H]^+$ 406.1, found 406.2; Crystal data (Mo *Kα* radiation) for $C_{20}H_{23}NO_4S_2$: M_r = 405.51, Monoclinic, $P2_1/n$, a = 16.029 (2) Å, b = 6.1465 (5) Å, c =

21.146 (3) Å, V = 1986.6 (4) Å^3, Z = 4, λ = 0.71073 Å, T = 170 K, $R[F^2 > 2\sigma(F^2)]$ = 0.048, $wR(F^2)$ = 0.123.

2.4.3 Ethyl 2-(4-methoxybenzyl)-3-(4-methoxyphenyl)-2-nitropropanoate

This compound was synthesized with 4-methoxybenzyl bromide (3.8 g, 18.8 mmol) as the benzyl halide and anhydrous acetonitrile (5 mL) as the solvent. The same basic procedure was followed as written in previous section (**2.4.1**). Yield, 0.41 g (15%); mp 72 – 73 °C; ^{1}H-NMR (250 MHz, $CDCl_3$) δ 7.09 (d, J=8.6 Hz, 4H), 6.84 (d, J=8.6 Hz, 4H), 4.14 (q, J=7.1 Hz, 2H), 3.79 (s, 6H), 3.41 (s, 4H), 1.16 (t, J=7.1 Hz, 3H); ^{13}C-NMR (250 MHz, $CDCl_3$) δ 166.3, 159.1, 131.1, 125.0, 113.9, 97.3, 62.5, 55.1, 39.1,13.5; MS (ESI) calculated for $C_{20}H_{23}NO_6$ $[M + H]^+$ 374.2, found 374.2; Crystal data (Cu $K\alpha$ radiation) for $C_{20}H_{23}NO_6$: M_r = 373.39, Orthorhombic, $Pna2_1$, a = 18.0681 (9) Å, b = 17.1151 (6) Å, c = 6.0216 (3) Å, V = 1862.10 (15) Å^3, Z = 4, λ = 1.54178 Å, T = 90 K, $R[F^2 > 2\sigma(F^2)]$ = 0.022, $wR(F^2)$ = 0.056.

2.5 References

1. Gazit, E., A Possible Role for π-Stacking in the Self-Assembly of Amyloid Fibrils. *FASEB J.* **2002**, 16, 77-83.

2. Azriel, R.; Gazit, E., Analysis of the Minimal Amyloid-forming Fragment of Islet Amyloid Polypeptide - An Experimental Support for the Key Role of the Phenylalanine Residue in Amyloid Formation. *J. Biol. Chem.* **2001**, 276, 34156-34161.

3. Rose, G. D.; Geselowitz, A. R.; Lesser, G. J.; Lee, R. H.; Zehfus, M. H., Hydrophobicity of Amino-Acid Residues in Globular-Proteins. *Science* **1985**, 229, 834-838.

4. Stains, C. I.; Mondal, K.; Ghosh, I., Molecules that Target beta-Amyloid. *ChemMedChem* **2007**, 2, 1674-1692.

5. Tracz, S. M.; Abedini, A.; Driscoll, M.; Raleigh, D. P., Role of Aromatic Interactions in Amyloid Formation by Peptides Derived from Human Amylin. *Biochemistry* **2004**, 43, 15901-15908.

6. Marek, P.; Abedini, A.; Song, B. B.; Kanungo, M.; Johnson, M. E.; Gupta, R.; Zaman, W.; Wong, S. S.; Raleigh, D. P., Aromatic Interactions Are Not Required for Amyloid Fibril Formation by Islet Amyloid Polypeptide but Do Influence the Rate of Fibril Formation and Fibril Morphology. *Biochemistry* **2007**, 46, 3255-3261.

7. Bemporad, F.; Taddei, N.; Stefani, M.; Chiti, F., Assessing the Role of Aromatic Residues in the Amyloid Aggregation of Human Muscle Acylphosphatase. *Protein Sci.* **2006**, 15, 862-870.

8. Mazor, Y.; Gilead, S.; Benhar, I.; Gazit, E., Identification and Characterization of a Novel Molecular-recognition and Self-assembly Domain within the Islet Amyloid Polypeptide. *J. Mol. Biol.* **2002**, 322, 1013-1024.

9. Slepko, N.; Bhattacharyya, A. M.; Jackson, G. R.; Steffan, J. S.; Marsh, J. L.; Thompson, L. M.; Wetzel, R., Normal-Repeat-Length Polyglutamine Peptides Accelerate Aggregation Nucleation and Cytotoxicity of Expanded Polyglutamine Proteins. *Proc. Natl. Acad. Sci. U. S. A.* **2006**, 103, 14367-14372.

10. Reches, M.; Porat, Y.; Gazit, E., Amyloid Fibril Formation by Pentapeptide and Tetrapeptide Fragments of Human Calcitonin. *J. Biol. Chem.* **2002**, 277, 35475-35480.

11. Fu, Y. W.; Hammarstrom, L. G. J.; Miller, T. J.; Fronczek, F. R.; McLaughlin, M. L.; Hammer, R. P., Sterically Hindered $C^{\alpha,\alpha}$-Disubstituted α-Amino Acids: Synthesis from α-Nitroacetate and Incorporation into Peptides. *J. Org. Chem.* **2001**, 66, 7118-7124.

12. Lee, E. C.; Hong, B. H.; Lee, J. Y.; Kim, J. C.; Kim, D.; Kim, Y.; Tarakeshwar, P.; Kim, K. S., Substituent Effects on the Edge-to-Face Aromatic Interactions. *J. Am. Chem. Soc.* **2005**, 127, 4530-4537.

13. Ringer, A. L.; Sinnokrot, M. O.; Lively, R. P.; Sherrill, C. D., The Effect of Multiple Substituents on Sandwich and T-Shaped π-π Interactions. *Chem. Eur. J.* **2006**, 12, 3821-3828.

14. Rashkin, M. J.; Waters, M. L., Unexpected Substituent Effects in Offset π-π Stacked Interactions in Water. *J. Am. Chem. Soc.* **2002**, 124, 1860-1861.

15. Baker, J. W., Reactions of ω-Substituted Acetophenone Derivatives. Part III. Comparison of the Mechanism of Interaction of ω-Halogenoacetophenones and of Benzyl Halides with Primary and Tertiary Bases. *J. Chem. Soc.* **1932**, 2631-2636.

16. Finkelstein, H., Darstellung organischer Jodide aus den entsprechenden Bromiden und Chloriden. *Ber. Dtsch. Chem. Ges.* **1910**, 43, 1528-1532.

17. Pace, R. D.; Regmi, Y., The Finkelstein Reaction: Quantitative Reaction Kinetics of an S_N2 Reaction Using Nonaqueous Conductivity. *J. Chem. Educ.* **2006**, 83, 1344-1348.

18. Miller, T. J.; Fu, Y. W.; Fronczek, F. R.; Hammer, R. P., Ethyl 2-benzyl-2-nitro-3-phenylpropanoate. *Acta Crystallogr. Sect. C-Cryst. Struct. Commun.* **2000**, 56, E574-E575.

CHAPTER 3

RADICAL BENZYLATION WITH ELECTRON WITHDRAWING GROUPS ON THE BENZYL HALIDE

3.1 Introduction

It seemed unusual that benzyl bromides with electron donating group (such as methoxy and methylthio) in the *para* position would have lower or equivalent yields than the unsubstituted benzyl bromides for the dialkylation experiments mentioned in **Chapter 2**. It was expected that these groups would help promote a S_N2 reaction (see **Figure 3.1**) by stabilizing the positive charge on the carbon between the halide and the aromatic ring. While comparing the yields to our previous publication,[1] another unusual observation was made. The benzyl bromides that contained electron withdrawing groups (such as nitro, cyano and methylcarboxyl) in the *para* position had higher yields than the unsubstituted benzyl bromides. This also seemed contrary to what one would expect. Shouldn't electron withdrawing groups inhibit a S_N2 reaction by destabilizing the positive charge on the carbon site for nucleophilic attack? (See **Figure 3.2**) What's going on here?

From the literature, it has been shown experimentally that both benzyl bromides containing electron donating and electron withdrawing groups in the *para* position promote benzylation. Swain and Langsdorf also noted that based on the "U" or "V" shape of the Hammet plot of various *para* substituents that there must be a difference in mechanism behind phenomena.[2] They rationalized the transition state favoring "bond breaking" with electron donating groups and "bond making" with electron withdrawing groups. This rationale was supported also by Bowden and Cook.[3] Hudson and Klopman reported that the unusual effect of the electron withdrawing groups may be due to a promoted conjugation between the phenyl ring

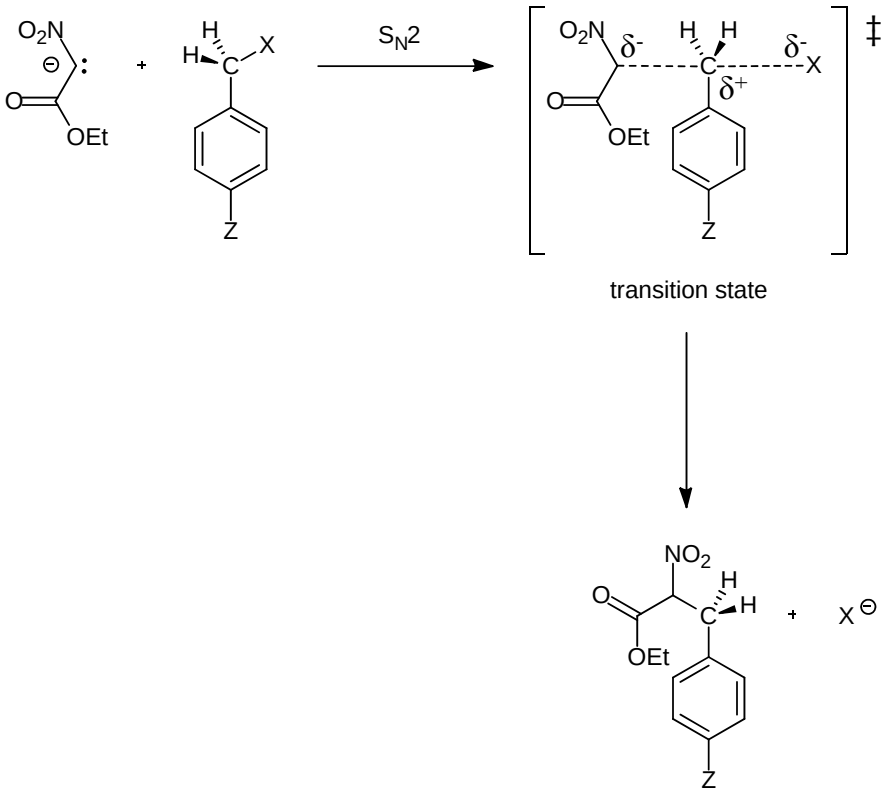

Figure 3.1. S_N2 reaction between the nucleophile, ethyl nitroacetate, and the electrophile, para benzyl halide.

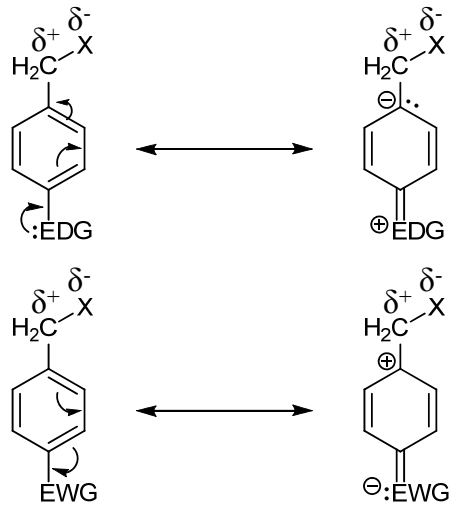

Figure 3.2. Resonance effects of electron donating group (EDG) and electron withdrawing group (EWG) in the *para* position.

and the "pseudo" *p*-orbital of the "CH_2" group connected to the *ispo* carbon.[4] But how does all this translate into a possible second benzylation mechanism?

In a review article with the *p*-nitrobenzyl "system", the mystery around the speculated change in mechanism is unraveled in detail.[5] There are two major forms of benzylation that can transpire during the substitution reaction between a deprotonated aliphatic nitro compound and alkyl halides. Since a lone pair of electrons can resonate between the nitro group and the adjacent carbon atom, a competition between *O*-alkylation, which ultimately leads to the formation of an aldehyde, versus *C*-alkylation exists. The balance between these two alkylations depends on both the substituent on the aromatic ring and the leaving group for the substitution. In the case of the *p*-nitrobenzyl "system", it became evident that *C*-alkylation dominants when a poorer leaving group is employed, which is contrary to the normal trends observed in both S_N2 and S_N1 reactions. Hence, it is better to perform *C*-alkylation with a 4-nitrobenzyl chloride instead of a bromide or iodide. For this reversal of the trend to occur, a different route or mechanism must be occurring.[5]

In the case of the *p*-nitrobenzyl "system", it has been proposed that a radical anion intermediate was the root cause for *C*-alkylation's preference for poor leaving groups. To prove this idea that a single electron transfer was taking place between a deprotonated aliphatic nitro compound, such as 2-nitropropane, and 4-nitrobenzyl chloride, a known electron capturer, 1,4-dinitrobenzene, was added to the reaction in order to steal an electron away from the α-nitro radical anion. This electron capture should be able to occur faster than the rate of the displacement of the chloride and, therefore, inhibit the possibility of *C*-alkylation. The addition of 1,4-dinitrobenzene in the same equivalents of 4-nitrobenzyl chloride led to a major reduction from 92 % to 2 % for *C*-alkylation.[5]

To test Kornblum's conclusions, a similar synthesis was performed to see if 4-nitrobenzyl chloride would be more reactive than the bromide version for the dialkylation of ethyl nitroacetate. To verify that a radical anion intermediate was being formed, *C*-alkylation inhibition with 1,4-dinitrobenzene was also evaluated with the more reactive 4-nitrobenzyl chloride.

3.2 Results and Discussion

4-Nitrobenzyl bromide was used for the dibenzylation of ethyl nitroacetate under similar reaction conditions as previously reported.[1] The only change was not adding tetrabutylammonium bromide to the reaction. This compound was previously used in catalytic amounts and it was suggested that this additive helped promote the dialkylation. But I did not know if it would help to the same degree (or hurt) when switching from a benzyl bromide to a benzyl chloride. Therefore, it was removed from the procedure since I was only interested in the influence of *para* substituents and halogen leaving groups on the dibenzylation. The previously reported yield of 75 % was not reproduced in this experiment.[1] In my hands, the reaction only yielded 29 % of dialkylated product.

Despite getting lower than expected yields, I pressed on with my experiments by switching to the chloride. After working up the reaction and purifying the desire product, I was quite pleased with the results. The effect of using 4-nitrobenzyl chloride for the dialkylation caused the yields to increase to 50 %. If this type of substitution was a normal S_N2 reaction, or S_N1 for those who believe otherwise, such an increase in reactivity would not happen. Something else is going on here. All signs point to a different mechanism (see **Figure 3.3**).

To evaluate the possibility of a mechanism involving a radical anion intermediate, the same electron scavenger was used.[5] When 1,4-dinitrobenzene was added in the same number equivalents as 4-nitrobenzyl chloride, no dialkylated product was formed. It is also interesting to

note that no trace of mono-benzylated product was observed based on NMR. It would appear that 1,4-dinitrobenzene shut down the possibility of any *C*-alkylation. This also gives credibility to the proposed radical anion intermediate mechanism.

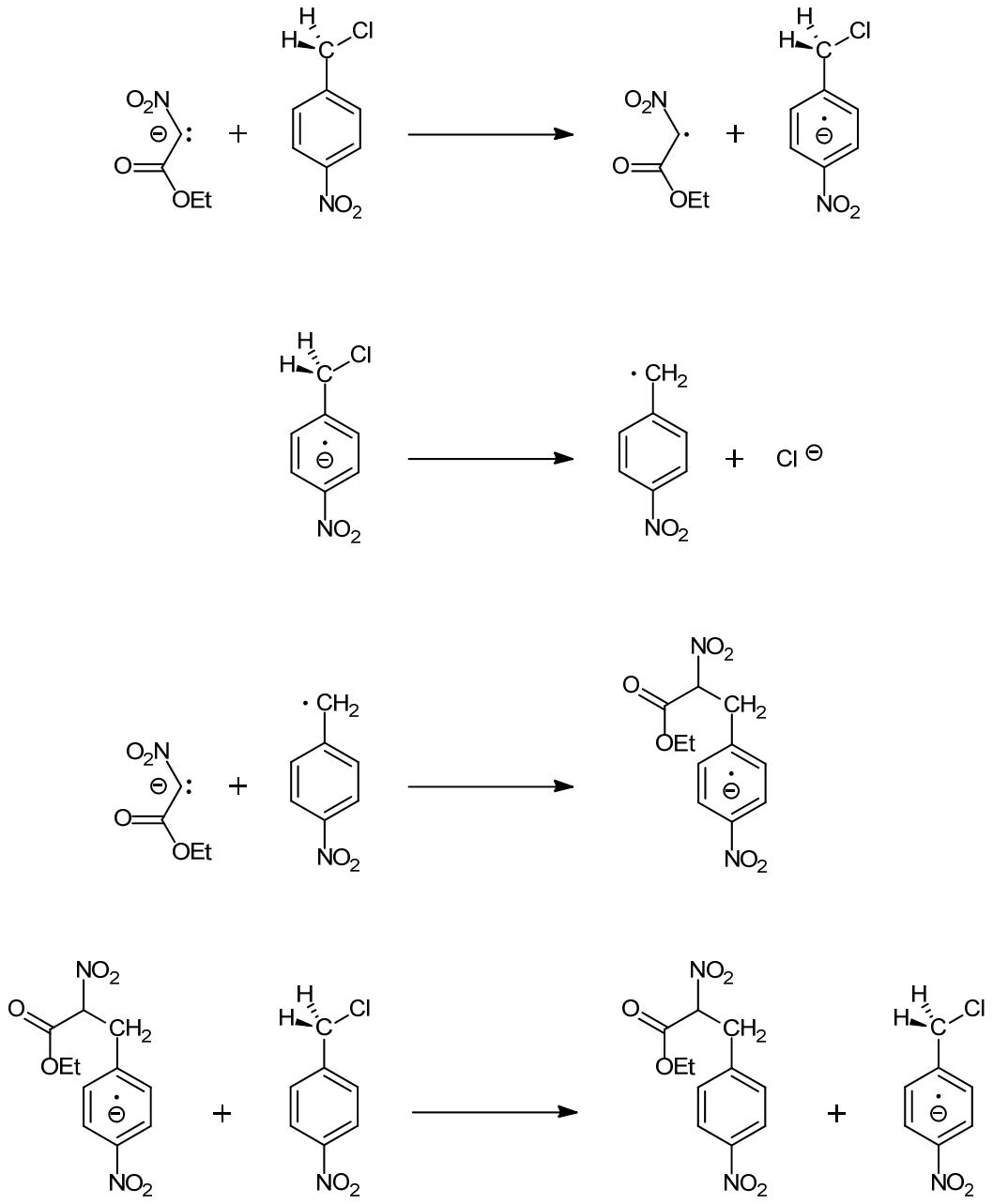

Figure 3.3. Reaction between ethyl nitroacetate and 4-nitrobenzyl chloride (adapted from the $S_{RN}1$ mechanism reported in the publication by Kim and Bunnett).[6]

3.3 Conclusions

It was quite rewarding to unravel this mystery by digging into the literature with the aid of Dr. Crowe. This knowledge will aid our synthetic methodology in designing dibenzylated analogs with *para* substituents. This unique change in mechanism that involves a radical anion intermediate has been shown with other electron withdrawing substituents, such as the cyano group.[7] It would be interesting to see if our previously reported dibenzylation yields using 4-cyanobenzyl bromide could be improved by switching to the chloride version.[1]

The formation of an aldehyde via *O*-alkylation has long been suspected as one of the reasons we have been plagued with mediocre yields when attempting dibenzylation of ethyl nitroacetate (see **Figure 3.4**). Attempts to dibenzylate with 4-(methylsulfonyl)benzyl chloride

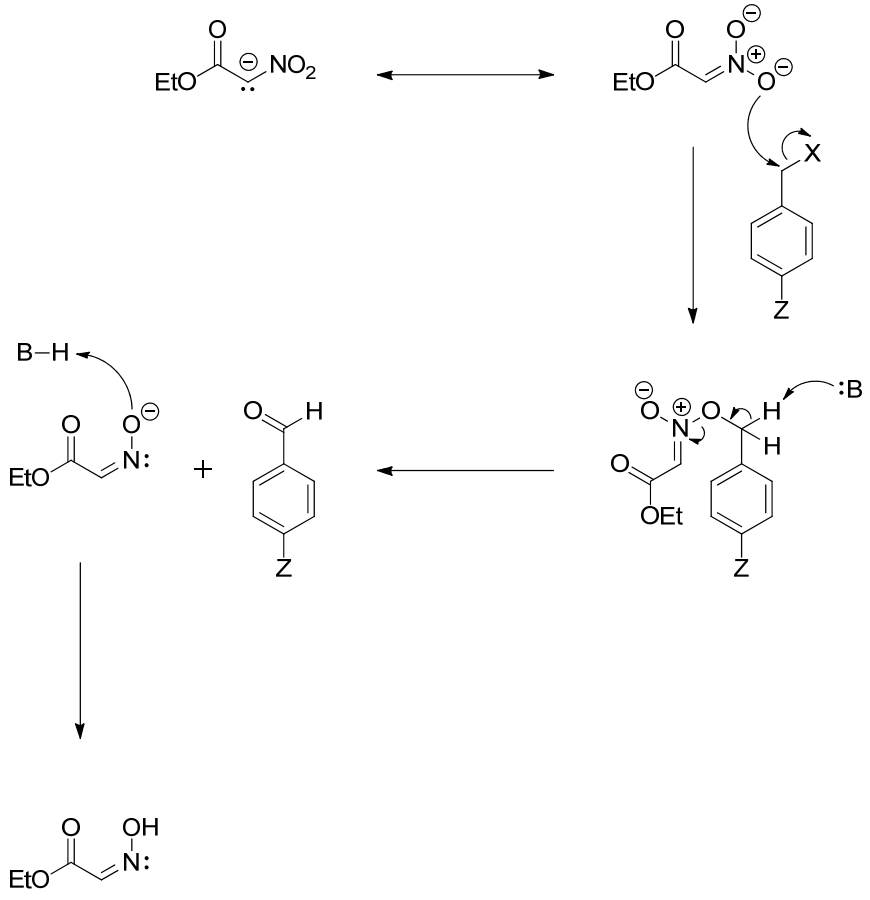

Figure 3.4. Mechanism for the formation of a benzaldehyde via *O*-alkylation of ethyl nitroacetate.

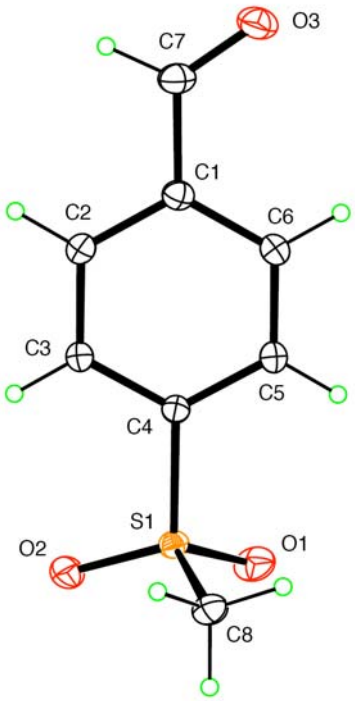

Figure 3.5. ORTEP representation (ellipsoids 50 %) of 4-(methylsulfonyl)benzaldehyde (which has not been previously reported). Crystal data (Mo $K\alpha$ radiation) for $C_8H_8O_3S$: M_r = 184.20, Monoclinic, $P2_1/c$, a = 6.0820 (6) Å, b = 7.9205 (9) Å, c = 16.639 (2) Å, V = 801.51 (15) Å^3, Z = 4, λ = 0.71073 Å, T = 90 K, $R[F^2 > 2\sigma(F^2)]$ = 0.037, $wR(F^2)$ = 0.104.

provides rock solid evidence that benzaldehyde is being produced (see **Figure 3.5**). Unfortunately, in the case of using 4-(methylsulfonyl)benzyl chloride, no traces of *C*-alkylated product was obtained.

3.4 Experimental

3.4.1 Ethyl 2-nitro-2-(4-nitrobenzyl)-3-(4-nitrophenyl)propanoate (Using NO_2BzBr)

Ethyl nitroacetate (1.0 g, 7.51 mmol) and 4-nitrobenzyl bromide (4.1 g, 18.8 mmol) were added to a round-bottom flask containing anhydrous N,N-dimethylformamide (5 mL). The reaction mixture was then cooled to 0 °C in an ice bath and N,N-diisopropylethylamine (2.4 g, 18.78 mmol) was added slowly while stirring. The reaction was carried out under argon at room

temperature. After diluting in diethyl ether (100mL), impurities were extracted by washing with 1N HCl (2 x 40 mL), saturated sodium carbonate solution (2 x 40 mL), and water (5 x 20 mL) in a separatory funnel. Magnesium sulfate was used to dry the organic layer and later removed by paper filtration. The filtrate was then concentrated on a rotary evaporator and the desired product was isolated using a silica gel column (hexanes / ethyl acetate 90:10). Recrystallization in hot ethanol followed by slow cooling resulted in colorless crystals. Yield, 0.87 g (29%); ^{1}H-NMR (250 MHz, DMSO-d_6) δ 8.21 (d, J=8.8 Hz, 4H), 7.51 (d, J=8.8 Hz, 4H), 4.12 (q, J=7.1 Hz, 2H), 3.72 (d, J= 3.8 Hz, 4H), 1.05 (t, J=7.1 Hz, 3H); ^{13}C-NMR (250 MHz, DMSO-d_6) δ 174.9, 147.5, 141.5, 132.0, 123.8, 97.3, 63.5, 28.4, 13.7

3.4.2 Ethyl 2-nitro-2-(4-nitrobenzyl)-3-(4-nitrophenyl)propanoate (Using NO_2BzCl)

This compound was synthesized with 4-nitrobenzyl chloride (3.22 g, 18.8 mmol) using the same procedure as written in previous section (**3.4.1**). Yield, 1.50 g (50%); ^{1}H-NMR (250 MHz, DMSO-d_6) δ 8.21 (d, J=8.9 Hz, 4H), 7.51 (d, J=8.9 Hz, 4H), 4.12 (q, J=7.1 Hz, 2H), 3.72 (d, J= 3.8 Hz, 4H), 1.05 (t, J=7.1 Hz, 3H)

3.4.3 Benzylation Experiment with 4-nitrobenzyl Chloride and 1,4-dinitrobenzene

This experiment was conducted using 4-nitrobenzyl chloride (3.22 g, 18.8 mmol) and 1,4-dinitrobenzene (3.16 g, 18.8 mmol) using the same procedure as written in previous section (**3.4.1**). The desired product, Ethyl 2-nitro-2-(4-nitrobenzyl)-3-(4-nitrophenyl)propanoate, was not formed and bulk of the final reaction mixture appears to be the benzyl halide starting material, 4-nitrobenzyl chloride (see **Figure 3.6**). Even before purification, the excessive amount of 4-nitrobenzyl chloride that remains can be seen visually if the crude reaction mixture is allowed to crystallize (see **Figure 3.7**).

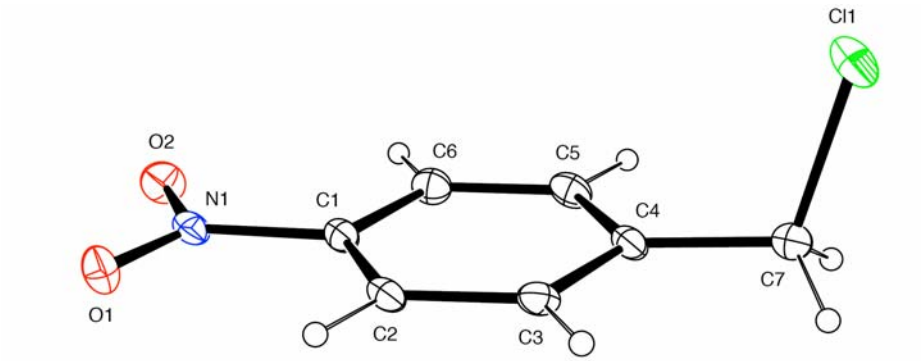

Figure 3.6. ORTEP representation (ellipsoids 50 %) of 4-nitrobenzyl chloride. Crystal data (Cu *Kα* radiation) for $C_7H_6ClNO_2$: M_r = 171.58, Orthorhombic, $P2_12_12_1$, a = 4.6952 (2) Å, b = 6.3691 (2) Å, c = 24.5393 (8) Å, V = 733.83 (5) Å^3, Z = 4, λ = 1.54178 Å, T = 90 K, $R[F^2 > 2\sigma(F^2)]$ = 0.041, $wR(F^2)$ = 0.119.[8]

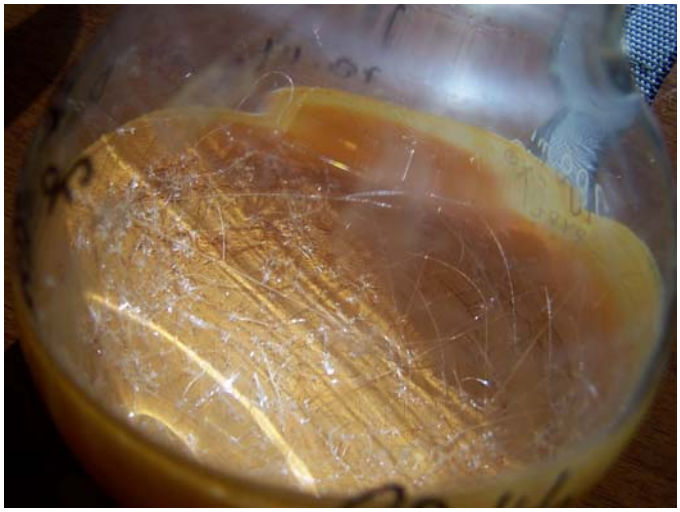

Figure 3.7. 4-Nitrobenzyl chloride (starting material) crystallizing out of the crude reaction mixture.

3.5 References

1. Fu, Y. W.; Hammarstrom, L. G. J.; Miller, T. J.; Fronczek, F. R.; McLaughlin, M. L.; Hammer, R. P., Sterically Hindered $C^{\alpha,\alpha}$-Disubstituted α-Amino Acids: Synthesis from α-Nitroacetate and Incorporation into Peptides. *J. Org. Chem.* **2001**, 66, 7118-7124.

2. Swain, C. G.; Langsdorf, W. P., Concerted Displacement Reactions. VI. *m*- and *p*-Substituent Effects as Evidence for a Unity of Mechanism in Organic Halide Reactions. *J. Am. Chem. Soc.* **1951**, 73, 2813-2819.

3. Bowden, K.; Cook, R. S., Reactions in Strongly Basic Solutions. Part I. Kinetics and Mechanism of Alkylation and Benzylation of 9-Cyanofluorenyl Anion. *J. Chem. Soc. B* **1968**, 1529-1533.

4. Hudson, R. F.; Klopman, G., Nucleophilic Reactivity. Part II. The Reaction between Substituted Thiophenols and Benzyl Bromides. *J. Chem. Soc.* **1962**, 1062-1067.

5. Kornblum, N., Substitution-Reactions Which Proceed via Radical-Anion Intermediates. *Angew. Chem. Int. Edit. Engl.* **1975**, 14, 734-745.

6. Kim, J. K.; Bunnett, J. F., Evidence for a Radical Mechanism of Aromatic Nucleophilic Substitution. *J. Am. Chem. Soc.* **1970**, 92, 7463-7464.

7. Kornblum, N.; Fifolt, M. J., Electron-Transfer Substitution-Reactions - Facilitation by the Cyano Group. *Tetrahedron* **1989**, 45, 1311-1322.

8. McCandless, G. T.; Fronczek, F. R., *Private communication CCDC 685650 to Cambridge Crystallographic Data Centre* **2008**.

CHAPTER 4

PALLADIUM-ASSISTED ALKYLATION WITH ALLYL METHYL CARBONATE AND SYTHESIS OF N^{α}-(9-FLUORENYLMETHOXYCARBONYL)-2,2-DIPROPYLGLYCINE

4.1 Introduction

2,2-Dipropylglycine, or Dpg, (see **Figure 4.1**) along with two other disubstituted amino acids (2,2-diisobutylglycine, or Dibg, and 2,2-dibenzylglycine, or Dbzg) have been previously incorporated into our inhibitors designed to bind to the central hydrophobic core within the amyloid beta peptide sequence and impede the aggregation process that is believed to be play an important role in Alzheimer's disease.[1] *In vitro* experiments have demonstrated AMY-1 inhibitor (sequence: H-Lys-Dibg-Val-Dbzg-Phe-Dpg-$(Lys)_6$-NH_2) can prevent peptide aggregation into fibrils at sub-stoichiometric concentrations (i.e. 5 μM AMY-1 : 50 μM amyloid beta). This is a boast few can claim. Most inhibitors developed by other research groups have only been successful at concentrations of at least one equivalent or higher. Therefore, we are confident that disubstituted amino acids should be included in future inhibitor designs. In order to continue our ongoing efforts to improve of our inhibitor design, it is necessary to maintain our supplies of disubstituted amino acids and explore experimental changes to improve the synthetic yields to produce each one in the most efficient manner.

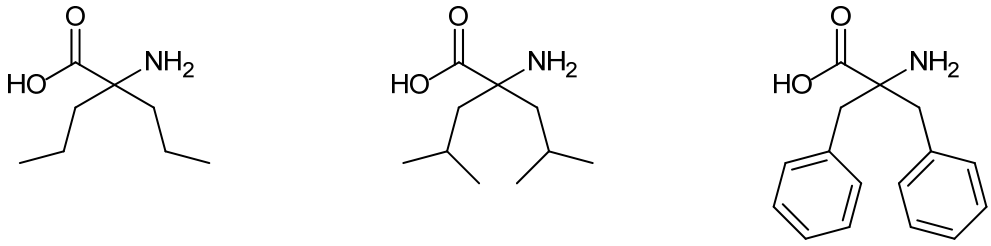

Figure 4.1. Three disubstituted amino acids: Dpg, Dibg and Dbzg (from left to right).

4.2 Results and Discussion

This synthesis was not really novel – the palladium-assisted alkylation to form the precursor to Dpg and the subsequent steps to convert it to an amino acid has already been reported by our research group (see **Figure 4.2** for overall reaction scheme).[2] However, the catalytic amounts (or mol %) of $Pd(PPh_3)_4$ truly needed for complete dialkylation has not been thoroughly investigated. My efforts focused on minimizing the amount of palladium catalyst and changing the electrophile from allyl acetate to allyl methyl carbonate.

Based on the work done by Tsuji,[3] there are three main advantages in using allyl methyl carbonate. In the case of using allyl acetate, every step is reversible (see **Figure 4.3**). This is not true for the catalytic cycle when employing allyl methyl carbonate as the alkylation reagent (see **Figure 4.4**). The irreversibility advantage that occurs between **6** and **7** comes from the decarboxylation step (conversion of methyl carbonate anion to methoxide anion) and the protonation step (methoxide anion is basic enough to pick up a proton from ethyl nitroacetate to

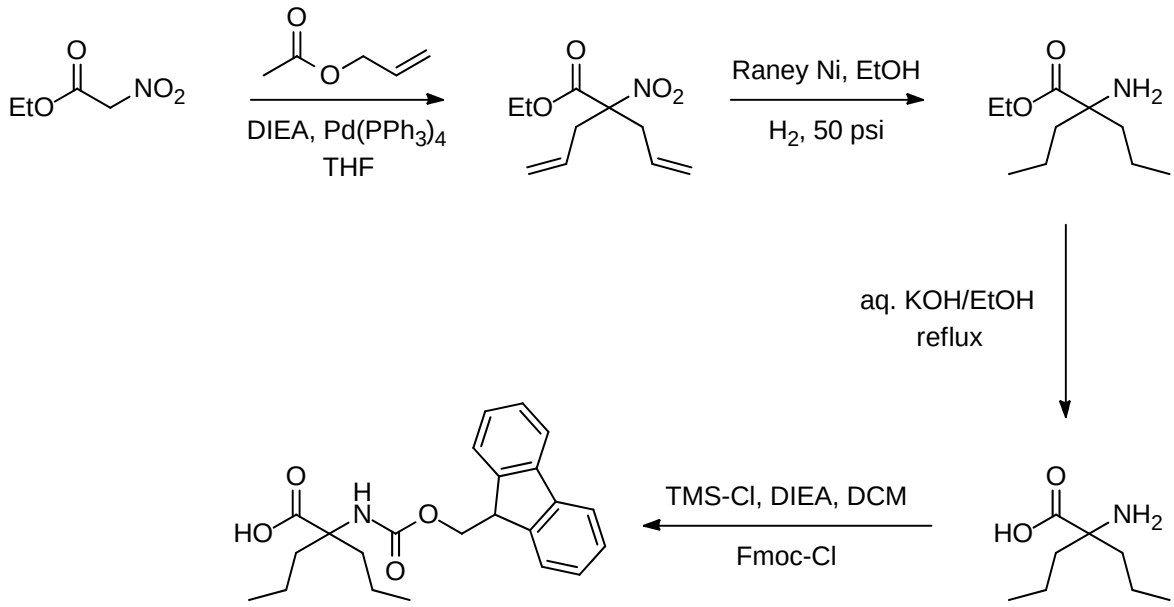

Figure 4.2. Previously reported reaction scheme for the synthesis of Fmoc (or 9-fluorenylmethoxycarbonyl) protected Dpg.[2]

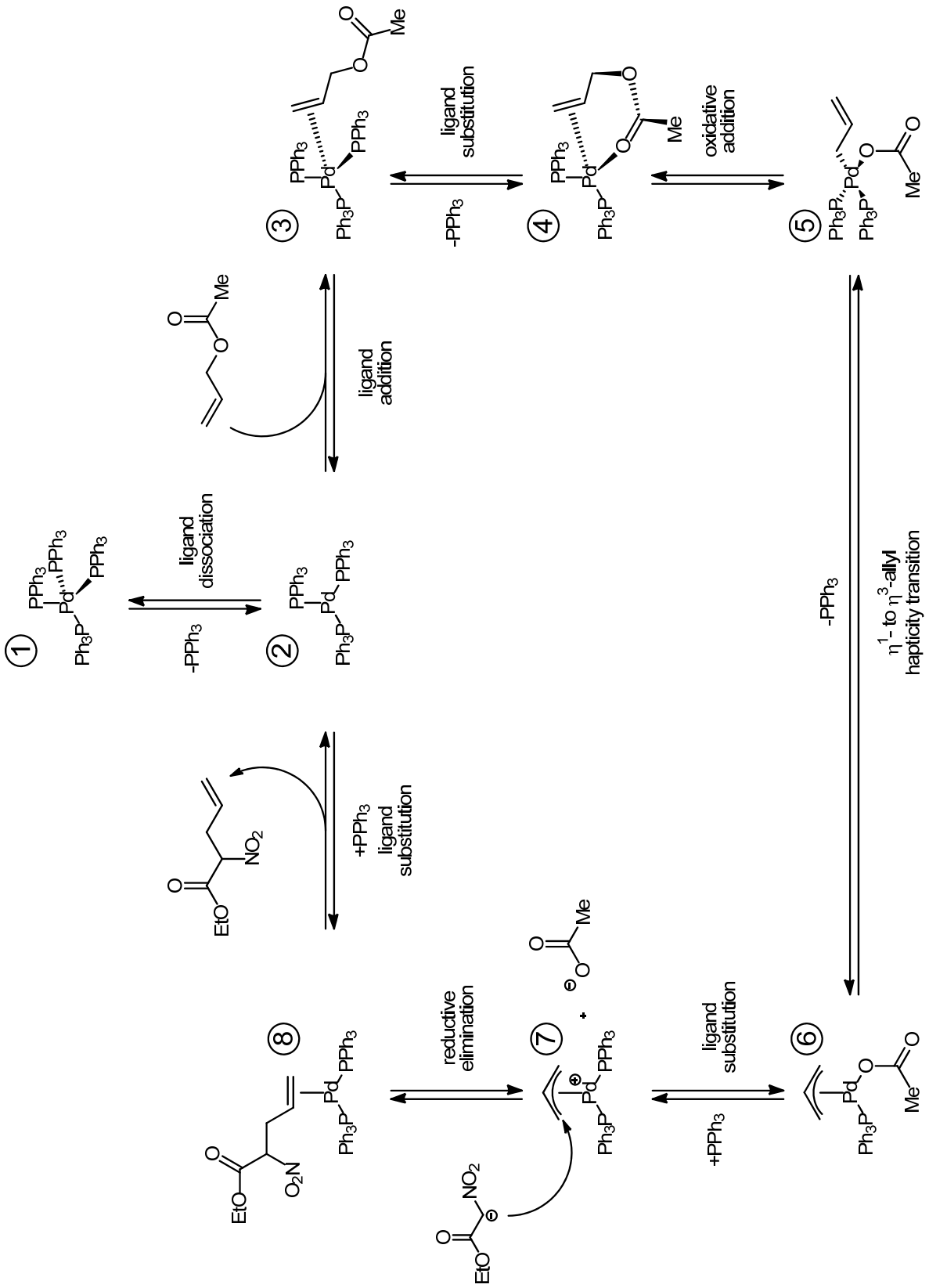

Figure 4.3. Catalytic cycle of palladium-assisted alkylation with allyl acetate.

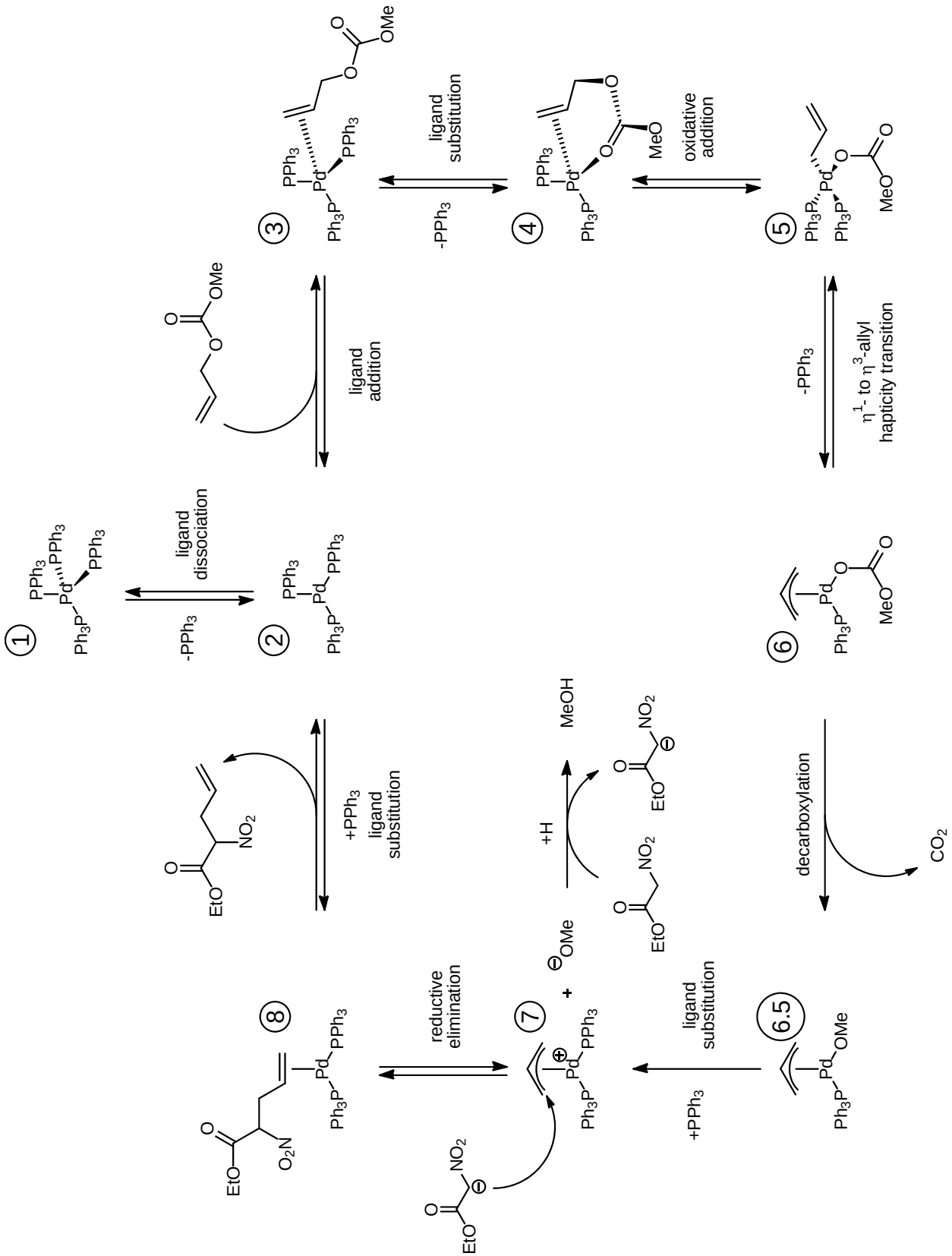

Figure 4.4. Catalytic cycle of palladium-assisted alkylation with allyl methyl carbonate.

form methanol). The protonation step leads to a second advantage. The acetate anion (conjugate acid pKa 4.75)[4] generated when using allyl acetate can not serve as a base to deprotonate the alpha carbon of a nucleophile, such as ethyl nitroacetate (pKa 5.75).[5] Therefore, the reaction would need to be run under basic conditions. In previous experiments with allyl acetate, we have added N,N-diisopropylethylamine (pKa 11.4)[6] as the base. Since methoxide anions (conjugate acid pKa 15.5)[4] are being generated with each catalytic cycle, alkylation with allyl methyl carbonate can be done under neutral conditions.[7] A third advantage is that the oxidative addition step between **4** and **5** is enhanced by the leaving group ability (due to its basicity, conjugate acid pKa 5.61)[8] of the carbonate group. By having a higher propensity to undergo oxidative addition, the reaction can be pushed toward the irreversible steps mentioned earlier.

Evidence of higher reactivities of carbonates over acetates was demonstrated by Tsuji and co-workers by an alkylation competition reaction of methyl 2-methyl-3-oxopentanoate with equal amounts of methallyl methyl carbonate, which is more sterically hindered than allyl methyl carbonate, and allyl acetate. Under neutral conditions at room temperature, the alkylated product favored the addition of an allyl from the carbonate vs. the acetate 84% to 16% using $Pd(PPh_3)_4$ as the catalyst. The carbonate advantage was increased even further by changing the catalyst to $Pd(P(OEt)_3)_4$ (97% to 3%).[3]

My findings demonstrated that the successful dialkylated product could be obtained in high yields (94%) when the amount of catalyst, $Pd(PPh_3)_4$, was reduced by an order of magnitude (0.5 mol %, instead of 5 mol %). Incomplete dialkylation was observed when the catalytic amounts were further reduced (0.05 mol %) – thus indicating the limits of the effectiveness of $Pd(PPh_3)_4$ has been reached. The two products isolated via silica gel column were the dialkylated (72%) and the monoalkylated product (21%).

Before proceeding in the discussion of the subsequent steps, it should be noted that there was an omission in the previously reported experimental for this palladium-assisted dialkylation. A strict interpretation of the synthetic write-up without prior experience working with polystyrene resins would lead to insufficient resin swelling when using ethyl acetate as the solvent. The importance of this swelling requirement, which allows the resin's functional groups to be more accessible for chemical bonding, cannot be understated as crucial to the palladium scavenging ability of polystyrene-triphenylphosphine. A more suitable solvent that maximizes swelling as well as dissolve the crude mixture into solution is dichloromethane. This will greatly enhance the scavenger's ability to remove the remaining palladium catalysts within the allowed parts per billion set by the pharmaceutical industry.[9]

The remaining steps were 1) hydrogenation with Raney nickel / H_2 (50 psi) to reduce the nitro and allyl groups, 2) hydrolysis of the ester by refluxing by refluxing in KOH / ethanol and 3) *N*-terminus protection with 9-fluorenylmethoxycarbonyl chloride after treatment with a temporary *C*-terminus protecting group, chlorotrimethylsilane. No deviation from the published procedures was attempted for these final steps since they have been well established as "tried and true". The hydrogenation step did not have the high 90 plus % yields as anticipated and only converted 79% of the starting compound, ethyl 2,2-bis(allyl)-2-nitroacetate. This may have been caused by a loss in "freshness" via oxidation of the Raney nickel that had a little age – the reagent's label indicated it was opened in 2003. The saponification went according to plan. After isolating the free amino acid, Dpg, with Dowex ion-exchange resin, nice synthetic yield of 94% was obtained. On the other hand, the Fmoc protection step proved to be problematic. Although the desired product is clearly present in the ^{1}H-NMR spectrum, its physical appearance resembles a sticky beige tar-like substance. Efforts to transform it to the typical white fluffy or clear crystalline solid were in vain, even with the assistance of a veteran graduate student.

Therefore, accurate product yields were never determined and the product was ultimately disposed of.

Additional work was done to try to indentify the origin of the unsuccessful Fmoc protection step. After the crude product was redissolved in ethyl acetate and diluted in water (ethyl acetate / water 2:1 v/v), it was noted that the pH was moderately acidic (~3). Typically at this point the pH should be neutral or just slightly basic. Under the suggestion of my advisor, the Fmoc protection step was repeated using a commercially available free amino acid, proline. The acidic pH was the same. Although, I had been temporary reassigned to work on surface plasmon resonance (SPR) inhibitor binding experiments, I still kept researching this matter. My findings ultimately led me to believe that in my inexperience, I was overlooking the production of HCl gas that was forming during the reflux with chlorotrimethylsilane. Periodic purging of the reaction with inert gas during the addition of the temporary acid labile trimethylsilyl protecting group to the C-terminus should remedy this situation and keep the pH from getting too low. Unfortunately, I never got around to testing this hypothesis by myself. However, an undergraduate student, Amber Scroggs, working with me demonstrated that this works well for the Fmoc protection of Dibg and Dbzg.

4.3 Conclusions

The limits of the Pd catalyst was investigated and found to be around 0.5 mol %. At this lower catalytic limit, a very small increase in yield (i.e. 1%) was achieved when using allyl methyl carbonate instead of allyl acetate. It would be interesting to test how well these two new reaction variables would fair at a larger synthetic scale. Also the allylic alkylation should be evaluated under neutral conditions at room temperature as done by Tsuji. The ability to use carbonates in the absence of base and heat was not realized until *ex post facto*.

4.4 Experimental

4.4.1 Ethyl 2,2-bis(allyl)-2-nitroacetate (Using 0.5 mol % Pd Catalyst)

Ethyl nitroacetate (2.0 g, 15.0 mmol), allyl methyl carbonate (3.7 g, 31.5 mmol) and tetrakis(triphenylphosphine)palladium(0) (0.17 g, 0.15 mmol) were added to a round-bottom flask containing anhydrous tetrahydrofuran (20 mL). N,N-Diisopropylethylamine (4.1 g, 31.5 mmol) was then added slowly to the mixture while stirring. The reaction was carried out under argon at 50 °C for approximately 7 hours. After filtering the reaction mixture through a fritted glass funnel containing Celite, the filtrate was concentrated on a rotary evaporator and then redissolved in ethyl acetate (15 mL). Impurities were extracted by washing with 10% potassium carbonate (10 mL) in a separatory funnel. Palladium catalyst was scavenged from the organic layer by allowing it to shake for half an hour with polystyrene-bound triphenylphosphine resin (0.14 g, 2.15 mmol/g). (Note: It was pointed out later that ethyl acetate is not a good PS resin swelling solvent.) After filtering off the resin using a fritted glass funnel, the desired product was isolated using a silica gel column (hexanes / ethyl acetate 90:10) and concentrated to a yellow oil. Yield, 3.0 g (94%); ^{1}H-NMR (250 MHz, $CDCl_3$) δ 5.71 – 5.55 (m, 2H), 5.24 – 5.17 (m, 4H), 4.27 (q, J=7.3 Hz, 2H), 3.02 – 2.85 (m, 4H), 1.29 (t, J=7.1 Hz, 3H); ^{13}C-NMR (250 MHz, $CDCl_3$) δ 166.3, 129.8, 121.8, 95.2, 63.1, 38.4, 14.3; GC/MS (EI) cald for $C_{10}H_{15}NO_4$ $[M + H]^+$ 214.1, found 213.8.

4.4.2 Ethyl 2,2-bis(allyl)-2-nitroacetate (Using 0.05 mol % Pd Catalyst)

This compound was synthesized with tetrakis(triphenylphosphine)palladium(0) (0.017 g, 0.015 mmol) using the same procedure as written in previous section (**4.4.1**). Yield, 2.3 g (72%); ^{1}H-NMR (250 MHz, $CDCl_3$) δ 5.71 – 5.54 (m, 2H), 5.24 – 5.16 (m, 4H), 4.27 (q, J=7.1 Hz, 2H), 3.02 – 2.85 (m, 4H), 1.29 (t, J=7.1 Hz, 3H); ^{13}C-NMR (250 MHz, $CDCl_3$) δ 166.4, 129.8, 121.8, 95.2, 63.2, 38.5, 14.3; GC/MS (EI) calculated for $C_{10}H_{15}NO_4$ $[M + H]^+$ 214.1, found 213.8.

4.4.3 Ethyl 2-amino-2,2-bis(propyl)acetate

Ethyl 2,2-bis(allyl)-2-nitroacetate (2.3 g, 10.8 mmol) and glacial acetic acid (2 mL) were added to a hydrogenation reaction vessel containing anhydrous ethanol (15 mL). 50% (w/w) slurry of Raney Nickel in water (1.0 g) was added carefully. The reaction was carried out under hydrogen (50 psi) for approximately 24 hours. Drops in hydrogen pressure were monitored as hydrogen was consumed and refilled as needed. After filtering the reaction mixture through a fritted glass funnel containing Celite, the filtrate was concentrated on a rotary evaporator and then redissolved in diethyl ether (40 mL). Impurities were extracted by successive washings with saturated sodium carbonate solution (30 mL) and brine (30 mL) in a separatory funnel. Sodium sulfate was used to dry the organic layer and later removed by paper filtration. The filtrate was then concentrated to a yellow oil. Yield, 1.6 g (79%); ^{1}H-NMR (300 MHz, $CDCl_3$) δ 4.16 (q, J=7.1 Hz, 2H), 1.76 – 1.62 (m, 4H), 1.56 – 1.31 (m, 4H), 1.27 (t, J=7.1 Hz, 3H), 0.91 (t, J=7.2 Hz, 6H); ^{13}C-NMR (250 MHz, $CDCl_3$) δ 177.8, 61.4, 61.2, 42.8, 17.6, 14.7, 14.7; GC/MS (EI) calculated for $C_{10}H_{21}NO_2$ $[M + H]^+$ 188.2, found 188.0.

4.4.4 2,2-Dipropylglycine

Ethyl 2-amino-2,2-bis(propyl)acetate (1.6 g, 8.55 mmol) was added to a round-bottom flask containing 3M potassium hydroxide (40 mL) and ethanol (20 mL). The reaction was refluxed under argon for approximately 24 hours. After reducing the volume of the reaction mixture on a rotary evaporator to 20 mL, the pH was lowered (or acidified) to 6.5 using 12N HCl. The crude product was then concentrated again and redissolved in water (10 mL). The desired product was isolated using Dowex 50x8-400 ion-exchange resin. This isolation process began by first washing and activating the resin (500 g) with water (2 L), 2N hydrochloric acid (2 L), water (4 L), 2N ammonium hydroxide (2 L), water (4 L) and methanol (2 L). Then the crude mixture was loaded on the resin and impurities were washed out of the resin with water (4 L)

leaving behind the bound amino acid product. Once all the impurities were removed, the remaining amino acid was eluted from the resin column using 2N ammonium hydroxide (2 L). The ammonium hydroxide filtrates were then heated to remove ammonia gas and concentrated to a white powder. Yield, 3.0 g (94%). ^{1}H-NMR (250 MHz, DMSO-d_6) δ 7.27 (bs, 3H) 1.57 – 1.46 (m, 4H), 1.42 – 1.09 (m, 4H), 0.81 (t, J=7.2 Hz, 6H). Elemental Analysis calculated for $C_8H_{17}NO_2$: C, 60.35; H, 10.76; N, 8.80. Found: C, 59.96; H, 10.53; N, 8.58.

4.4.5 N^{α}-(9-Fluorenylmethoxycarbonyl)-2,2-dipropylglycine

2,2-Dipropylglycine (1.2 g, 7.8 mmol) and chlorotrimethylsilane (1.7 g, 15.9 mmol) were added to a round-bottom flask containing anhydrous dichloromethane (15 mL). This mixture was refluxed under argon at 50 °C for approximately 8 hours while stirring. Then N,N-diisopropylethylamine (2.1 g, 15.9 mmol) and 9-fluorenylmethoxycarbonyl chloride were added slowly to the mixture. The reaction was continued at room temperature for approximately 20 hours. After the reaction mixture was concentrated on a rotary evaporator, redissolved in ethyl acetate (45 mL) and diluted with water (22.5 mL), the pH was lowered (or acidified) to 2.0 using 2N HCl. The organic layer was isolated using a separatory funnel and dried with magnesium sulfate. The drying agent was removed by paper filtration and the filtrate was then concentrated to a yellow solid. Impurities were further removed by triturating in hexanes overnight. Yield, undetermined; ^{1}H-NMR (250 MHz, DMSO-d_6) δ 7.88 (d, J=7.3 Hz, 2H), 7.69 (d, J=7.3 Hz, 2H), 7.40 (t, J=7.3 Hz, 2H), 7.31 (t, J=7.4 Hz, 2H), 6.91 (s, 1H), 4.28 (d, J=5.8 Hz, 2H), 4.19 (t, J=6.3 Hz, 1H), 1.78 – 1.70 (m, 4H), 1.25 (t, J=6.3 Hz, 6H).

4.5 References

1. Etienne, M. A.; Aucoin, J. P.; Fu, Y. W.; McCarley, R. L.; Hammer, R. P., Stoichiometric Inhibition of Amyloid β-Protein Aggregation with Peptides Containing Alternating α,α-Disubstituted Amino Acids. *J. Am. Chem. Soc.* **2006**, 128, 3522-3523.

2. Fu, Y. W.; Etienne, M. A.; Hammer, R. P., Facile Synthesis of α,α-Diisobutylglycine and Anchoring Its Derivatives onto PAL-PEG-PS Resin. *J. Org. Chem.* **2003**, 68, 9854-9857.

3. Tsuji, J.; Shimizu, I.; Minami, I.; Ohashi, Y.; Sugiura, T.; Takahashi, K., Allylic Carbonates - Efficient Allylating Agents of Carbonucleophiles in Palladium Catalyzed-Reactions under Neutral Conditions. *J. Org. Chem.* **1985**, 50, 1523-1529.

4. Bordwell, F. G., Equilibrium Acidities in Dimethyl Sulfoxide Solution. *Accounts Chem. Res.* **1988**, 21, 456-463.

5. Adolph, H. G.; Kamlet, M. J., Fluoronitroaliphatics. I. Effect of α Fluorine on Acidities of Substituted Nitromethanes. *J. Am. Chem. Soc.* **1966**, 88, 4761-4763.

6. Faltin, C.; Fleming, E. M.; Connon, S. J., Acrylamide in the Baylis-Hillman Reaction: Expanded Reaction Scope and the Unexpected Superiority of DABCO over More Basic Tertiary Amine Catalysts. *J. Org. Chem.* **2004**, 69, 6496-6499.

7. Tsuji, J., New General Synthetic Methods Involving π-Allylpalladium Complexes as Intermediates and Neutral Reaction Conditions. *Tetrahedron* **1986**, 42, 4361-4401.

8. Gattow, G.; Behrendt, W., Methyl Hydrogen Carbonate. *Angew. Chem. Int. Edit.* **1972**, 11, 534-535.

9. Garrett, C. E.; Prasad, K., The Art of Meeting Palladium Specifications in Active Pharmaceutical Ingredients Produced by Pd-Catalyzed Reactions. *Adv. Synth. Catal.* **2004**, 346, 889-900.

CHAPTER 5

DESIGN OF SHORT PEPTIDE INHIBITORS

5.1 Introduction

Peptide mimics of the same length as its target can be used to inhibit the formation of fibrils, which has been associated with amyloid diseases.[1] However, the synthetic advantages of using short peptides are several fold. Peptides with less than ~20 residues typically results in higher yields due to the fewer couplings necessary. In addition, aggregation of the inhibitor during short peptide synthesis is not as susceptible as peptide chain grows. Also, it is more probable for short peptides with a molecular weight below 400 to 700 g/mol to pass through the highly selective blood brain barrier.[2-4] The lower molecular weight requirement translates into a limit of peptide sequences between 4 to 6 amino acids residues. Inhibitors of higher molecular weight can overcome this limitation if it is conformationally flexible.[2] But most often, the key to an inhibitor's ability to prevent or reduce peptide aggregation is the incorporation of conformationally restricted residues,[5] which will be discussed in this chapter. Another critical factor in drug delivery is permeability. The rule of thumb is that with each additional hydrogen bonding element (i.e. functional groups such as hydroxyls, carboxylic acids, amines, etc.) in a peptide sequence, the blood brain barrier permeability drops by an order of magnitude.[2-4] Therefore, it is unavoidable to have lower permeability with longer peptide sequences. It is best to keep it short. The next variable to consider is the selection of the sequence.

When searching for the shortest peptide sequence with the most affinity to amyloid beta peptide, Nordstedt and co-workers identified the peptide sequence H-Lys-Leu-Val-Phe-Phe-NH_2 (see **Figure 5.1**) as the highest binding fragment based on the native sequence by comparing results from a combination of radioligand binding and surface plasmon resonance (SPR) experiments.[6] Since this identification, several modifications of this peptide motif have been

suggested and evaluated in order to design inhibitors of peptide aggregation that leads to the formation of amyloid fibrils linked to the neurologically degenerative disorder, Alzheimer's disease.

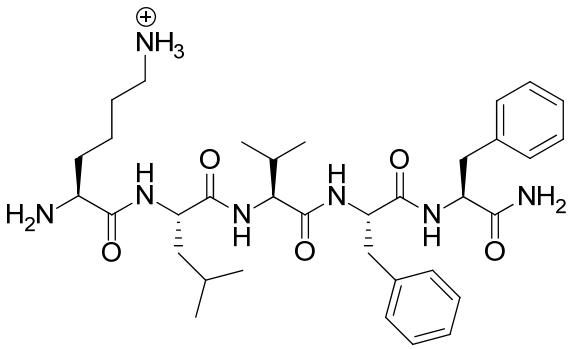

Figure 5.1. Peptide sequence H-Lys-Leu-Val-Phe-Phe-NH_2.

The incorporation of proline, a well known beta-sheet breaker,[7] into this hydrophobic sequence has been used in conjunction with the charged amino acid residues, arginine and aspartate, by Soto et al. (see **Figure 5.2**).[8] Due to proline's sidechain that uniquely reconnects to the residue's amine terminus, it is both conformationally restricted, which decreases the propensity to form beta-sheets, and hydrogen bonding limited.[9] Its ability to inhibit peptide aggregation is so highly regarded that even removable pseudoproline derivatives have been recently used in the synthesis of aggregation prone peptide sequences, such as human islet amyloid polypeptide (IAPP).[10]

The addition of charged residues can improve the inhibitor in three ways. First, it will cause the hydrophobic sequence become more soluble.[11] Second, it can serve as a disruptor, especially in the case of a connecting a tetramer or hexamer of lysines or glutamates to the inhibitor's *C*-terminus, that can potentially impose electrostatic interactions with other charged residues in the target peptide.[12] Finally, it has the ability to prevent inhibitor self-aggregation.[13]

This is a common major problem with short hydrophobic peptide fragments that share the same propensity to form fibrils as the full-length target peptide sequence.

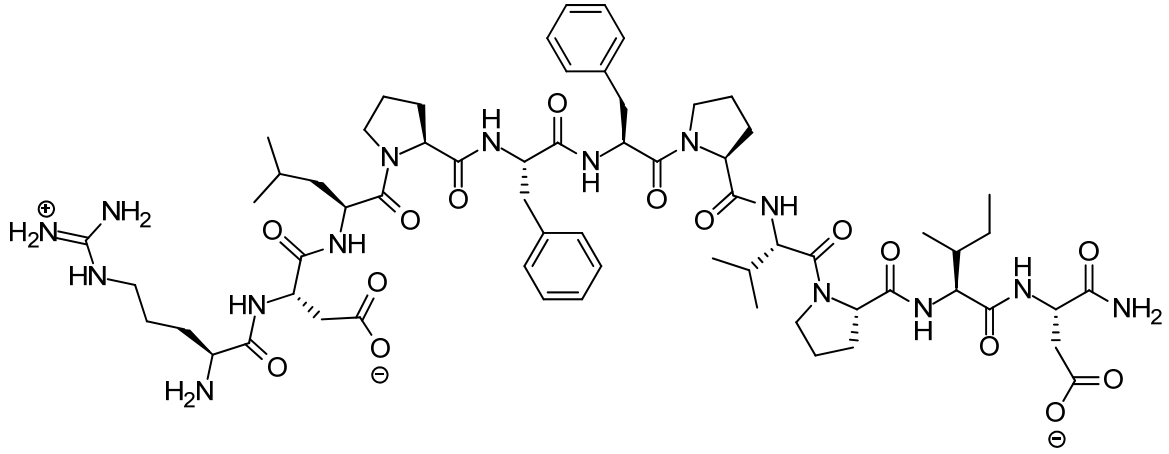

Figure 5.2. Peptide sequence H-Arg-Asp-Leu-Pro-Phe-Phe-Pr-Val-Pro-Ile-Asp-NH_2 (iAβ1).

Peptide solubility can also be increased, surprisingly, by substituting in a few *N*-methylated residues in spite of increases in hydrophobicity and decreases in hydrogen bonding it causes.[14] The decrease in hydrogen bonding created by *N*-methyl groups can provide a "blocking" face to avoid interaction with another monomer of peptide that could potentially lead to amyloidic aggregation.[15] The effectiveness of incorporating *N*-methylated amino acids in order to reduce aggregation and toxicity depends heavily on position within the sequence and works best when placed as every other residue.[16] The capacity for self-recognition of the "binding" face is retained by having all the *N*-methyl groups on the opposite face, or side, of the inhibitor. Interestingly, the reduction in aggregation when using this method is linked more to a decline in hydrogen bonding capacity than to the conformational restrictions it places on the peptide backbone as demonstrated by Gordon and Meredith (see **Figure 5.3**).[17] This was confirmed by replacing the *N*-methyl groups with ester groups in the sequence without a decline in inhibition. *N*-methylated inhibitors have also been used for other amyloid disease-linked

peptides, such as IAPP,[18] and shown to be protease resistant when the natural peptide version was not.[14]

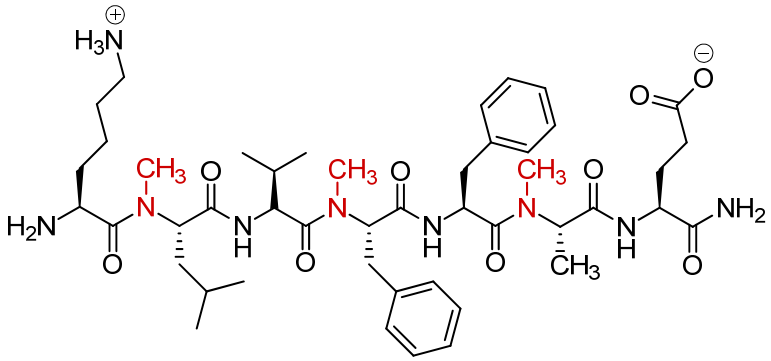

Figure 5.3. Peptide sequence H-Lys-(Me)Leu-Val-(Me)Phe-Phe-(Me)Ala-Glu-NH_2.

Moving closer to an approach similar to our inhibitor designs, the incorporation of disubstituted amino acids in alternating positions of the short peptide sequence has been very effective in reducing the propensity for fibril formation. Gilead and Gazit used the disubstituted analog of alanine, α-aminoisobutyric acid or Aib (see **Figure 5.4**), in the synthesis of three inhibitors of IAPP, which is strikingly similar in sequence to amyloid beta peptide.[19] Aib is a strong beta-sheet breaker and possesses a more restricted allowable conformation than the amino acid proline. Evaluation of the φ, ψ torsion angles for this disubstituted residue explains why it favors alpha-helical formation. This beta-sheet breaker in alternating positions works in similar fashion (i.e. the two-faced approach) as demonstrated with inhibitors containing *N*-methylated residues. Evidence obtained from transmission electron microscopy (TEM), Congo red birefringence and Fourier transformed infrared (FTIR) assays shows the effectiveness in using disubstituted amino acids by an absence of amyloidic fibrils.

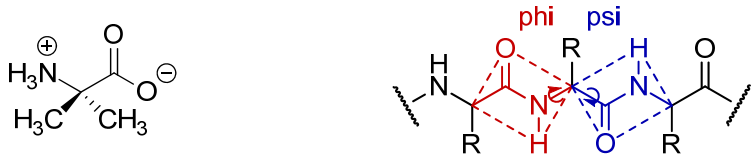

Figure 5.4. Disubstituted amino acid Aib (left) and illustration of the φ, ψ torsion angles (right).

With the incorporation of three disubstituted amino acids, dipropylglycine (Dpg), diisobutylglycine (Dibg) and dibenzylglycine (Dbzg), the Hammer group has developed a potent inhibitor of the harmful fibrillization associated with amyloid beta peptide by promoting the formation of non-fibrillic amorphous aggregates.[20, 21] This inhibitor, called AMY-1 (see **Figure 5.5**), has a "binding" face with the natural amino acid residues and a "blocking" face with the sterically bulky disubstituted amino acid residues.[22] The "two-faced" peptide works so well that inhibition of peptide aggregation can be achieved even with **sub-stoichiometric** amounts of inhibitor (i.e. 50 μM amyloid beta : 5μM AMY-1).[23] In my efforts to build on this success and address three major issues, inhibitor blood brain barrier permeability, cellular toxicity and protease resistance, I have worked on the design of a few new short peptide sequences using standard Fmoc solid phase peptide synthesis techniques.[24]

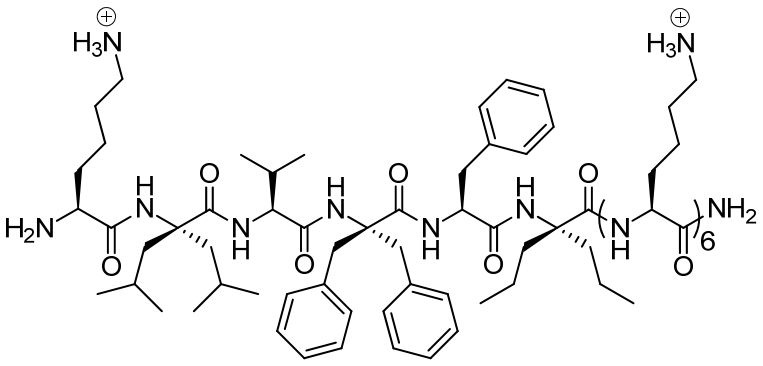

Figure 5.5. Peptide sequence H-Lys-Dibg-Val-Dbzg-Phe-Dpg-$(Lys)_6$-NH_2 (AMY-1).

5.2 Results and Discussion

To address the issue of blood brain barrier permeability and cellular toxicity, my first peptide sequence (H-mPEG-Val-Phe-Phe-Ala-mPEG-NH_2, see **Figure 5.6**) was shorter in length and used polyethylene glycol chains ("miniPEG" or mPEG) for solubility, instead of a hexamer of lysines as used in the inhibitor, AMY-1. Although it is not a requirement, peptides of shorter lengths have a higher probability of passing through the highly selective blood brain barrier.[2-4] Passage through this barrier might also be hampered by an abundance of charged residues, such as lysine. Large cationic polylysine peptides (greater than 900 g/mol), which can be used to increase the uptake of neutral molecules, are believed to specifically bind to the surface of brain microvessels that are saturated with anionic sialic acid residues.[25] To maintain the solubility the chain of lysines provides to the hydrophobic sequence (Val-Phe-Phe-Ala), PEG chains with amine and carboxylic termini, which are sold under the trademark name of "mini-PEG", were utilized. Wantanabe et al. found a series of these PEG chains could serve as a better disruptor of fibril formation and preventer of cytotoxicity than lysine repeats because of the conformational flexibility they provide.[26] The added flexibility could also allow for higher peptide molecular weight as discussed at the opening of this chapter. This peptide was synthesized without the inclusion of disubstituted amino acids for two reasons. First, it was important to evaluate its capacity to bind to amyloid beta peptide with a shorter self-recognition motif. A significant reduction in binding was reported for the tetrapeptide, H-Leu-Val-Phe-Phe-NH_2, by Nordstedt and co-workers in comparison to the pentapeptide, H-Lys-Leu-Val-Phe-Phe-NH_2, as determined by their surface plasmon resonance (SPR) experiments.[6] Interestingly, the peptide sequence, H-Val-Phe-Phe-Ala-NH_2, was not evaluated in their study, hence it would be prudent to evaluate the effect of a decrease in length without adding the additional variable of disubstituted amino acids. Coupling each residue by hand, the synthetic yields (18%) and peptide purity were both

quite good (see **Figure 5.7** and **5.8**). A sample of this peptide, along with a similar peptide sequence (H-mPEG-Leu-Val-Phe-Phe-mPEG-NH_2, see **Figure 5.9**) that was synthesized by a former undergraduate student (Sarah Curtis) working with me, was sent off to one of our collaborators at Winthrop University for aggregation studies.

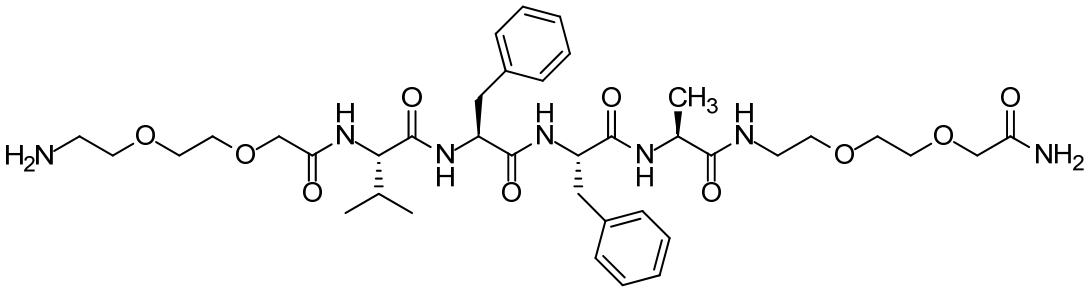

Figure 5.6. Peptide sequence H-mPEG-Val-Phe-Phe-Ala-mPEG-NH_2.

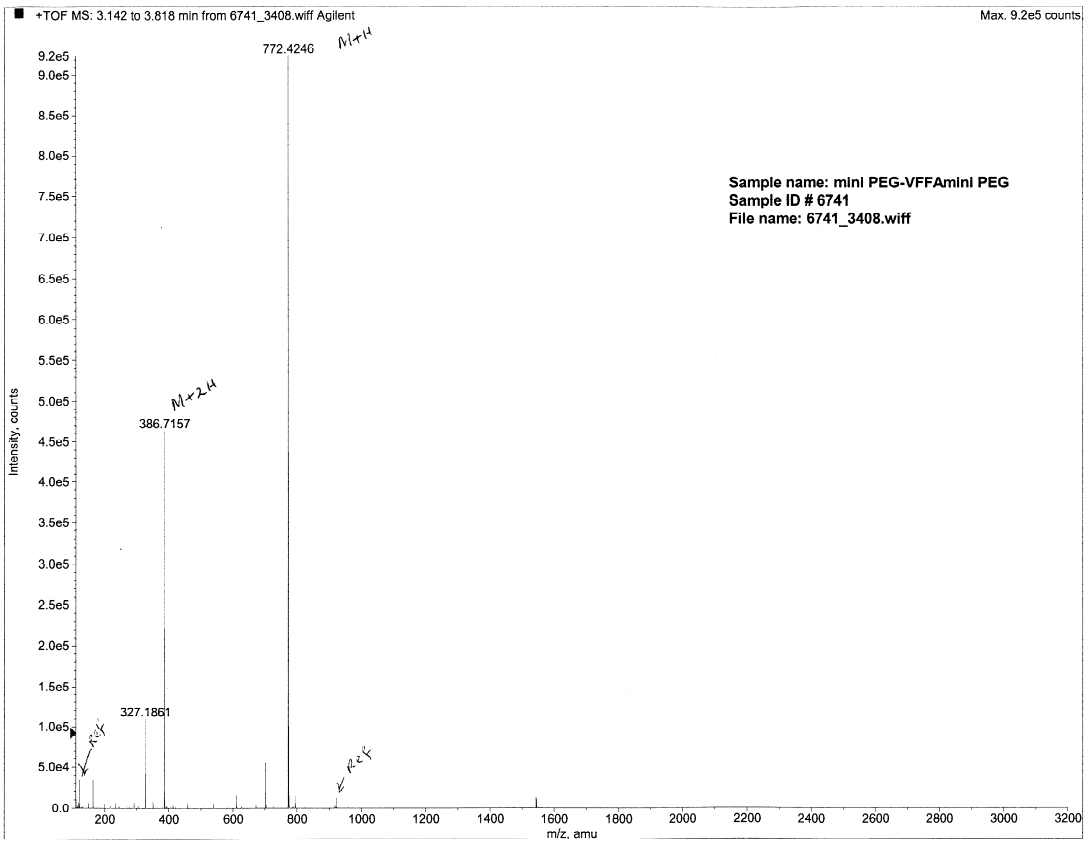

Figure 5.7. MS of H-mPEG-Val-Phe-Phe-Ala-mPEG-NH_2 showing the $[M + H]^+$ (772.4246) and $[M + 2H]^+$ (386.7157).

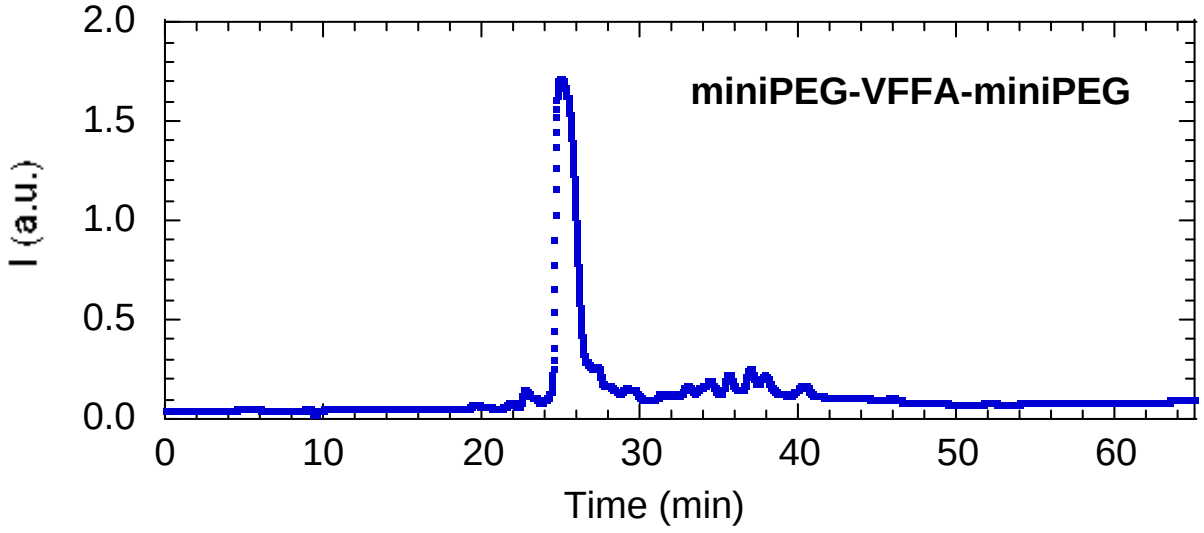

Figure 5.8. HPLC (Preparative) of H-mPEG-Val-Phe-Phe-Ala-mPEG-NH_2.

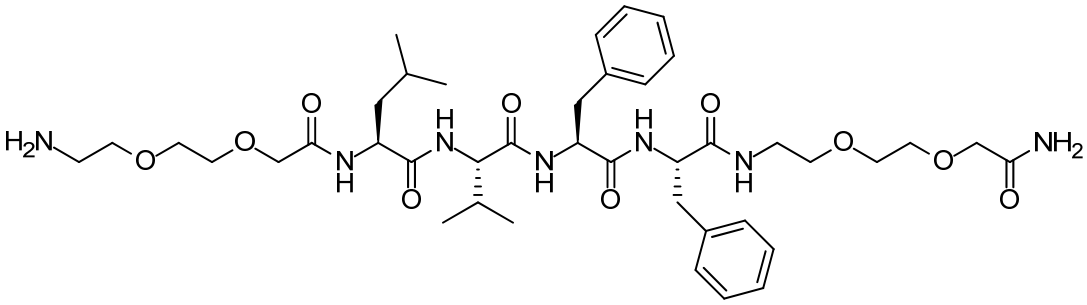

Figure 5.9. Peptide sequence H-mPEG-Leu-Val-Phe-Phe-mPEG-NH_2 (synthesized by former undergraduate student, Sarah Curtis).

D-Amino acids have a proven track record to be protease resistant and have been used in the design of inhibitors of amyloid diseases.[27-30] The peptide sequence of amyloid beta peptide contains peptide bonds that are subject to cleavage by proteases. Examples of this type of proteolysis are cleavage on the carboxyl side of aromatic amino acids with chymotrypsin and after the positively charged amino acids, lysine and arginine, with trypsin. It has been proposed that in its effort to become more protease resistant, that the peptide alters its conformation which inevitably leads to the aggregation process.[31] There is a temptation to go *au un-naturel* with the

use of an inhibitor with D-amino acids. This added protease resistance does come at a price. It has been reported that D-amino acids sequences have a significant decrease in brain influx via the blood brain barrier and might not be delivered to its target in the necessary concentration levels. Poduslo and co-workers reported the average permeability based on the "permeability coefficient-surface area product" (PS) of the L-enantiomer of amyloid beta (1-40) across the blood brain barrier was almost 25 times higher than the D-version when examining various regions of the brain.[32] However, this set back in permeability can be reversed by coupling of a putrescine[29] or cholyl[30] functional group on the *N*-terminus. The PS of a D-version of the peptide inhibitor iAβ11 (H-Arg-Asp-Leu-Pro-Phe-Phe-Pro-Val-Pro-Ile-Asp-NH_2) was increased by four fold with the addition of putrescine. Interestingly, the bioactivity of the inhibitor's ability to reduce fibril formation and disassemble preformed fibrils *in vitro* was significantly enhanced when used in excess (0.5 μg/μL amyloid beta : 1 μg/μL inhibitor and 0.5 mg/ml amyloid beta : 2 μg/μL inhibitor, respectively).[29] Peptides with D-amino acids and cholyl groups, on the other hand, can be effect inhibitor in **submolar equivalents** while having an order of magnitude higher "brain uptake index" (BUI), which is another type of permeability measurement, than sucrose and cholic acid. This union of an organic group and the D-version of the peptide sequence (H-Leu-Val-Phe-Phe-Ala-NH_2) was used by Findeis et al. (see **Figure 5.10**) in 1.6 μM concentration for an inhibition assay with 50 μM of amyloid beta (1-40).[30]

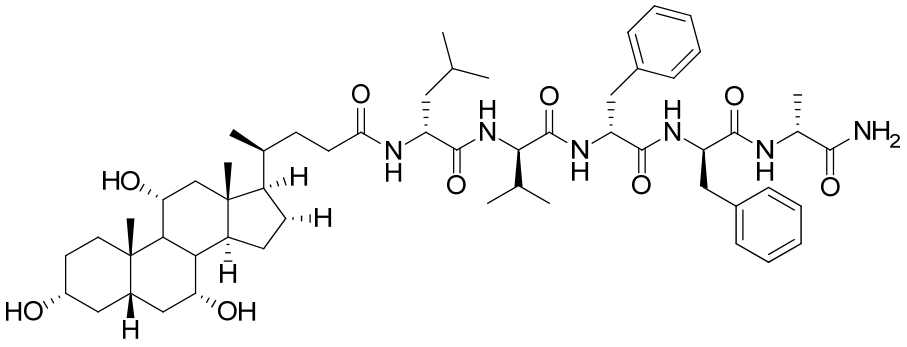

Figure 5.10. Peptide sequence Cholyl-Leu-Val-Phe-Phe-Ala-NH_2.

In order to see the affects of D-amino acids for designs closer to the ones we have experimented with, two more peptides were synthesized. The first peptide was a D-version similar to the previous one discussed earlier in this chapter. An additional modification to this sequence is the replacement of two amino acids, the second phenylalanine from *C*-terminus and alanine, with the disubstituted amino acid, Aib (see **Figure 5.11**). Aib is a conservative disubstituted amino acid incorporation in terms of size, or bulk. This could help us understand the necessity of disubstituting with larger and/or aromatic sidechains as done for the inhibitor, AMY-1. Based on the crude MS results (see **Figure 5.12**), this peptide was successfully synthesized (calculated $[M + H]^+$ 724.4240, found 724.4253). However, there was difficulty in the attempts to purify the crude product by HPLC due to the solubility of the peptide. Based on the work of a former group member, we believe the solubility problems arise from the incorporation of Aib residues in the sequence. We may be able to overcome this problem by adding longer PEG chains to this sequence.

A second sequence attempted was a D-analog of AMY-1 with all the disubstituted amino acids replaced with Aib (see **Figure 5.13**). This would give us another indication of the possible improvements that might occur by going to the shorter peptide sequence with PEG chains instead of lysines. The synthesis of this peptide appeared to proceed without any complications. But once again, the same solubility issue using Aib residues occurs. Based on the crude MS results, which shows several mass peaks (see **Figure 5.14**), this peptide was not successfully synthesized (calculated $[M + H]^+$ 1423.0446, found 1415.9964). Efforts were made to determine the problems that may have occurred during the synthesis by match up calculated mass values to the actual mass values (see **Table 5.1**). The differences between the highest actual masses indicate successful couplings were still occurring toward the end of the peptide sequence (i.e. 1228.8263 - 1129.7757 = 99.0506, addition of Val; 1313.8816 - 1228.8263 = 85.0553, addition of Aib).

However, these mass values are off by ~ 20 amu. This would suggest that something occurred in the middle of the sequence, such as a residue deletion or coupling of wrong amino acid by mistake.

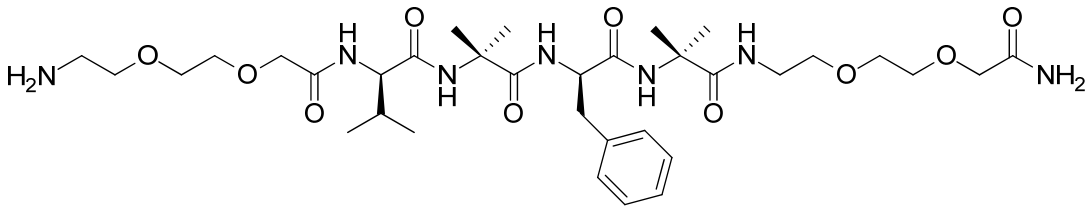

Figure 5.11. Peptide sequence H-mPEG-(DVal)-Aib-(DPhe)-Aib-mPEG-NH_2.

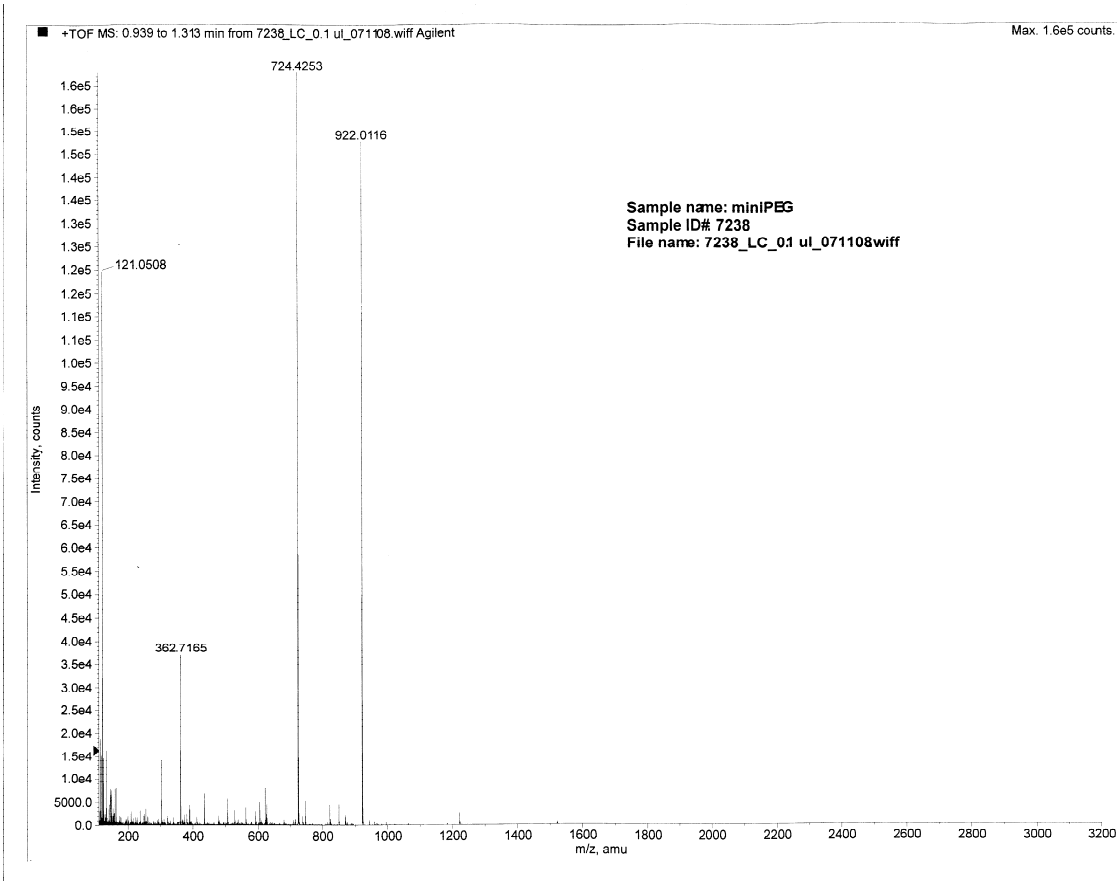

Figure 5.12. MS of crude mixture for H-mPEG-(DVal)-Aib-(DPhe)-Aib-mPEG-NH_2 showing the $[M + H]^+$ (724.4253) and $[M + 2H]^+$ (362.7165). Internal standards (or reference compounds) are indicated by the peaks at 121.0508 and 922.0116.

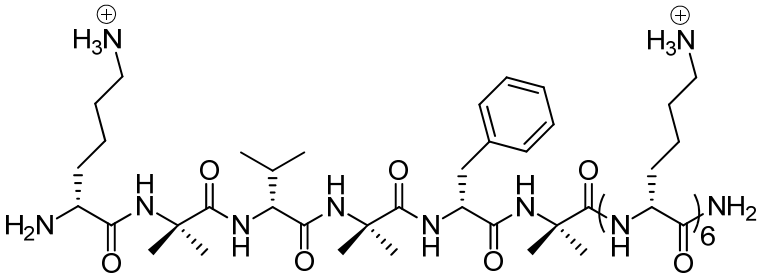

Figure 5.13. Peptide sequence H-(DLys)-Aib-(DVal)-Aib-(DPhe)-Aib-(DLys)$_6$-NH_2.

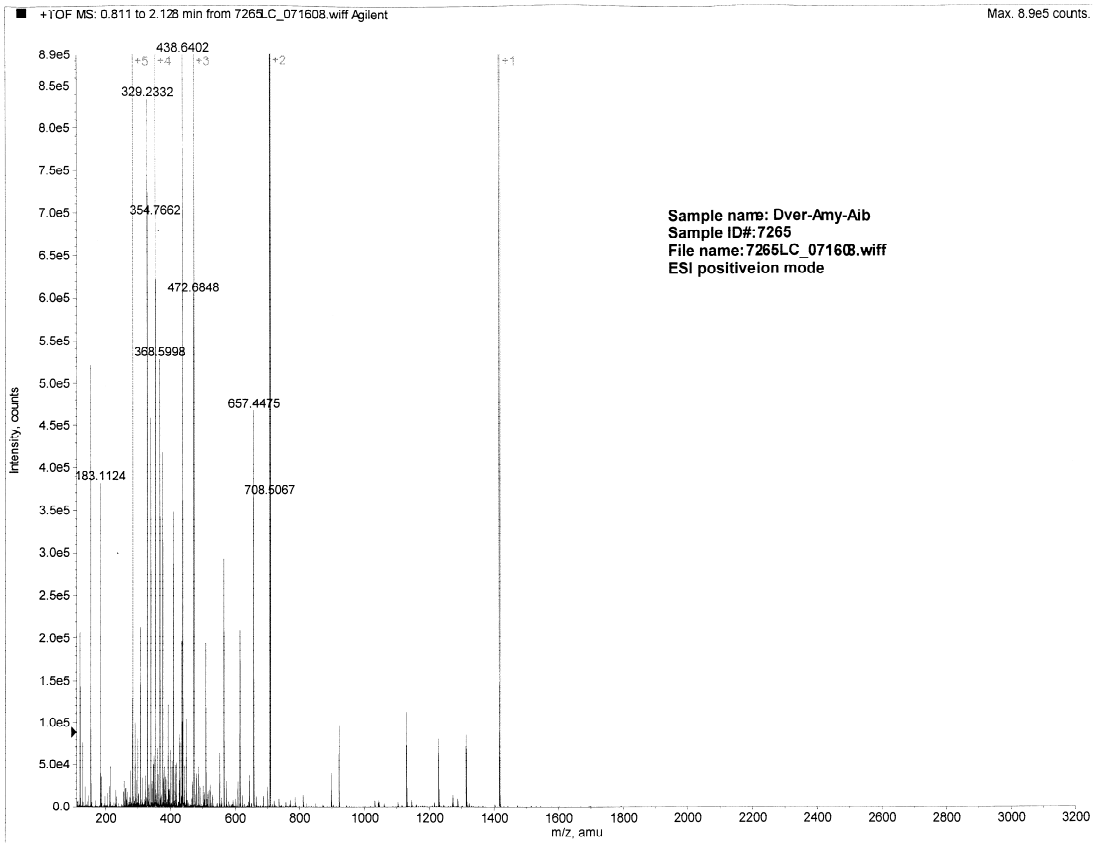

Figure 5.14. MS of crude mixture for H-(DLys)-Aib-(DVal)-Aib-(DPhe)-Aib-(DLys)$_6$-NH_2 indicates that the peptide synthesis was not successful due to incomplete couplings (calculated $[M + H]^+$ 1423.0446, found 1415.9964). Internal standards (or reference compounds) are located at 121.0510 and 922.0105.

Table 5.1. Comparison of the calculated mass with the nearest found mass in the MS (**Figure 5.14**) for all the possible peptide fragments that could result during the synthesis of the peptide sequence H-(DLys)-Aib-(DVal)-Aib-(DPhe)-Aib-$(DLys)_6$-NH_2. The mass associated with the final amino acid coupling for each fragment is also indicated.

Peptide Sequence	Calculated Mass (amu)	Nearest Found Mass (amu)	Last Coupled Amino Acid
H-(DLys)-NH_2	147.1361	153.1429	Addition of DLys (129.10 amu)
H-$(DLys)_2$-NH_2	276.2383	283.1987	Addition of DLys (129.10 amu)
H-$(DLys)_3$-NH_2	405.3405	410.2854	Addition of DLys (129.10 amu)
H-$(DLys)_4$-NH_2	534.4428	565.3948	Addition of DLys (129.10 amu)
H-$(DLys)_5$-NH_2	663.5450	708.5068	Addition of DLys (129.10 amu)
H-$(DLys)_6$-NH_2	792.6473	-	Addition of DLys (129.10 amu)
H-Aib-$(DLys)_6$-NH_2	877.7000	-	Addition of Aib (85.06 amu)
H-(DPhe)-Aib-$(DLys)_6$-NH_2	1024.7684	-	Addition of DPhe (147.07 amu)
H-Aib-(DPhe)-Aib-$(DLys)_6$-NH_2	1109.8212	1129.7757	Addition of Aib (85.06 amu)
H-(DVal)-Aib-(DPhe)-Aib-$(DLys)_6$-NH_2	1208.8896	1228.8263	Addition of DVal (99.07 amu)
H-Aib-(DVal)-Aib-(DPhe)-Aib-$(DLys)_6$-NH_2	1293.9424	1313.8816	Addition of Aib (85.06 amu)
H-(DLys)-Aib-(DVal)-Aib-(DPhe)-Aib-$(DLys)_6$-NH_2	1423.0446	1415.9964	Addition of DLys (129.10 amu)

5.3 Conclusions

Three new peptide inhibitors have been synthesized, but only one has been successfully purified. It is speculated that the Aib residues are the cause of the purification problems by their influence on the solubility of the peptide. Precipitation of peptide in cold ether (see experimental for details) did not occur with the peptides containing Aib as it did with the peptide containing all natural L-amino acids. But it would be exciting to see if these new modifications can lead to a better understanding of the design elements needed for highly effective inhibitors of peptide aggregation.

5.4 Experimental

5.4.1 H-mPEG-Val-Phe-Phe-Ala-mPEG-NH_2 (0.2 mmol Scale Synthesis)

Each amino acids or residue (Fmoc-mini-PEG, Fmoc-Val-OH, Fmoc-Phe-OH and Fmoc-Ala-OH) was weighed out in the desired amounts (4.4 equivalents) and mixed with the coupling reagents, TBTU (0.26 g, 4.0 equivalents) and HOBt (0.12 g, 4.4 equivalents). Then H-Rink-Amide ChemMatrix resin (0.39 g, 0.52 mmol/g) was weighed out into a 10 mL polypropylene disposable syringe containing a polypropylene fritted disc (20 – 40 μm pore size, 0.125 in tk.) flush to the bottom of the syringe barrel (i.e. the injection outlet). The resin was allowed to swell for 30 minutes in dichloromethane (~ 3 times the resin volume) with periodic stirring with the polyethylene plunger from a 1 mL disposable syringe. The solvent was removed by vacuum aspiration and the resin was washed several times with dimethylformamide. While the resin is still wet, the amino acid / coupling reagent mixture are dissolved to 0.2 M concentration in dimethylformamide (4.4 mL), combined with N,N-diisopropylethylamine (0.23 g, 8.8 equivalents) and immediately transferred to the syringe containing the resin. The coupling process was allowed at least one hour with a combination of gentle shaking and stirring of the reaction mixture. The completeness of the amine coupling was accessed by visual inspection

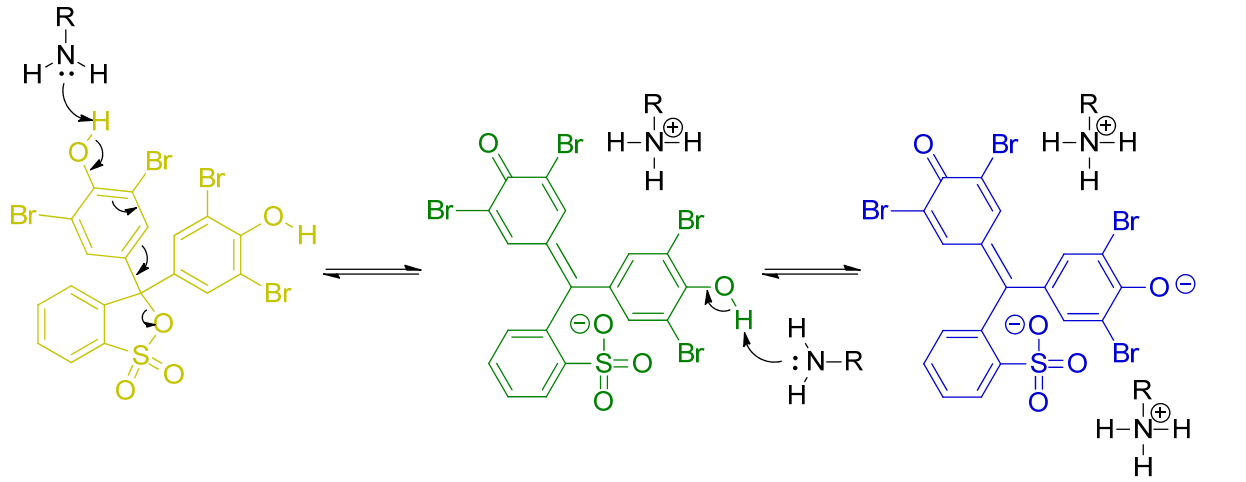

293 nm
UV

410 nm
UV

580 nm
UV

Resin with Fmoc
Protected Amines
Solvent - DCM

Resin with Free Amines
Solvent - DCM

Figure 5.15. Monitoring the completion of coupling (left picture with yellow resin beads) and deprotection (right picture with blue resin beads) with the aid of bromophenol blue.[33]

(bromophenol blue test, see **Figure 5.15**). Between couplings, the "Fmoc" (or 9-fluorenylmethyloxycarbonyl) protecting groups were removed from the N terminus by a deprotection cocktail (1,8-diazabicyclo[5.4.0]undec-7-ene / piperidene / dimethylformamide 2:5:93). The bromophenol blue test was also used after deprotection to make certain all the terminal amines had been exposed. This coupling / deprotection process (with generous dimethylformamide washings in between the steps) was continued until the peptide sequence

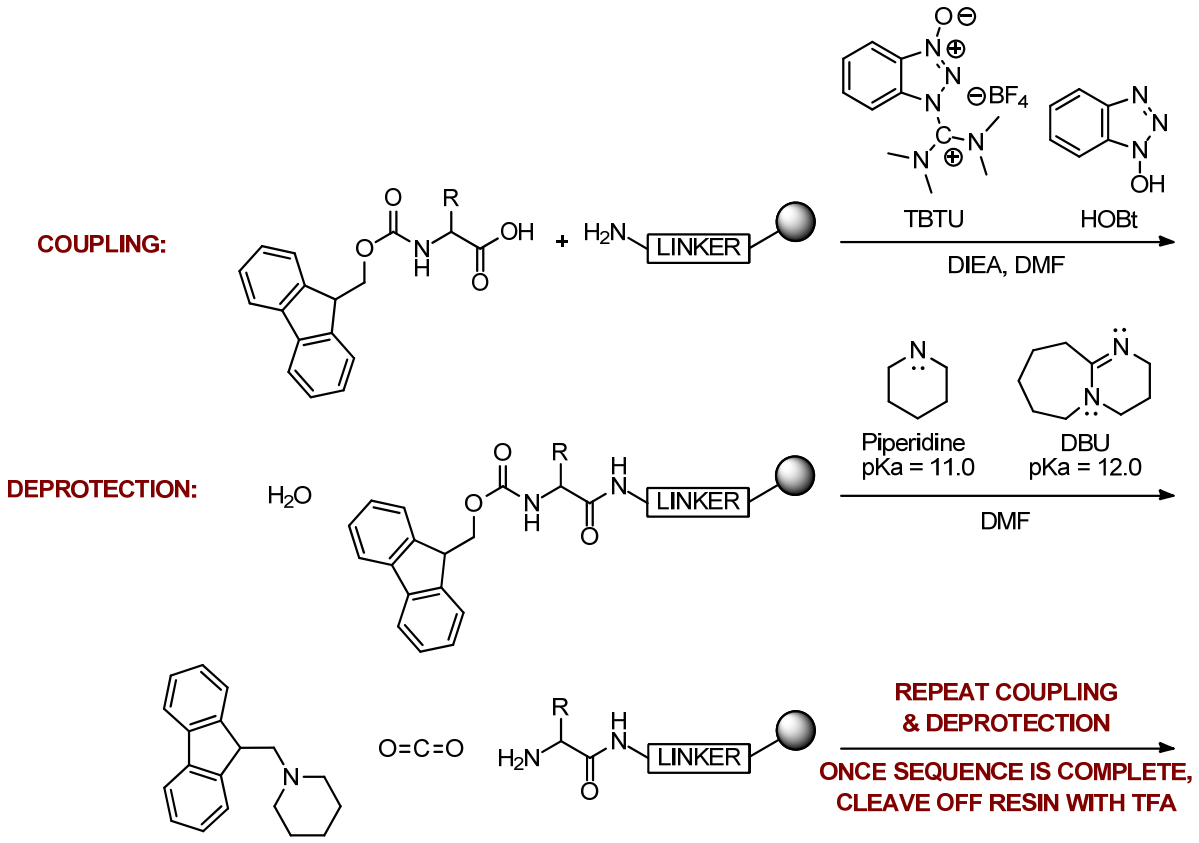

Figure 5.16. Fmoc solid phase peptide synthesis.[24]

was complete (see **Figure 5.16**). After the final "Fmoc" deprotection, the peptide was released from the resin by reacting it for 3 hours in a cleavage mixture (trifluoroacetic acid / triisopropylsilane / phenol / water 88:2:5:5). The peptide solution was removed from the syringe by vacuum aspiration and the resin is washed with neat trifluoroacetic acid twice. The filtrate was concentrated by evaporation under a stream of nitrogen to a volume of 1 mL. Then the peptide was precipitated in cold ether (20 mL) and immediately centrifuged for 10 minutes at 4000 rpm. After carefully decanting out the ether, a gummy peptide residual remained. It proven that the peptide got purer by repeating the process of dissolving in trifluoroacetic acid, precipitating in cold ether and centrifuging. After checking its purity by MS, the desired peptide was isolated by HPLC (solvent gradient of 10:90 to 70:30 acetonitrile/water at a percent change

of 1% per minute). The collected fractions were lyophilized until completely dry. Yield, 27.9 mg (18%); MS (ESI) calculated for $C_{38}H_{57}N_7O_{10}$ $[M + H]^+$ 772.4240, found 772.4246.

5.4.2 H-mPEG-(ᴅVal)-Aib-(ᴅPhe)-Aib-mPEG-NH_2 (0.2 mmol Scale Synthesis)

This peptide was prepared in similar fashion as previously described in section **5.4.1** using ᴅ-amino acids (Fmoc-ᴅVal-OH and Fmoc-ᴅPhe-OH), a disubstituted amino acid (Fmoc-Aib-OH) and PEG chains (Fmoc-mini-PEG). Each residue was coupled once and appeared to be successfully attached (based on bromophenol blue test). There was difficulty getting the crude peptide to the precipitate out in cold ether and isolating the desired product on the HPLC. Therefore, the peptide was concentrated and lyophilized twice in acetonitrile and water to produce white solid. Crude yield, 0.35 g (theoretical yield, 0.15 g); crude MS calculated for $C_{34}H_{57}N_7O_{10}$ $[M + H]^+$ 724.4240, found 724.4253.

5.4.3 H-(ᴅLys)-Aib-(ᴅVal)-Aib-(ᴅPhe)-Aib-$(ᴅLys)_6$-NH_2 (0.2 mmol Scale Synthesis)

This peptide was prepared in similar fashion as previously described in section **5.4.1** using ᴅ-amino acids (Fmoc-ᴅLys(Boc)-OH, Fmoc-ᴅVal-OH and Fmoc-ᴅPhe-OH) and a disubstituted amino acid (Fmoc-Aib-OH). Each residue was coupled once and appeared to be successfully attached (based on bromophenol blue test). There was difficulty getting the crude peptide to the precipitate out in cold ether. Therefore, the peptide was concentrated and lyophilized twice in acetonitrile and water to produce solid particles in an oily film. Crude yield, 0.33 g (theoretical yield, 0.28 g); crude MS does not show signs of the calculated $C_{68}H_{133}N_{20}O_{12}^{7+}$ $[M + H]^+$ 1423.0446, found 1415.9964.

5.5 References

1. Yan, L. M.; Tatarek-Nossol, M.; Velkova, A.; Kazantzis, A.; Kapurniotu, A., Design of a Mimic of Nonamyloidogenic and Bioactive Human Islet Amyloid Polypeptide (IAPP) as Nanomolar Affinity Inhibitor of IAPP Cytotoxic Fibrillogenesis. *Proc. Natl. Acad. Sci. U. S. A.* **2006**, 103, 2046-2051.

2. Navia, M. A.; Chaturvedi, P. R., Design Principles for Orally Bioavailable Drugs. *Drug Discov. Today* **1996**, 1, 179-189.

3. Pardridge, W. M., Transport of Small Molecules through the Blood-Brain-Barrier - Biology and Methodology. *Adv. Drug Deliv. Rev.* **1995**, 15, 5-36.

4. Lipinski, C. A.; Lombardo, F.; Dominy, B. W.; Feeney, P. J., Experimental and computational approaches to estimate solubility and permeability in drug discovery and development settings. *Adv. Drug Deliv. Rev.* **2001**, 46, 3-26.

5. Stains, C. I.; Mondal, K.; Ghosh, I., Molecules that Target beta-Amyloid. *ChemMedChem* **2007**, 2, 1674-1692.

6. Tjernberg, L. O.; Naslund, J.; Lindqvist, F.; Johansson, J.; Karlstrom, A. R.; Thyberg, J.; Terenius, L.; Nordstedt, C., Arrest of β-Amyloid Fibril Formation by a Pentapeptide Ligand. *J. Biol. Chem.* **1996**, 271, 8545-8548.

7. Chou, P. Y.; Fasman, G. D., Prediction of Protein Conformation. *Biochemistry* **1974**, 13, 222-245.

8. Soto, C.; Kindy, M. S.; Baumann, M.; Frangione, B., Inhibition of Alzheimer's Amyloidosis by Peptides That Prevent β-Sheet Conformation. *Biochem. Biophys. Res. Commun.* **1996**, 226, 672-680.

9. Soto, C.; Sigurdsson, E. M.; Morelli, L.; Kumar, R. A.; Castano, E. M.; Frangione, B., β-Sheet Breaker Peptides Inhibit Fibrillogenesis in a Rat Brain Model of Amyloidosis: Implications for Alzheimer's Therapy. *Nat. Med.* **1998**, 4, 822-826.

10. Abedini, A.; Raleigh, D. P., Incorporation of Pseudoproline Derivatives Allows the Facile Synthesis of Human IAPP, a Highly Amyloidogenic and Aggregation-prone Polypeptide. *Org. Lett.* **2005**, 7, 693-696.

11. Pallitto, M. M.; Ghanta, J.; Heinzelman, P.; Kiessling, L. L.; Murphy, R. M., Recognition Sequence Design for Peptidyl Modulators of β-Amyloid Aggregation and Toxicity. *Biochemistry* **1999**, 38, 3570-3578.

12. Cairo, C. W.; Strzelec, A.; Murphy, R. M.; Kiessling, L. L., Affinity-Based Inhibition of β-Amyloid Toxicity. *Biochemistry* **2002**, 41, 8620-8629.

13. Lowe, T. L.; Strzelec, A.; Kiessling, L. L.; Murphy, R. M., Structure-Function Relationships for Inhibitors of β-Amyloid Toxicity Containing the Recognition Sequence KLVFF. *Biochemistry* **2001**, 40, 7882-7889.

14. Gordon, D. J.; Sciarretta, K. L.; Meredith, S. C., Inhibition of β-Amyloid(40) Fibrillogenesis and Disassembly of β-Amyloid(40) Fibrils by Short β-Amyloid Congeners Containing N-Methyl Amino Acids at Alternate Residues. *Biochemistry* **2001**, 40, 8237-8245.

15. Kokkoni, N.; Stott, K.; Amijee, H.; Mason, J. M.; Doig, A. J., N-Methylated Peptide Inhibitors of β-Amyloid Aggregation and Toxicity. Optimization of the Inhibitor Structure. *Biochemistry* **2006**, 45, 9906-9918.

16. Hughes, E.; Burke, R. M.; Doig, A. J., Inhibition of Toxicity in the β-Amyloid Peptide Fragment β-(25-35) Using N-Methylated Derivatives: A General Strategy to Prevent Amyloid Formation. *J. Biol. Chem.* **2000**, 275, 25109-25115.

17. Gordon, D. J.; Meredith, S. C., Probing the Role of Backbone Hydrogen Bonding in β-Amyloid Fibrils with Inhibitor Peptides Containing Ester Bonds at Alternate Positions. *Biochemistry* **2003**, 42, 475-485.

18. Yan, L. M.; Velkova, A.; Tatarek-Nossol, M.; Andreetto, E.; Kapurniotu, A., IAPP Mimic Blocks Aβ Cytotoxic Self-Assembly: Cross-Suppression of Amyloid Toxicity of Aβ and IAPP Suggests a Molecular Link Between Alzheimer's Disease and Type II Diabetes. *Angew. Chem. Int. Ed.* **2007**, 46, 1246-1252.

19. Gilead, S.; Gazit, E., Inhibition of Amyloid Fibril Formation by Peptide Analogues Modified with α-Aminoisobutyric Acid. *Angew. Chem. Int. Edit.* **2004**, 43, 4041-4044.

20. Fu, Y. W.; Etienne, M. A.; Hammer, R. P., Facile Synthesis of α,α-Diisobutylglycine and Anchoring Its Derivatives onto PAL-PEG-PS Resin. *J. Org. Chem.* **2003**, 68, 9854-9857.

21. Fu, Y. W.; Hammarstrom, L. G. J.; Miller, T. J.; Fronczek, F. R.; McLaughlin, M. L.; Hammer, R. P., Sterically Hindered $C^{\alpha,\alpha}$-Disubstituted α-Amino Acids: Synthesis from α-Nitroacetate and Incorporation into Peptides. *J. Org. Chem.* **2001**, 66, 7118-7124.

22. Fu, Y. W.; Hammer, R. P., Efficient Acylation of the N-Terminus of Highly Hindered $C^{\alpha,\alpha}$-Disubstituted Amino Acids via Amino Acid Symmetrical Anhydrides. *Org. Lett.* **2002**, 4, 237-240.

23. Etienne, M. A.; Aucoin, J. P.; Fu, Y. W.; McCarley, R. L.; Hammer, R. P., Stoichiometric Inhibition of Amyloid β-Protein Aggregation with Peptides Containing Alternating α,α-Disubstituted Amino Acids. *J. Am. Chem. Soc.* **2006**, 128, 3522-3523.

24. Chan, W. C.; White, P. D., Basic Procedures. In *Fmoc Solid Phase Peptide Synthesis - A Practical Approach*, Chan, W. C.; White, P. D., Eds. Oxford University Press Inc.: New York, 2000; pp 41-76.

25. Fiori, A.; Ceci, F.; Savi, M. R.; Strom, R.; Cardelli, P., Effect of the Cationic Polypeptide Polylysine on Neutral Amino Acid Transport in Isolated Brain Microvessels. *Amino Acids* **1992**, 3, 253-260.

26. Watanabe, K.; Nakamura, K.; Akikusa, S.; Okada, T.; Kodaka, M.; Konakahara, T.; Okuno, H., Inhibitors of Fibril Formation and Cytotoxicity of β-Amyloid Peptide Composed of KLVFF Recognition Element and Flexible Hydrophilic Disrupting Element. *Biochem. Biophys. Res. Commun.* **2002**, 290, 121-124.

27. Cribbs, D. H.; Pike, C. J.; Weinstein, S. L.; Velazquez, P.; Cotman, C. W., All-D-Enantiomers of β-Amyloid Exhibit Similar Biological Properties to All-L-β-Amyloids. *J. Biol. Chem.* **1997**, 272, 7431-7436.

28. Tjernberg, L. O.; Lilliehook, C.; Callaway, D. J. E.; Naslund, J.; Hahne, S.; Thyberg, J.; Terenius, L.; Nordstedt, C., Controlling Amyloid β-Peptide Fibril Formation with Protease-stable Ligands. *J. Biol. Chem.* **1997**, 272, 17894-17894.

29. Poduslo, J. F.; Curran, G. L.; Kumar, A.; Frangione, B.; Soto, C., β-Sheet Breaker Peptide Inhibitor of Alzheimer's Amyloidogenesis with Increased Blood-Brain Barrier Permeability and Resistance to Proteolytic Degradation in Plasma. *J. Neurobiol.* **1999**, 39, 371-382.

30. Findeis, M. A.; Musso, G. M.; Arico-Muendel, C. C.; Benjamin, H. W.; Hundal, A. M.; Lee, J. J.; Chin, J.; Kelley, M.; Wakefield, J.; Hayward, N. J.; Molineaux, S. M., Modified-Peptide Inhibitors of Amyloid β-Peptide Polymerization. *Biochemistry* **1999**, 38, 6791-6800.

31. Nordstedt, C.; Naslund, J.; Tjernberg, L. O.; Karlstrom, A. R.; Thyberg, J.; Terenius, L., The Alzheimer Aβ Peptide Develops Protease Resistance in Association with Its Polymerization into Fibrils. *J. Biol. Chem.* **1994**, 269, 30773-30776.

32. Poduslo, J. F.; Curran, G. L.; Sanyal, B.; Selkoe, D. J., Receptor-Mediated Transport of Human Amyloid β-Protein 1-40 and 1-42 at the Blood-Brain Barrier. *Neurobiol. Dis.* **1999**, 6, 190-199.

33. Crooks, J. E.; Sheridan, P. J.; O'Donnell, D., Thermodynamics and Kinetics of Proton-Transfer Reactions between Bromophenol Blue and Aliphatic Amines in Chlorobenzene Solution. *J. Chem. Soc. B* **1970,** 1285-1288.

CHAPTER 6

AFFINITY EXPERIMENTS WITH SURFACE PLASMON RESONANCE (SPR) OF DESIGNED INHIBITORS OF PEPTIDE AGGREGATION

6.1 Introduction

Widely used qualitative techniques such as transmission electron microscopy, atomic force microscopy, and circular dichroism have been used to characterize the nature of the inhibitors for amyloid beta aggregation. However, the results from these methods may not represent the bulk characteristics and the nature of the inhibitor binding. Surface plasmon resonance (SPR) is a promising technique because mechanisms and kinetics of inhibitors binding to substrate can be evaluated. Furthermore, this technique requires very low peptide amounts (5-10 μg) and real time molecular interactions can be obtained without labeling. This detection method is not particularly wide-spread in part because of the variables involved in sample preparation and detection.[1, 2]

Surface plasmon resonance is a very sensitive optical technique where a light of frequency below the plasma frequency is reflected off the surface of a metal (see **Figure 6.1**). A light source (λ = 800 nm) can be directed towards a thin metal surface (50 nm thick) that causes total internal reflection.[3] Because of the sensitivity to the material's surface, any change in the intensity of the refracted light can be measured. When light strikes the surface of a metal, a portion of its energy is transmitted and surface plasmons are propagated to the sample. The transmitted energy can in turn excite the valence electrons of the metal. These mobile electrons, which are known collectively as surface plasmons, can resonate at the frequency of the incident light and form an electron cloud or sea of electrons on the metal surface opposing the light source. If the thin surface is placed on top of the fluidic media whose refractive properties can be manipulated, the intensity can be correlated to the nature of the media.[1, 4]

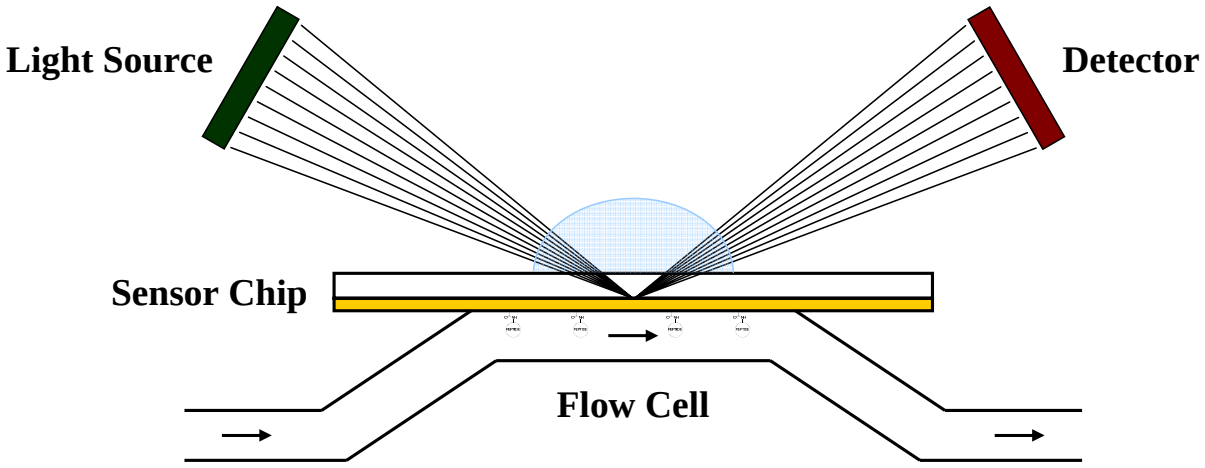

Figure 6.1. Illustration of the setup used for surface plasmon resonance (adapted from figure in Biacore Sensor Surface Handbook).[5]

Instruments using SPR for measuring protein interactions take advantage of these plasmons and the sensitivity of the detector to measure very small changes in the electron density on the surface. Through a variety of surface chemistry techniques, such as amine bond coupling (see **Figure 6.2**), the refractive environment can be modified by the attachment of protein or peptide of interest within the plasmonic domain (roughly within 300 nm of the metal's surface). The change in intensity recorded by the detector in "response units" (RU) is related to the amount of protein successfully bound to the surface. This protein, which is often referred to as the "ligand" in the literature, is permanently stuck to the surface under normal operating conditions and its affinity to other molecules of interest, or "analyte", and can be detected multiple times by simply flowing them across the modified surface at a set flow rate and concentration. Since the changes in response units are measured in real-time, the instrument can obtain very useful kinetic information describing the protein interaction.[1, 2, 6]

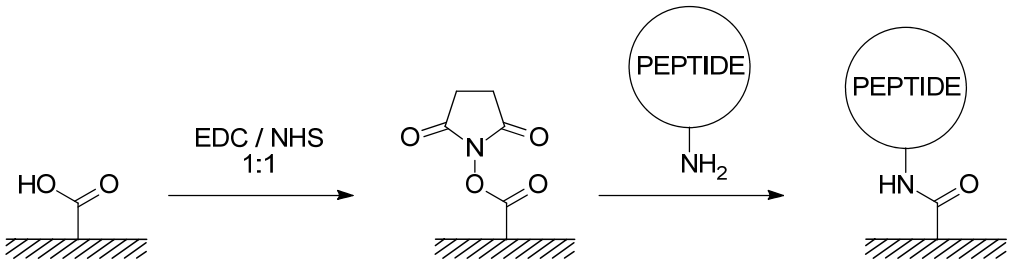

Figure 6.2. Scheme for peptide immobilization to a gold surface via amine coupling.

We attempted to model our affinity experiments on the work done by Cairo *et al.* using a fragment of the peptide sequence, amyloid beta [10-35] amide.[7] For direct comparison, our initial studies began with using one of their inhibitors, which we call "Murphy", as a reference. The "Murphy" inhibitor has similarities in sequence to our reported successful inhibitor, "AMY1".[8] It was anticipated that the use of SPR would help us screen and in turn design inhibitors by determining the peptide features that enhance a strong interaction with the target region (i.e. hydrophobic core) of amyloid beta.

6.2 Results and Discussion

Freshly prepared monomeric amyloid beta [10-35] amide peptide (H-Tyr-Glu-Val-His-His-Gln-Lys-Leu-Val-Phe-Phe-Ala-Glu-Asp-Val-Gly-Ser-Asn-Lys-Gly-Ala-Ile-Ile-Gly-Leu-Met-NH_2) was coupled to the carboxymethyl dextran matrix of a gold surface, Biacore CM5 sensor chip. Based on the Biacore X Surface Plasmon Resonance (SPR) instrument response units (20,886 RU, see **Figure 6.3**), it was estimated that approximately 25 ng of peptide has been immobilized within a 1.2 mm^2 surface area. This measurement was almost 8 times the amount reported by Cairo et al. on a CM5 sensor chip and over 26 times for the B1 sensor chip which has 10-fold lower amount of carboxylic groups than the CM5 version.[7] This gross overshot in peptide density was attributed to an omission in the reference paper and the inexperience we had using the instrument. Unfortunately, it was also noted that the flow was not diverted from going

over the reference (or control) surface during the peptide coupling process. This meant that "background" responses, such as nonspecific binding, injection noise and instrument drift, could not be subtracted to give a more accurate affinity response.[2] Despite these challenges, the decision was made to press on to see what information could be gleaned under these circumstances.

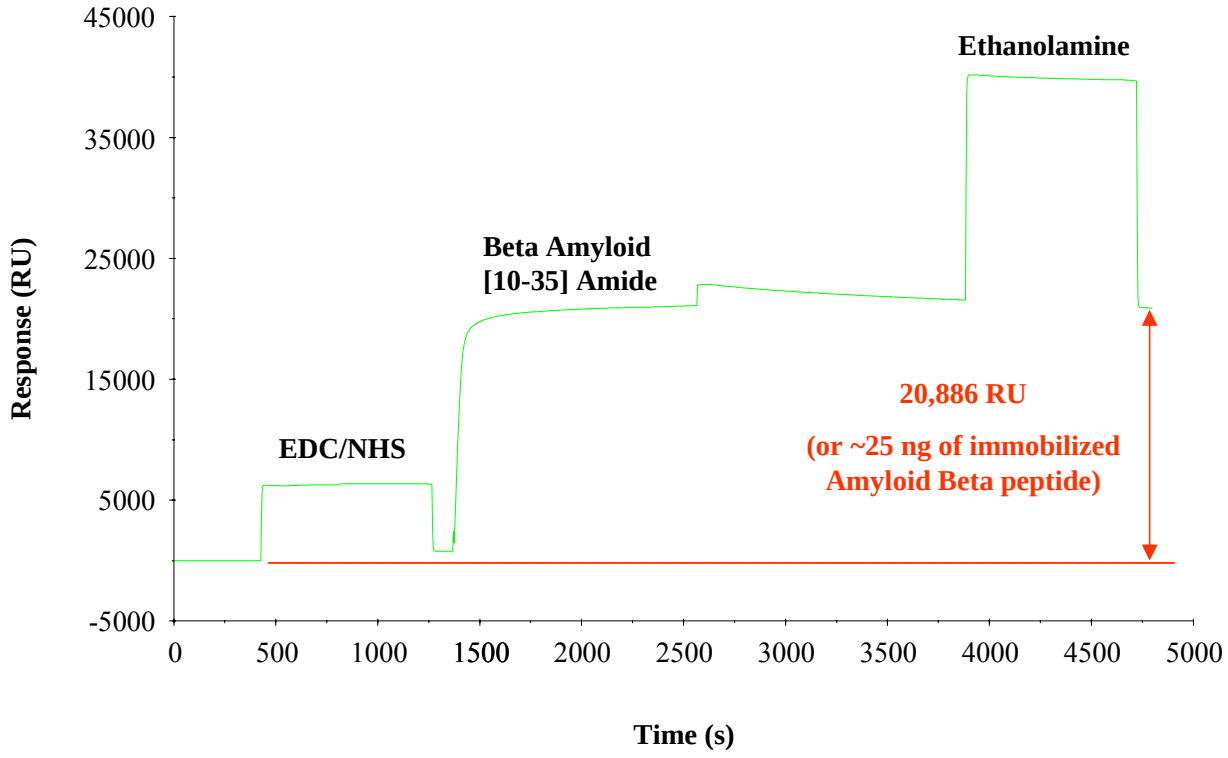

Figure 6.3. Biacore SPR sensorgram of the immobilization of Amyloid Beta peptide to the surface of CM5 sensor chip via amine coupling.

Interactions between the "Murphy" inhibitor (H-Lys-Leu-Val-Phe-Phe-$(Lys)_6$-NH_2) at various concentration levels (see **Section 6.4.4**) and the permanently bound peptide were observed through a series of injections over the peptide saturated surface (see **Figure 6.4** and **6.5**). The responses seemed reasonable when compared to those reported in the reference paper. However, the Biacore software statistical analysis of the calculated dissociation constant, K_D (4.62 μM), which is an order of magnitude lower than reported by Cairo et al., shows a very poor

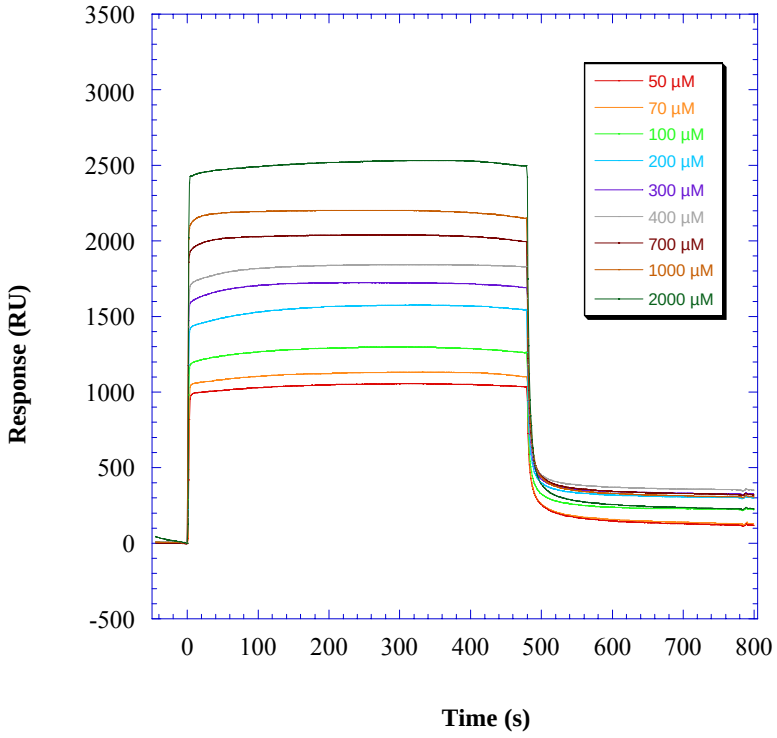

Figure 6.4. 1st series of injection with "Murphy" inhibitor at various concentration levels.

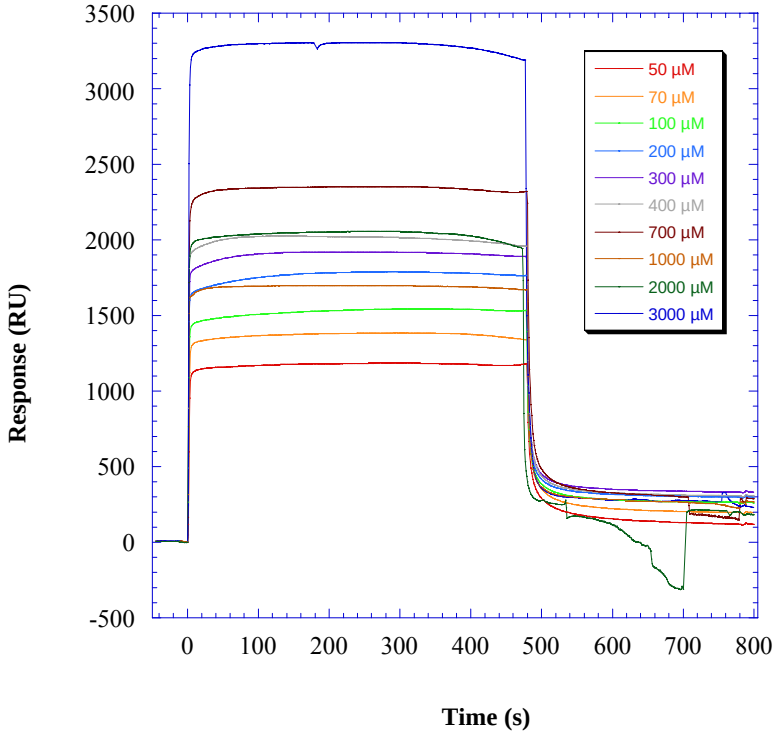

Figure 6.5. 2nd series of injection with "Murphy" inhibitor at various concentration levels.

goodness-of-fit (χ^2 = 36,000) to the data (i.e. all the "Murphy" injections). This means that we cannot use this information as a reliable assessment of the binding affinity for the "Murphy" peptide. Further study on this matter has led us to believe that the over-saturated surface, which cause rebinding, mass transport, aggregation and steric hindrance, may be the root of this problem.[2, 6, 9]

In our efforts to achieve better results, the idea of using competition between the amyloid beta [10-35] amide and ethanolamine as a means of reducing the amount of peptide coupled to the sensor chip surface emerged. The rationale behind this approach was to not only lower the bound peptide, but also make sure that it was uniformly spread throughout the available surface area. A series of injections were tested with mixtures of amyloid beta [10-35] amide and ethanolamine at certain mole ratios. As the concentration of ethanolamine increased, the response units decreases indicating that the competition approach was achieving the desired results. Our final injection of amyloid beta [10-35] amide and ethanolamine at a 1:40 mole ratio lead to 3,276 RU or 4 ng of peptide (see **Figure 6.6**).

6.3 Conclusions

It was hoped that SPR could be used as a screening tool in the amyloid beta aggregation inhibitor design process. Experts agree that the instrument's ease of use is very deceiving.[1, 6, 9] We gained some expertise on how to avoid or reduce potential pitfalls in using this technique. Should this approach be retried in the future, there is now some knowledge base to build from. It is also recommended that future studies include trials with the B1 sensor chip. With a lower carboxylic groups surface density (10-fold lower than the CM5 sensor chip), it should help alleviate the problems associated with over-saturating the surface with amyloid beta peptide.

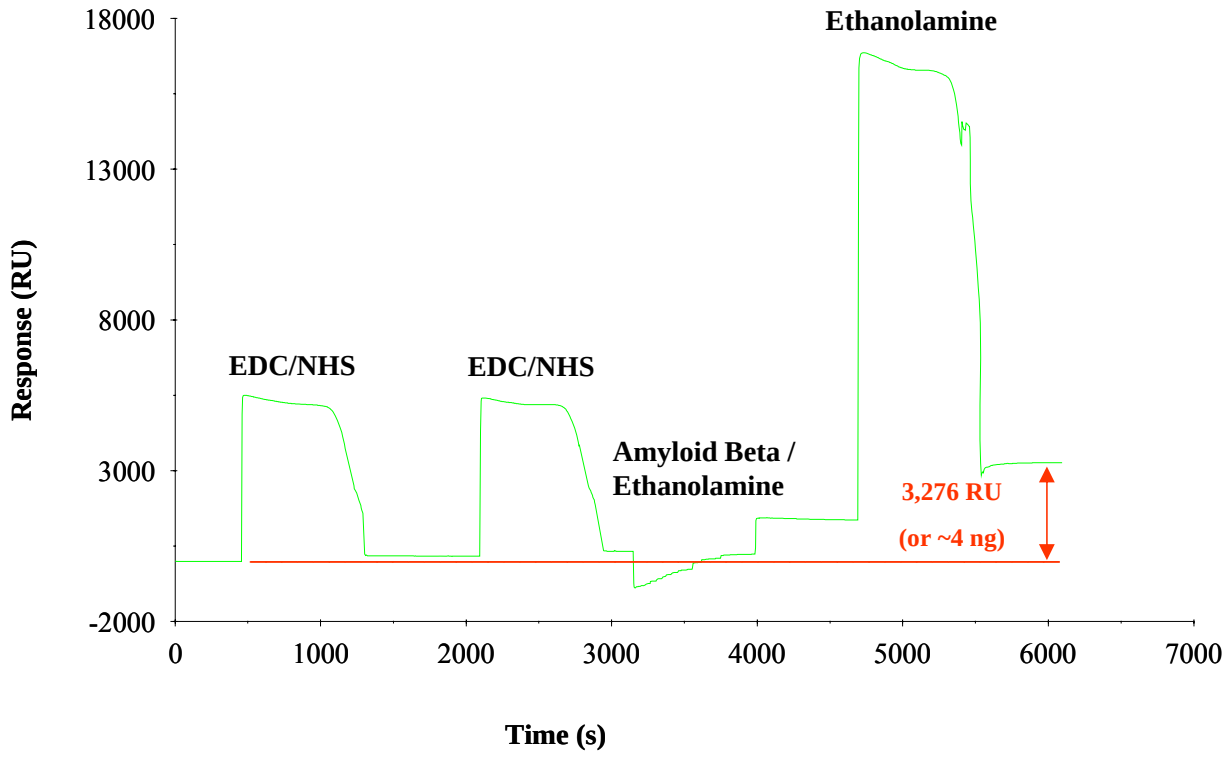

Figure 6.6. Biacore SPR sensorgram of the competition between the amyloid beta [10-35] amide and ethanolamine at a 1:40 mole ratio.

6.4 Experimental

6.4.1 Preparation of Amyloid Beta [10-35] Amide[10]

Amyloid beta [10-35] amide (peptide sequence: H-Tyr-Glu-Val-His-His-Gln-Lys-Leu-Val-Phe-Phe-Ala-Glu-Asp-Val-Gly-Ser-Asn-Lys-Gly-Ala-Ile-Ile-Gly-Leu-Met-NH_2, MW: 2902.4) was removed from -20 °C storage and allowed to warm to room temperature in a dessicator for 30 minutes. The peptide (1.0 g, 0.34 mmol) was weighed out in test tubes, dissolved in trifluoroacetic acid (1 mL), sonicated for 15 minutes. The acid was removed by evaporation under a stream of nitrogen to a thin peptide film. This film was redissolved in hexafluoroisopropanol (1 mL) and incubated at 38 °C for an hour. After evaporating the peptide back down to a thin film, it was redissolved in hexafluoroisopropanol (1 mL). This evaporation followed by redissolving in hexafluoroisopropanol (1 mL) was done one more time. At this

point, the peptide solution was split equally (0.5 mL) into two test tubes and evaporated again to a thin film. The peptide was then lyophilized for 2 hours and mixed with 10 mM sodium acetate (0.5 mL, pH 5.0). The peptide solutions were centrifuged overnight (~50,000 G) to pellet peptide aggregates (dimers, trimers, etc.) and leave monomer in solution. The supernate containing monomeric peptide was removed and stored in -80 °C freezer until needed. Amino acid analysis (AAA) of peptide concentration: 0.052 ± 0.003 mM (or 0.15 ± 0.01 mg/mL).

6.4.2 Amine Coupling of Peptide to Carboxymethyl Dextran Matrix on Gold Surface[7]

The carboxymethyl dextran matrix on the gold surface of a Biacore CM5 sensor chip was "activated" by converting the carboxylic groups to esters by injecting a 1:1 (v/v) mixture of N-ethyl-N'-[(dimethylamino)propyl]-carbodiimide (EDC) and N-hydroxysuccinimide (NHS) (70 μL, 200 mM EDC, 50 mM NHS) into a Biacore X Surface Plasmon Resonance (SPR) instrument, which was set to a flow rate of 5 μL/min. (Note: EDC and NHS should remain separate until ready to use.) The surface was then washed with a recommended running buffer solution, HBS-EP (0.01 M HEPES pH 7.4, 0.15 M NaCl, 3 mM EDTA, 0.005% v/v Surfactant P20). The peptide mixture (100 μL, 0.052 mM or 0.15 mg/mL) prepared in section **6.4.1** was injected over the surface and washed with HBS-EP. (It should be noted that the actual peptide mixture volume was not stated in the reference paper. Therefore, we choose 100 μL under the advisement of others with prior experience.) Any remaining esters on the surface were "deactivated" by amine coupling with 1M ethanolamine (70 μL, pH 8.0). The surface was washed a final time with HBS-EP and the amount of peptide bounded to the surface was calculated by converting the response units (RU) to nanograms. (1000 RU is approximately 1 ng protein/mm^2; surface area is 1.2 mm^2)[1, 2] Results: 20,886 RU or ~25 ng.

It is very important to note that each sensor chip has two individual surface areas that can be used for experiments. The SPR instrument allows the user to control the flow over one

surface area at a time or flow over both. One of the surface areas should be used as a reference surface during binding experiments. Therefore, peptide should not be coupled in this area. It should be "activated" and "deactived" to provide a surface coupled with ethanolamine. The response units for the reference surface will be subtracted from the response units for the peptide bound surface during the binding experiments which will be described in section **6.4.4**. (This subtraction is similar to removing background in IR, UV, etc.)

6.4.3 Peptide / Ethanolamine Competition to Lower Peptide Amount on Chip Surface

The same basic procedure was following as written in section **6.4.2** with one exception. The peptide solution (0.052 mM or 0.15 mg/mL) prepared in section **6.4.1** was mixed with 10 mM ethanolamine (in 10mM sodium acetate, pH 5.0) to achieve a desired peptide / ethanolamine mole ratio. An example of this mixing is combining 95 μL of 0.052 mM peptide solution and 5 μL of 10 mM ethanolamine solution to get a 1:10 mole ratio (peptide / ethanolamine). This example resulted in 11,641 RU or 14 ng.

6.4.4 Procedure for Binding Experiments with "Murphy" Inhibitor[7]

"Murphy" inhibitor (peptide sequence: H-Lys-Leu-Val-Phe-Phe-$(Lys)_6$-NH_2, MW: 1420.9) was removed from -20 °C storage and allowed to warm to room temperature in a dessicator for 30 minutes. A 3000 μM inhibitor stock solution was made that was diluted to the concentrations tested. Those concentrations were 3000, 2000, 1000, 700, 400, 300, 200, 100, 70, and 50 μM. With the flow rate set to 5 μL/min, each concentration (40 μL) was injected across both surface areas on the sensor chip (the peptide bound surface and the reference surface) for 5 minutes. In between the injection of various inhibitor concentrations, the surfaces areas where then washed with the running buffer (HBS-EP), regenerated with 4 M guanidine-HCl in 10 mM Tris-HCl (pH 8.0) and washed again with HBS-EP. By regenerating the surfaces, the response

units (RU) recorded by the instrument returned to the original baseline (or 0 RU if instrument was re-zeroed prior to injection of inhibitor solutions). Results: K_D = 4.62 μM, χ^2 = 36,000

6.5 References

1. van der Merwe, P. A., Surface Plasmon Resonance. In *Protein-Ligand Interactions: Hydrodynamics and Calorimetry*, Harding, S. E.; Chowdhry, B. Z., Eds. Oxford University Press: New York, 2001; pp 137-170.

2. Myszka, D. G.; Wood, S. J.; Biere, A. L., Analysis of Fibril Elongation Using Surface Plasmon Resonance Biosensors. In *Amyloid, Prions, and Other Protein Aggregates*, Wetzel, R., Ed. Academic Press Inc: San Diego, 1999; Vol. 309, pp 386-402.

3. O'Shannessy, D. J.; Brigham-Burke, M.; Soneson, K. K.; Hensley, P.; Brooks, I., Determination of Rate and Equilibrium Binding Constants for Macromolecular Interactions Using Surface-Plasmon Resonance - Use of Nonlinear Least-Squares Analysis-Methods. *Anal. Biochem.* **1993**, 212, 457-468.

4. Kittle, C., *Introduction to Solid State Physics*. 7th ed.; John Wiley & Sons, Inc.: New York, 1996; p 269-304.

5. *Biacore Sensor Surface Handbook*. October 2003 ed.; BR-1005-71 (Version AA); p 3.

6. Morton, T. A.; Myszka, D. G., Kinetic Analysis of Macromolecular Interactions Using Surface Plasmon Resonance Biosensors. In *Energetics of Biological Macromolecules, Pt B*, Ackers, G. K.; Johnson, M. L., Eds. Academic Press Inc: San Diego, 1998; Vol. 295, pp 268-294.

7. Cairo, C. W.; Strzelec, A.; Murphy, R. M.; Kiessling, L. L., Affinity-Based Inhibition of β-Amyloid Toxicity. *Biochemistry* **2002**, 41, 8620-8629.

8. Etienne, M. A.; Aucoin, J. P.; Fu, Y. W.; McCarley, R. L.; Hammer, R. P., Stoichiometric Inhibition of Amyloid β-Protein Aggregation with Peptides Containing Alternating α,α-Disubstituted Amino Acids. *J. Am. Chem. Soc.* **2006**, 128, 3522-3523.

9. Myszka, D. G., Kinetic, Equilibrium, and Thermodynamic Analysis of Macromolecular Interactions with BIACORE. In *Energetics of Biological Macromolecules, Pt C*, Johnson, M. L.; Ackers, G. K., Eds. Academic Press Inc: San Diego, 2000; Vol. 323, pp 325-340.

10. Zagorski, M. G.; Yang, J.; Shao, H. Y.; Ma, K.; Zeng, H.; Hong, A., Methodological and chemical factors affecting amyloid beta peptide amyloidogenicity. In *Amyloid, Prions, and Other Protein Aggregates*, Academic Press Inc: San Diego, 1999; Vol. 309, pp 189-204.

CHAPTER 7

FUTURE DIRECTIONS

Based on the inhibition results of the AMY-1 peptide and the similarity in peptide sequence between amyloid beta and islet amyloid polypeptide (IAPP), it seems logical that incorporation of disubstituted amino acids into short peptide inhibitors for Type II diabetes research should be a viable area to explore. The 20-29 region of IAPP has been the most investigated as the source of aggregation.[1] A possible first candidate would be based on the peptide sequence for residues 22-27 (H-Asn-Phe-Gly-Ala-Ile-Leu-NH_2). The disubstituted amino acid replacements could be 1) Dbzg for phenylalanine, 2) Dpg or Aib for alanine and 3) Dibg for leucine (see **Figure 7.1**). Another region that have been targeted within the IAPP sequence is 8-20. The peptide sequence for residues 12-17 (H-Leu-Ala-Asn-Phe-Leu-Val-NH_2) has been demonstrated to form fibrils.[2] The disubstituted amino acid replacements could be 1) Dpg or Aib for alanine, 2) Dbzg for phenylalanine and 3) Dibg for valine (see **Figure 7.2**).

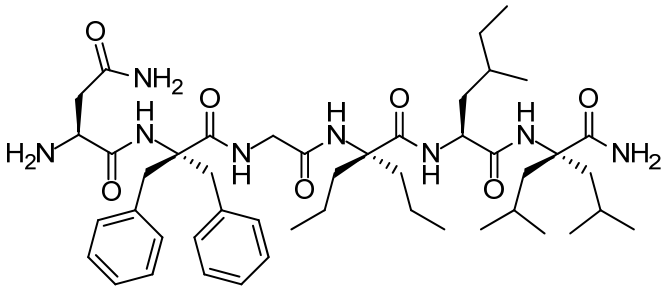

Figure 7.1. Inhibitor idea based on residues 22-27 of IAPP.

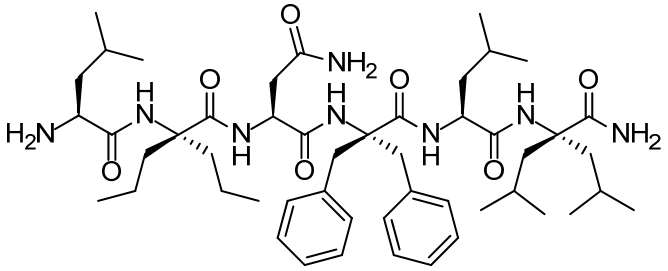

Figure 7.2. Inhibitor idea based on residues 12-17 of IAPP.

Due to hydrophobicity of these two sequences, these inhibitors will need additional solubility elements (such as charges residues and PEG chains) added to one or both of the peptide's termini.

Also it would be interesting to synthesize peptide inhibitors that contain aromatic amino acids which have either electron withdrawing groups or electron donating groups in the *para* position. As discussed in **Chapter 2**, this would serve as an evaluation of the role of aromaticity within peptide interactions, such as π-stacking. The possibility of being able to tune an inhibitors binding on one face and blocking on the other by exchanging the *para* substituent would be worth investigating.

7.1 References

1. Moriarty, D. F.; Raleigh, D. P., Effects of Sequential Proline Substitutions on Amyloid Formation by Human Amylin(20-29). *Biochemistry* **1999**, 38, 1811-1818.

2. Scrocchi, L. A.; Ha, K.; Chen, Y.; Wu, L.; Wang, F.; Fraser, P. E., Identification of Minimal Peptide Sequences in the (8-20) Domain of Human Islet Amyloid Polypeptide Involved in Fibrillogenesis. *J. Struct. Biol.* **2003**, 141, 218-227.

APPENDIX A - NMR SPECTRA

A.1 ^{1}H-NMR (250 MHz, $CDCl_3$)

Ethyl 2-benzyl-2-nitro-3-phenylpropanoate (**2.4.1**)

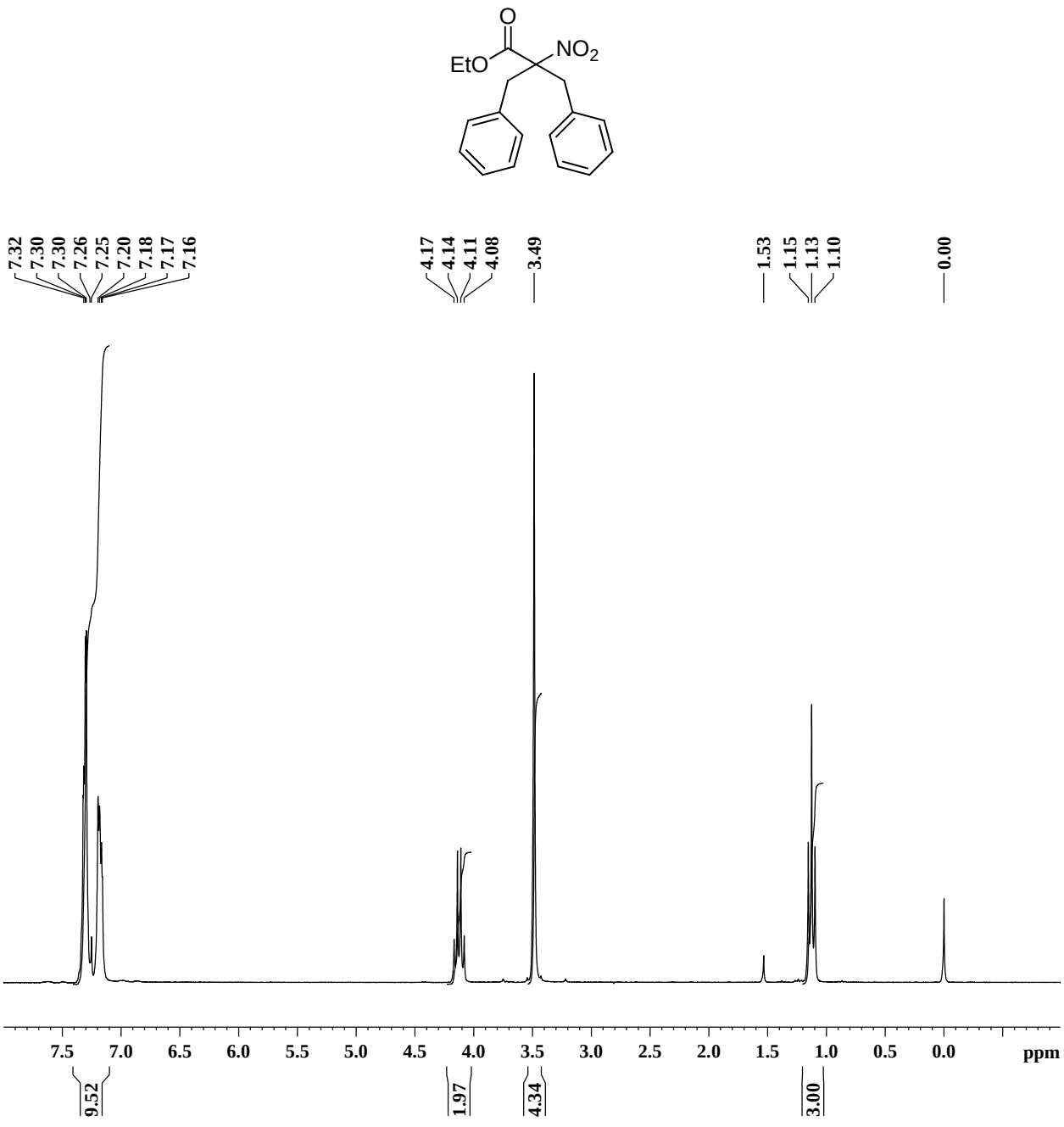

A.2 ^{13}C-NMR (250 MHz, $CDCl_3$)

Ethyl 2-benzyl-2-nitro-3-phenylpropanoate (**2.4.1**)

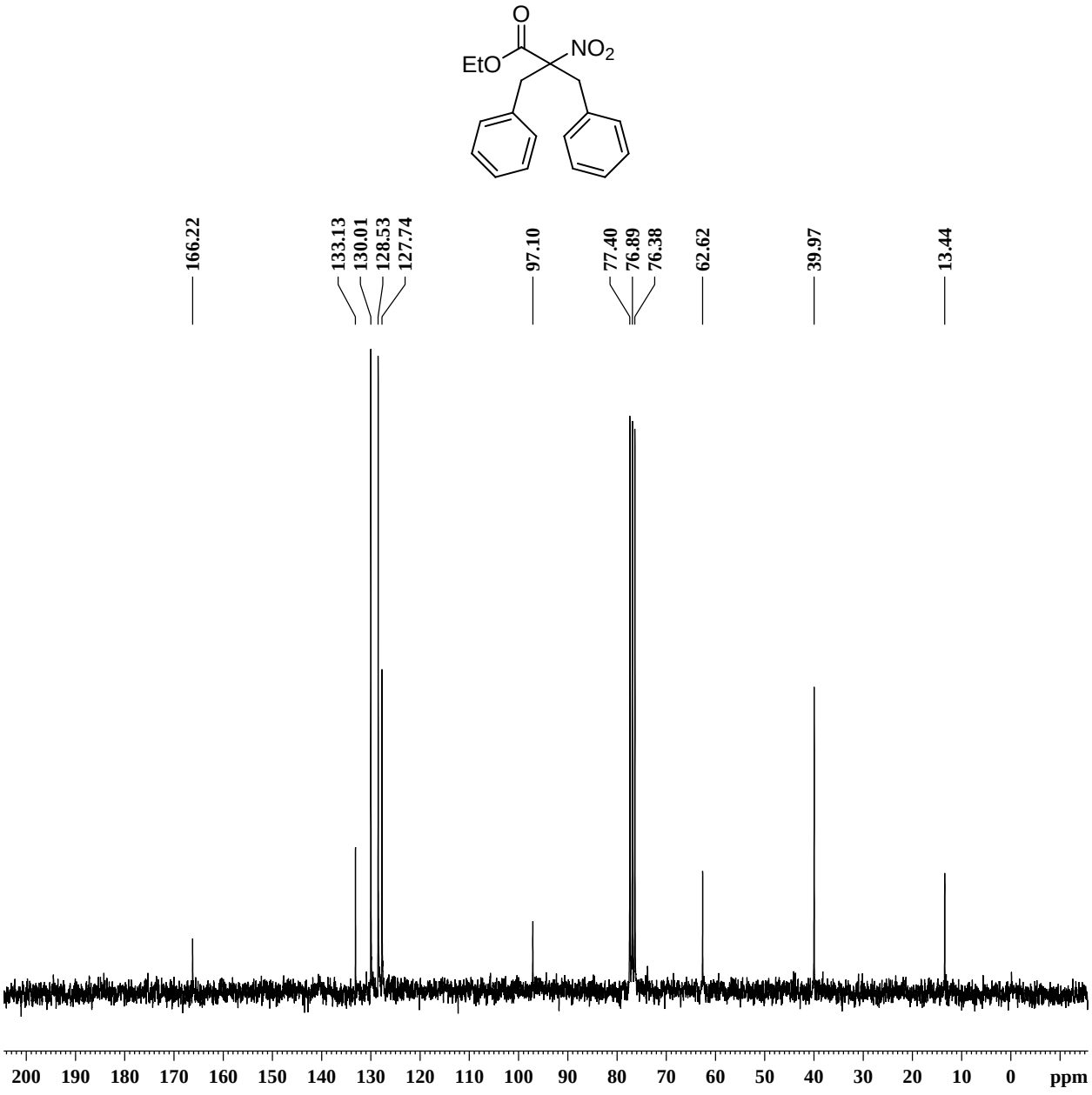

A.3 ^{1}H-NMR (250 MHz, $CDCl_3$)

Ethyl 2-(4-(methylthio)benzyl)-3-(4-(methylthio)phenyl)-2-nitropropanoate (**2.4.2**)

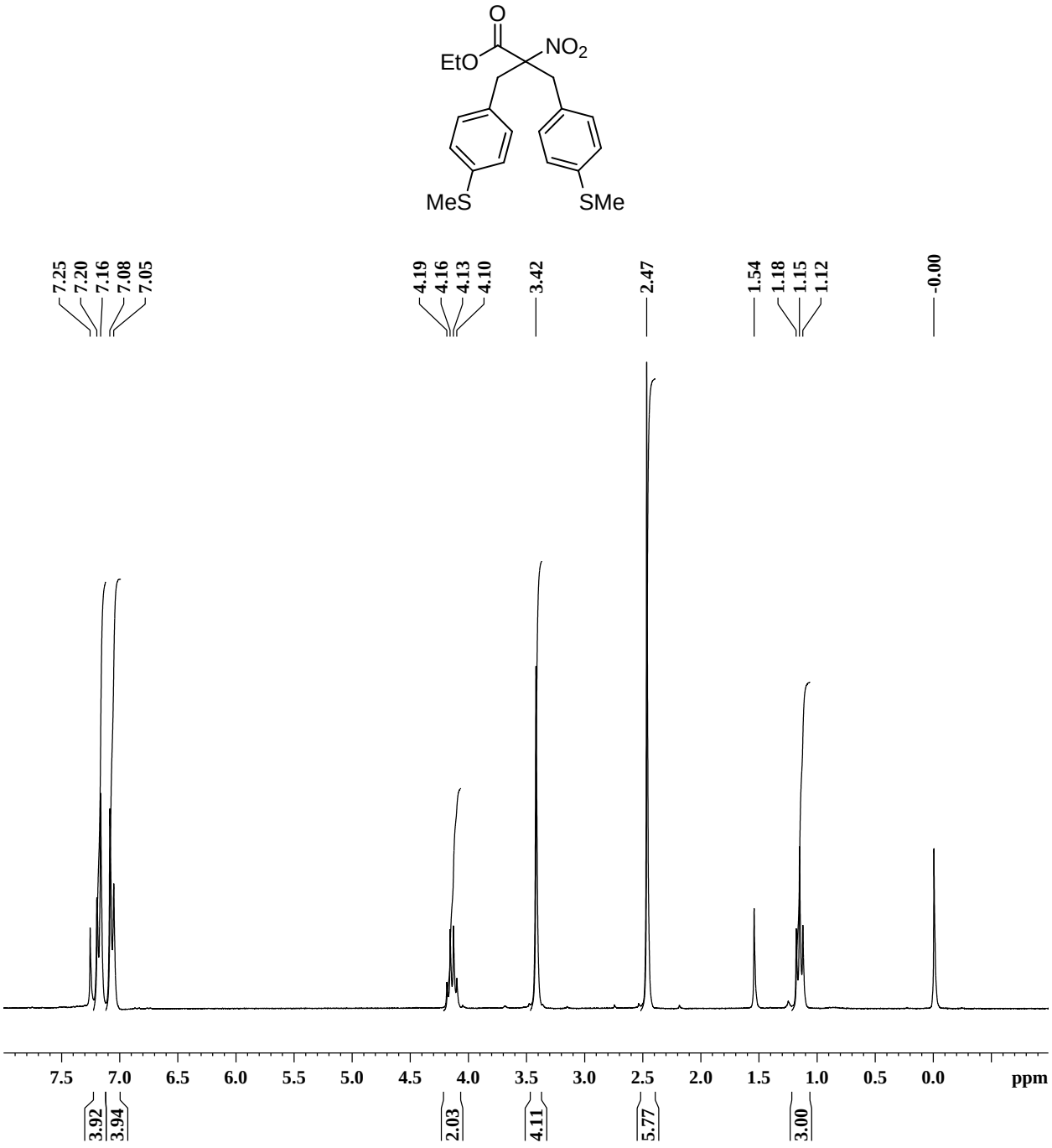

A.4 ^{13}C-NMR (250 MHz, $CDCl_3$)

Ethyl 2-(4-(methylthio)benzyl)-3-(4-(methylthio)phenyl)-2-nitropropanoate (**2.4.2**)

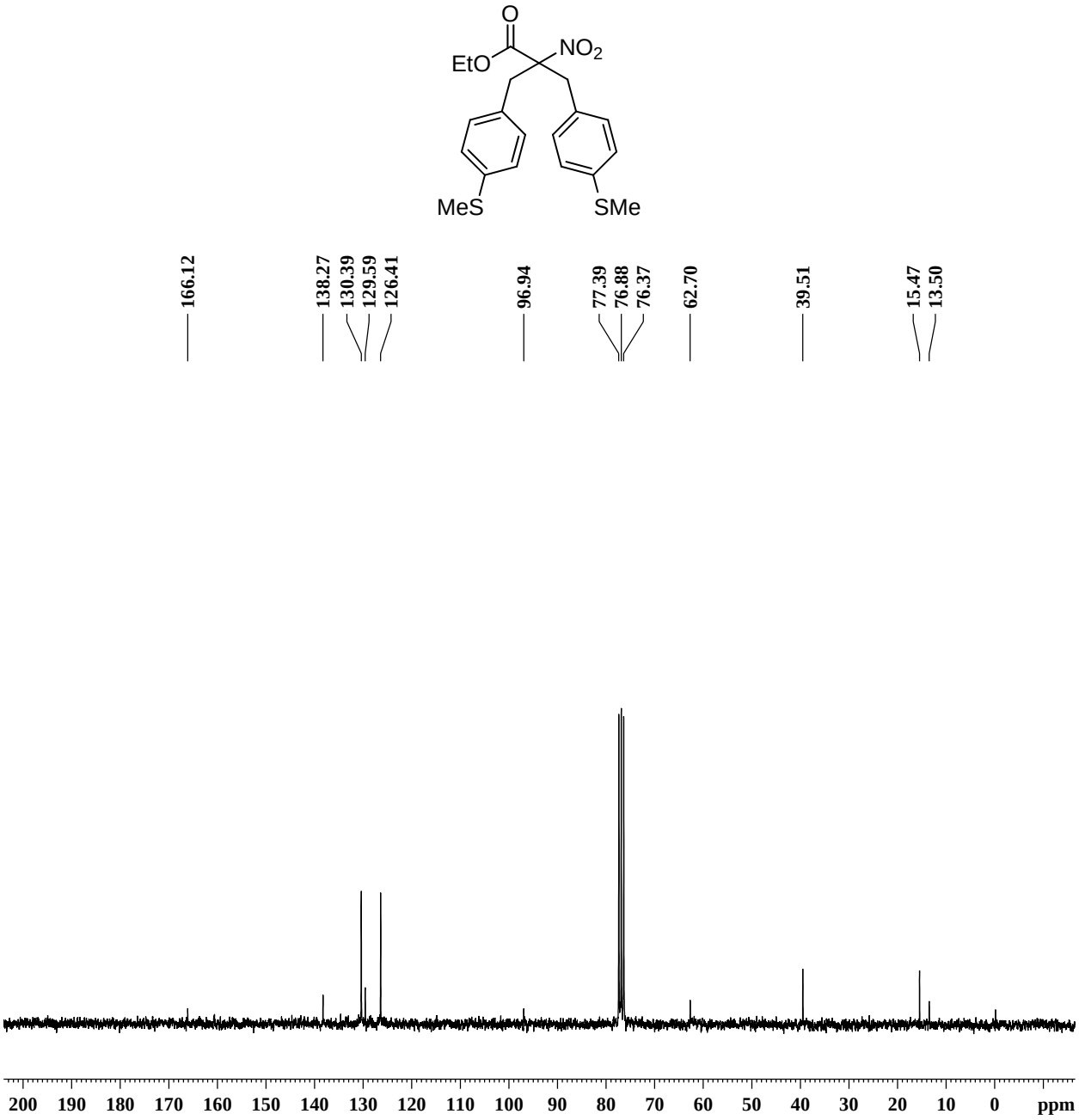

A.5 ^{1}H-NMR (250 MHz, $CDCl_3$)

Ethyl 2-(4-methoxybenzyl)-3-(4-methoxyphenyl)-2-nitropropanoate (**2.4.3**)

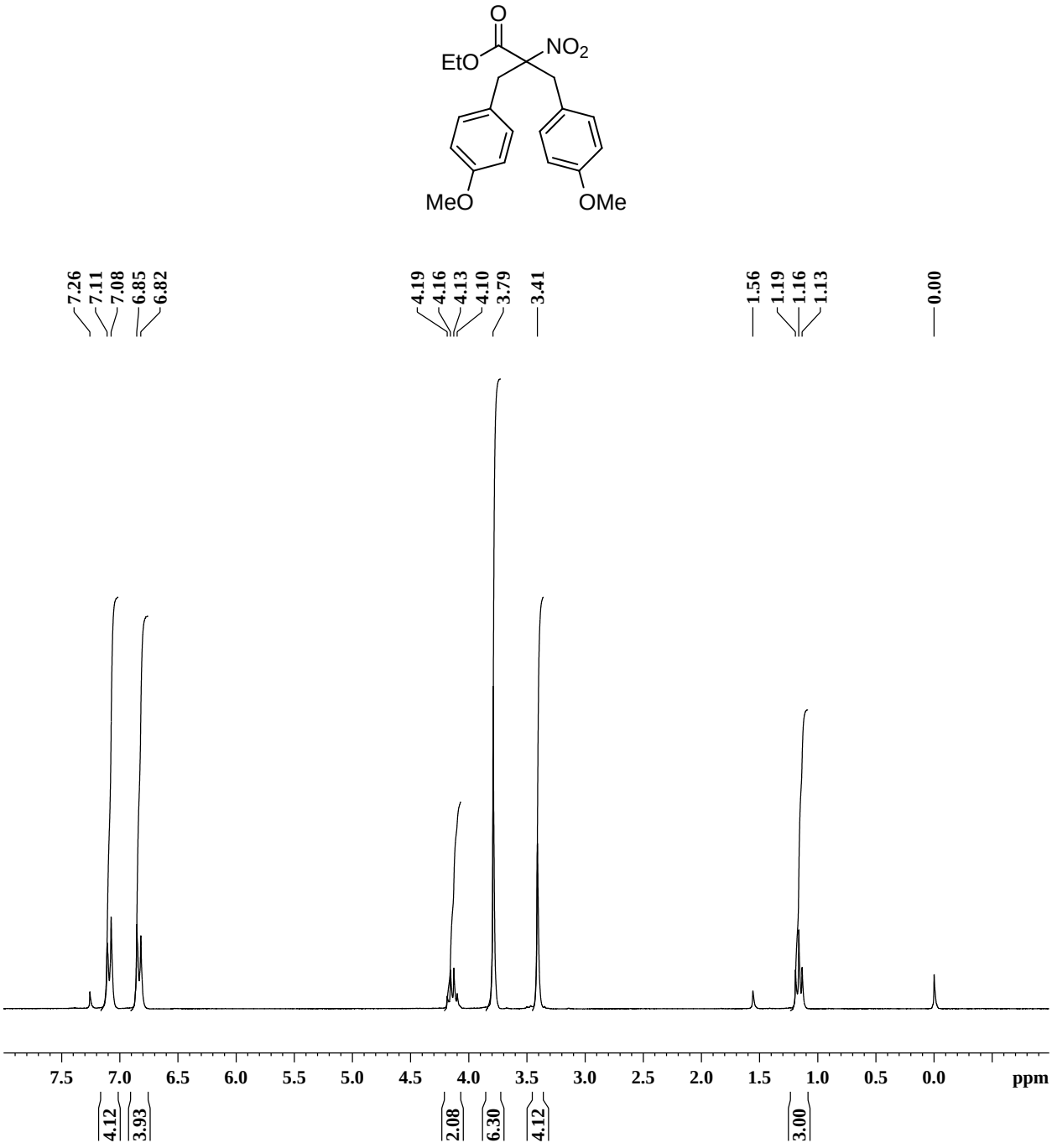

A.6 ^{13}C-NMR (250 MHz, $CDCl_3$)

Ethyl 2-(4-methoxybenzyl)-3-(4-methoxyphenyl)-2-nitropropanoate (**2.4.3**)

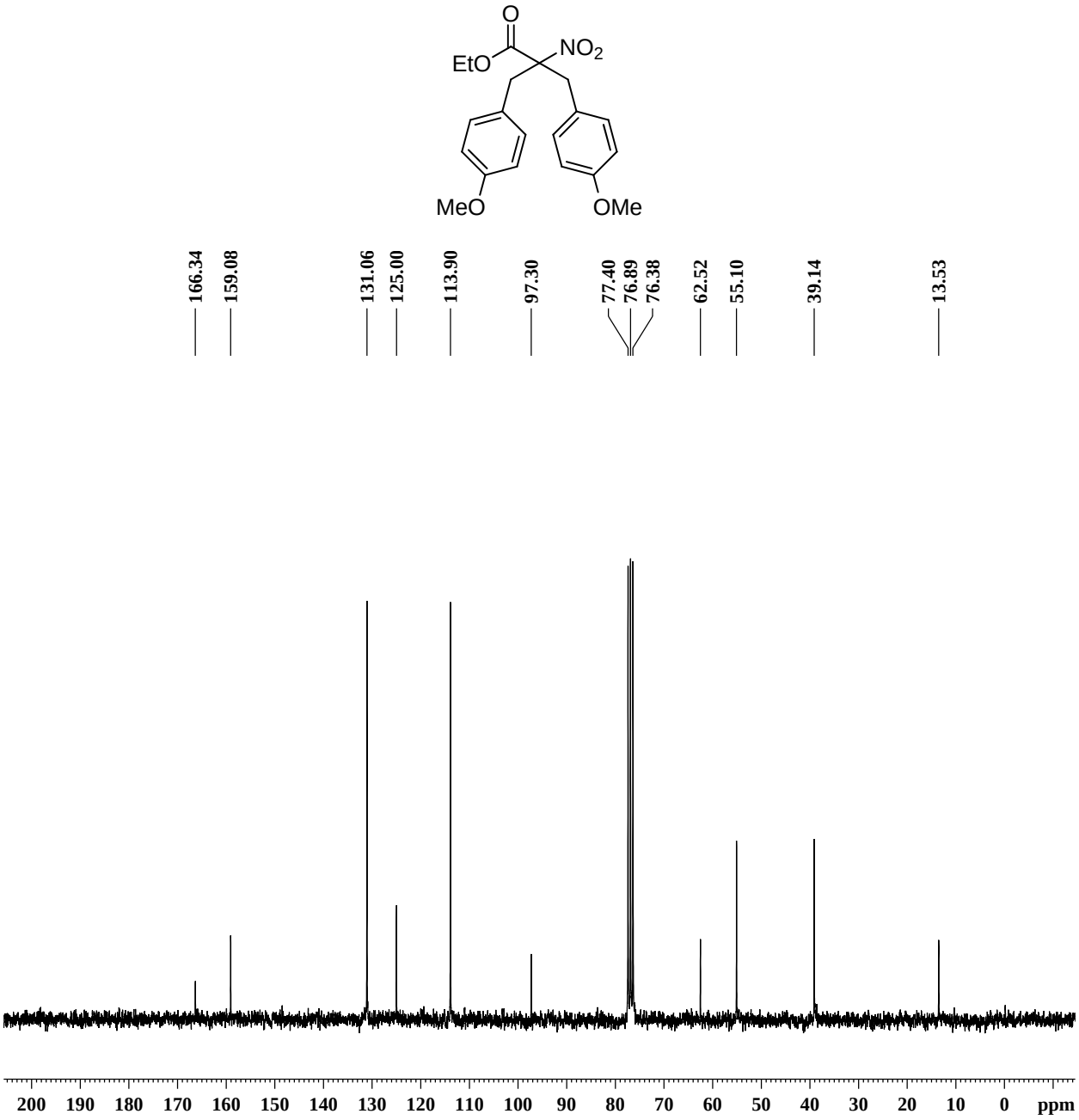

A.7 ^{1}H-NMR (250 MHz, DMSO-d_6)

Ethyl 2-nitro-2-(4-nitrobenzyl)-3-(4-nitrophenyl)propanoate (**3.4.1**)

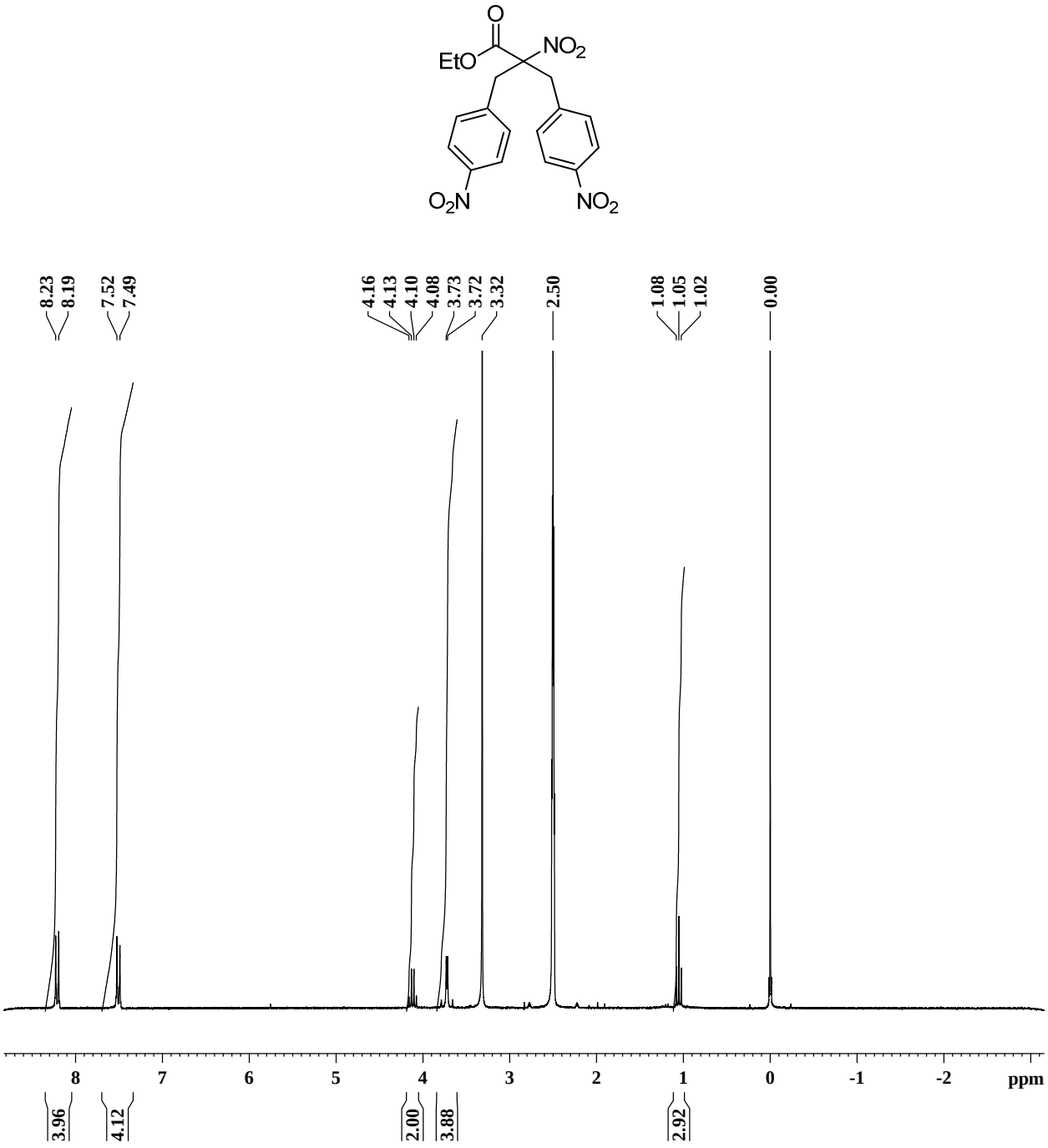

A.8 ^{13}C-NMR (250 MHz, DMSO-d_6)

Ethyl 2-nitro-2-(4-nitrobenzyl)-3-(4-nitrophenyl)propanoate (**3.4.1**)

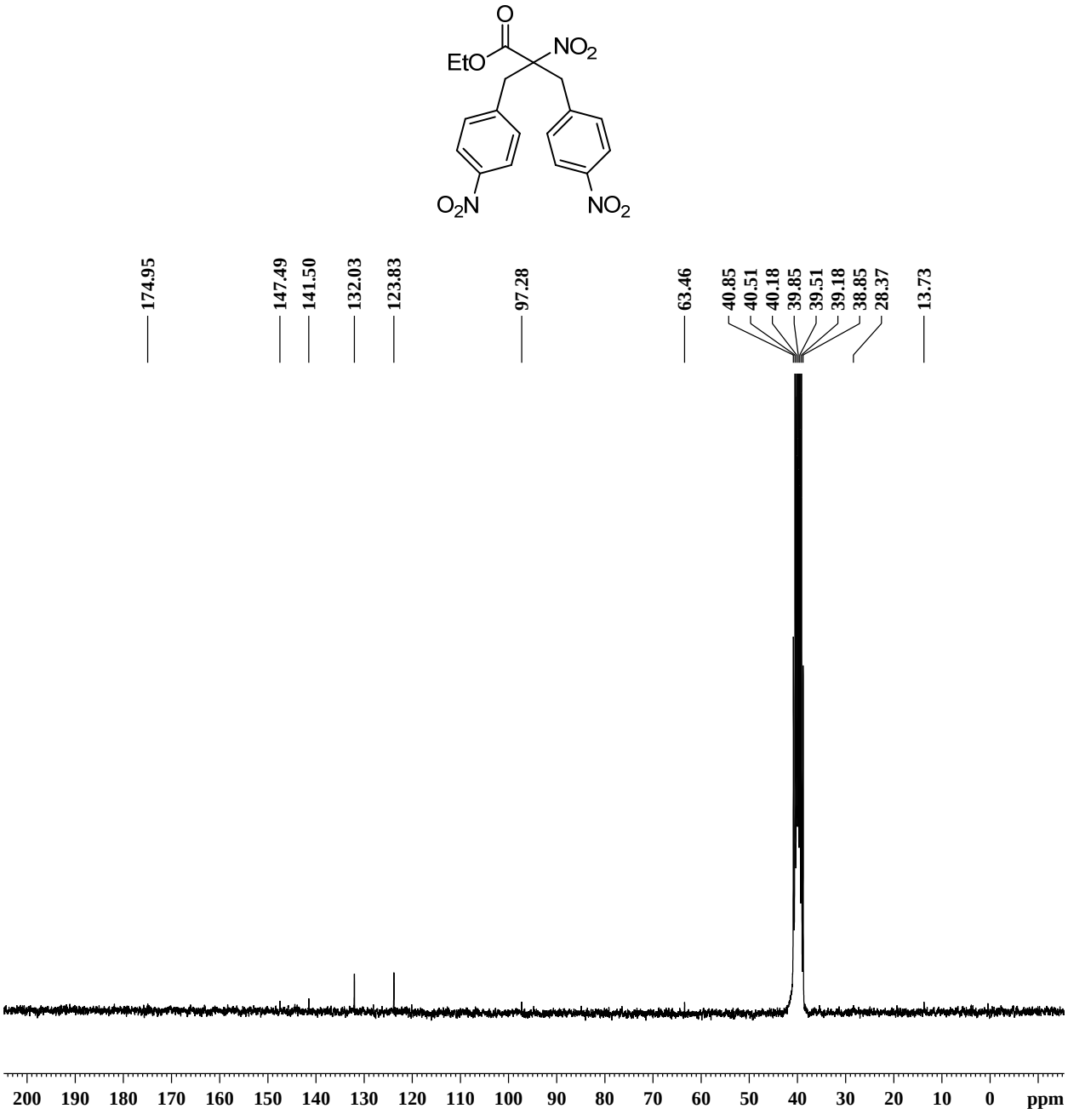

A.9 ^{1}H-NMR (250 MHz, $CDCl_3$)

Ethyl 2,2-bis(allyl)-2-nitroacetate (using 0.5 mol % Pd catalyst) (**4.4.1**)

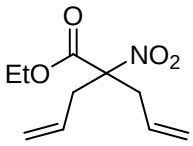

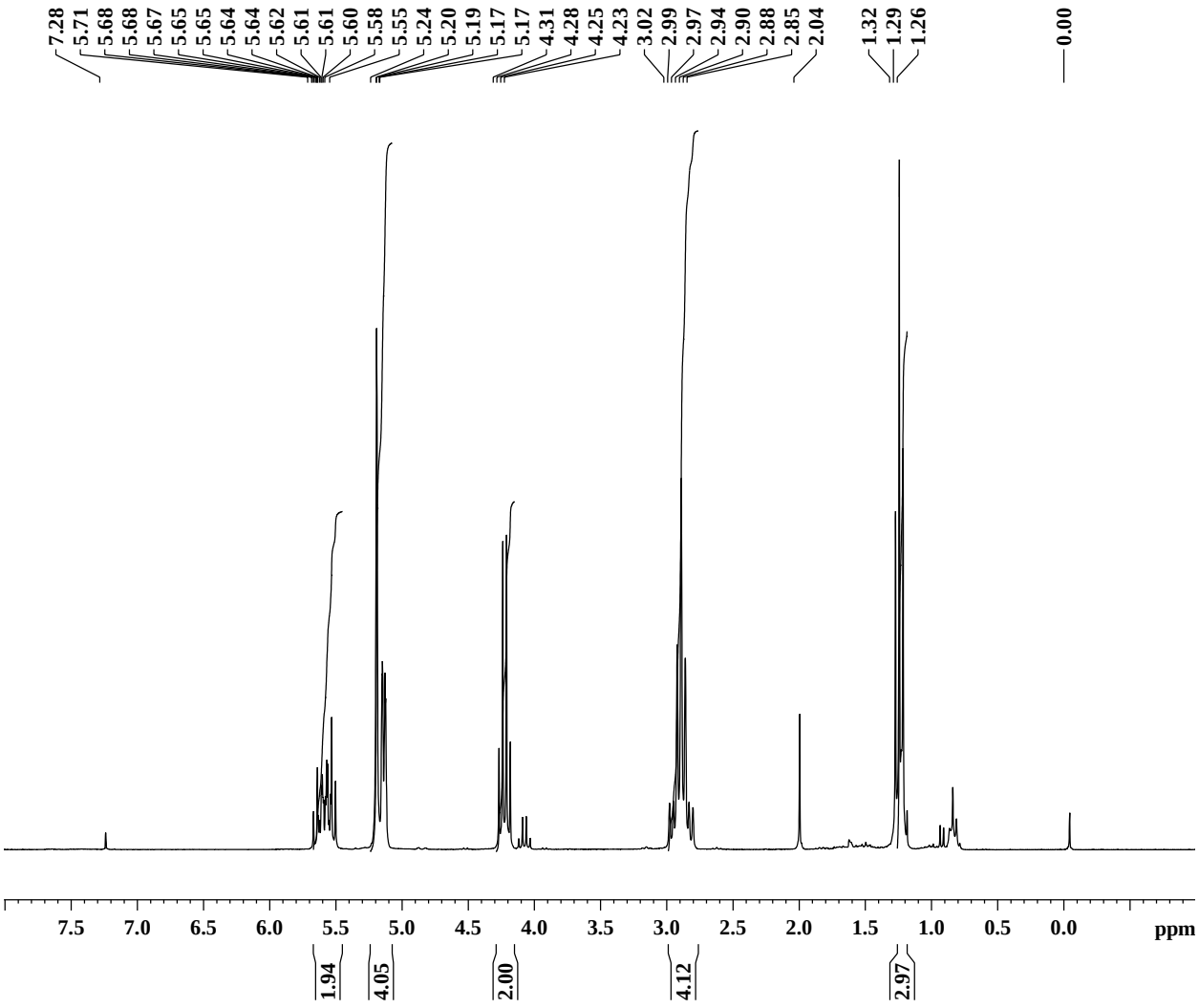

A.10 ^{13}C-NMR (250 MHz, $CDCl_3$)

Ethyl 2,2-bis(allyl)-2-nitroacetate (using 0.5 mol % Pd catalyst) (**4.4.1**)

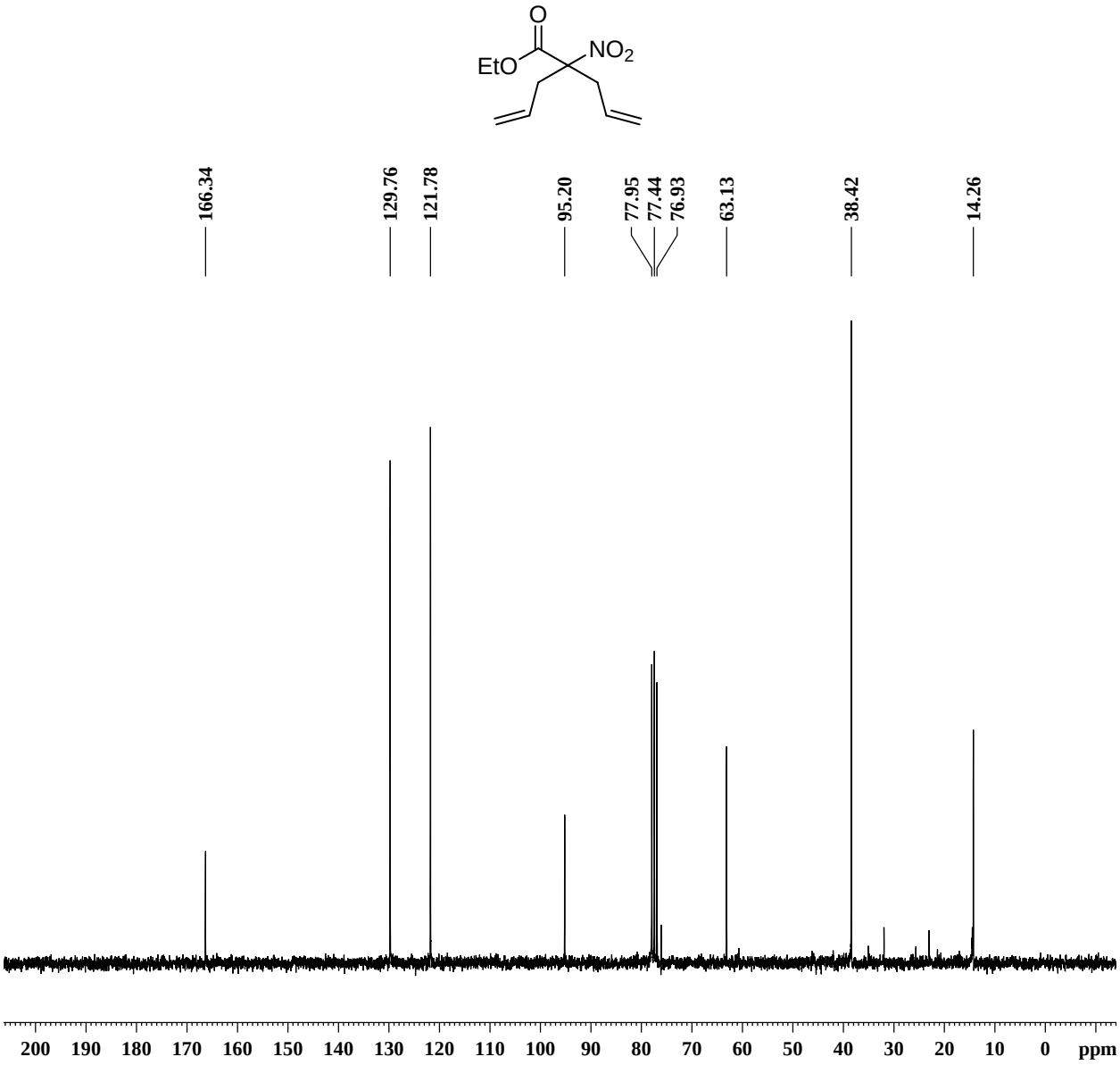

A.11 ^{1}H-NMR (250 MHz, $CDCl_3$)

Ethyl 2,2-bis(allyl)-2-nitroacetate (using 0.05 mol % Pd catalyst) (**4.4.2**)

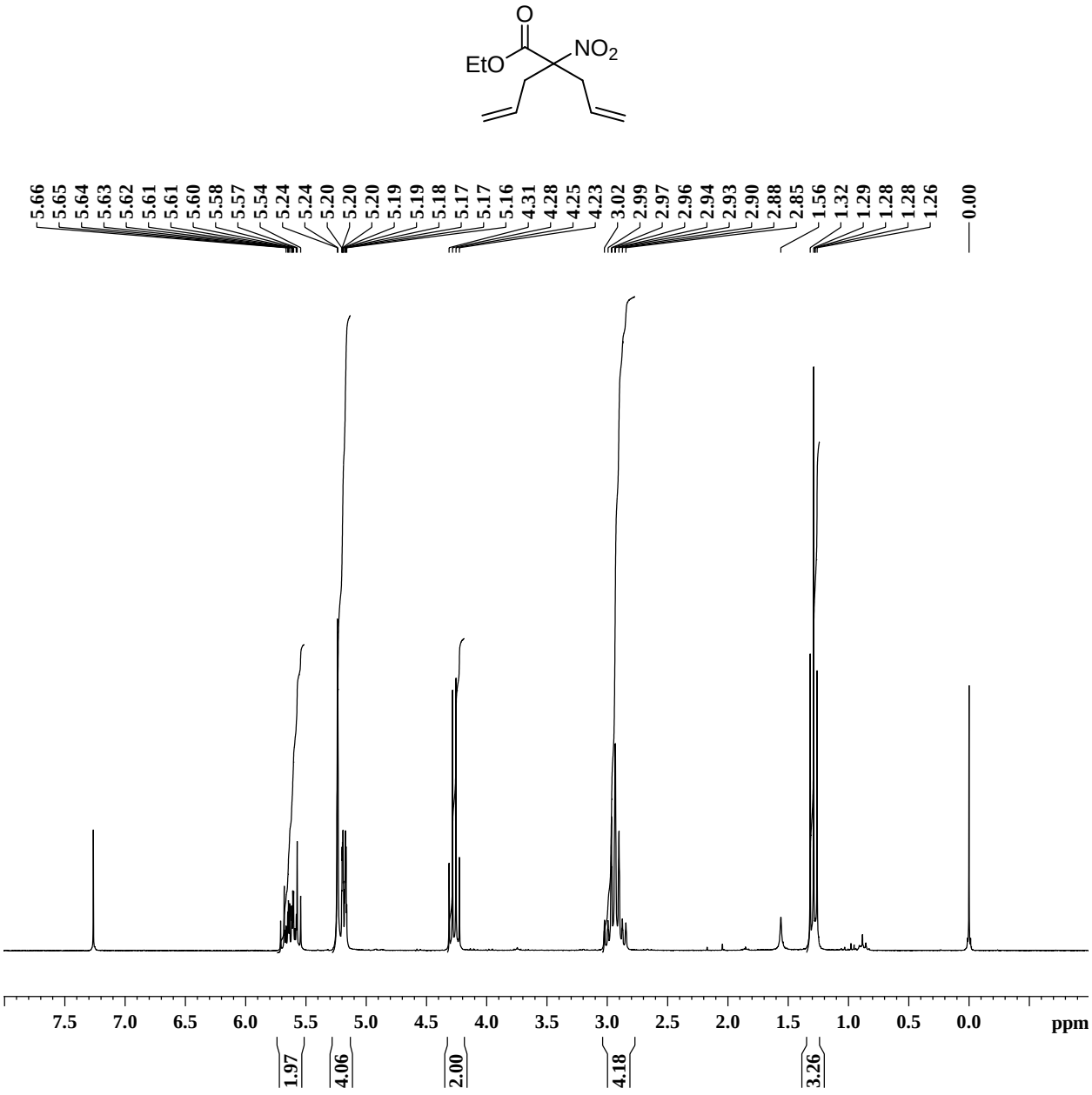

A.12 ^{13}C-NMR (250 MHz, $CDCl_3$)

Ethyl 2,2-bis(allyl)-2-nitroacetate (using 0.05 mol % Pd catalyst) (**4.4.2**)

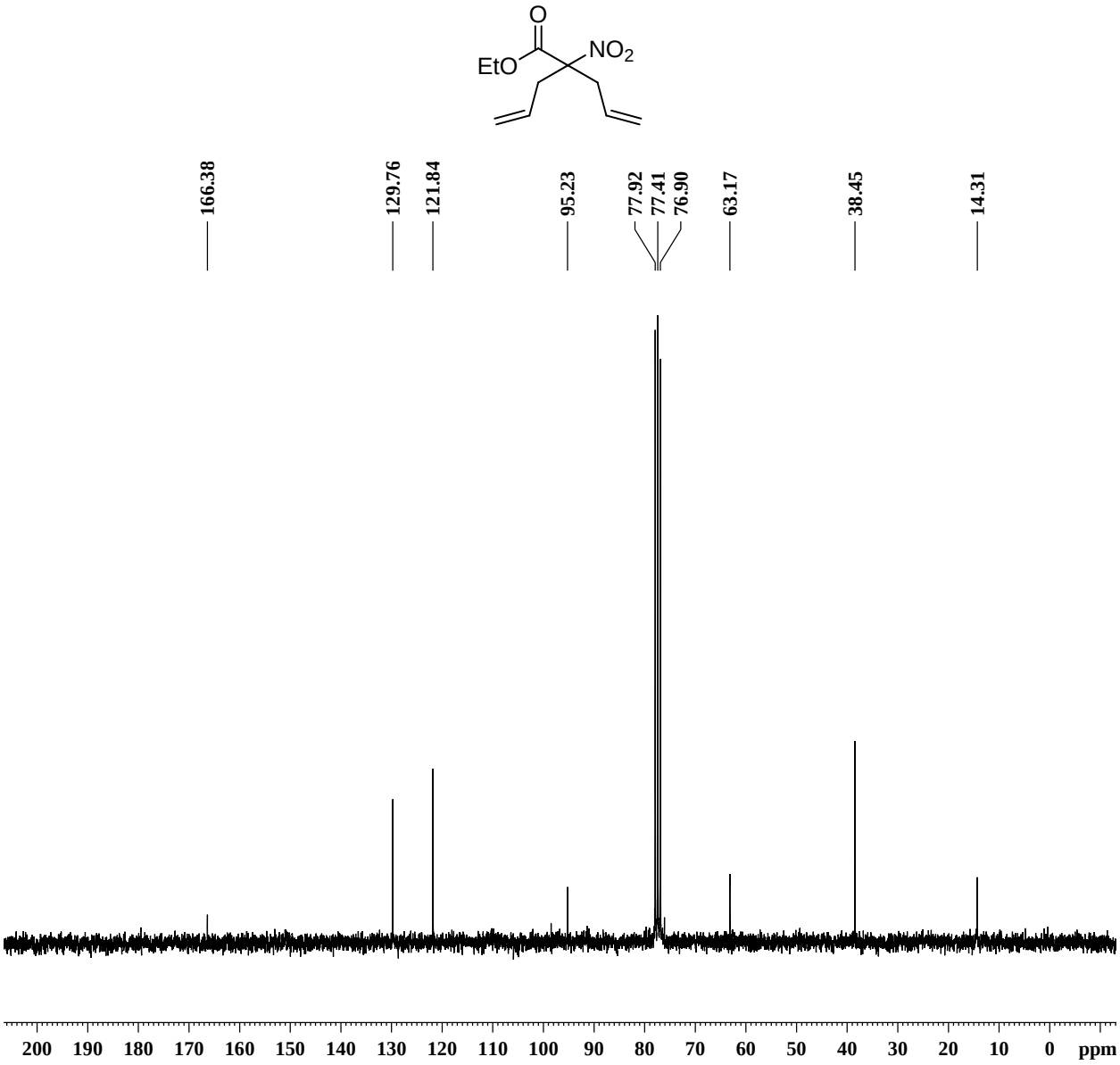

A.13 ^{1}H-NMR (300 MHz, $CDCl_3$)

Ethyl 2-amino-2,2-bis(propyl)acetate (**4.4.3**)

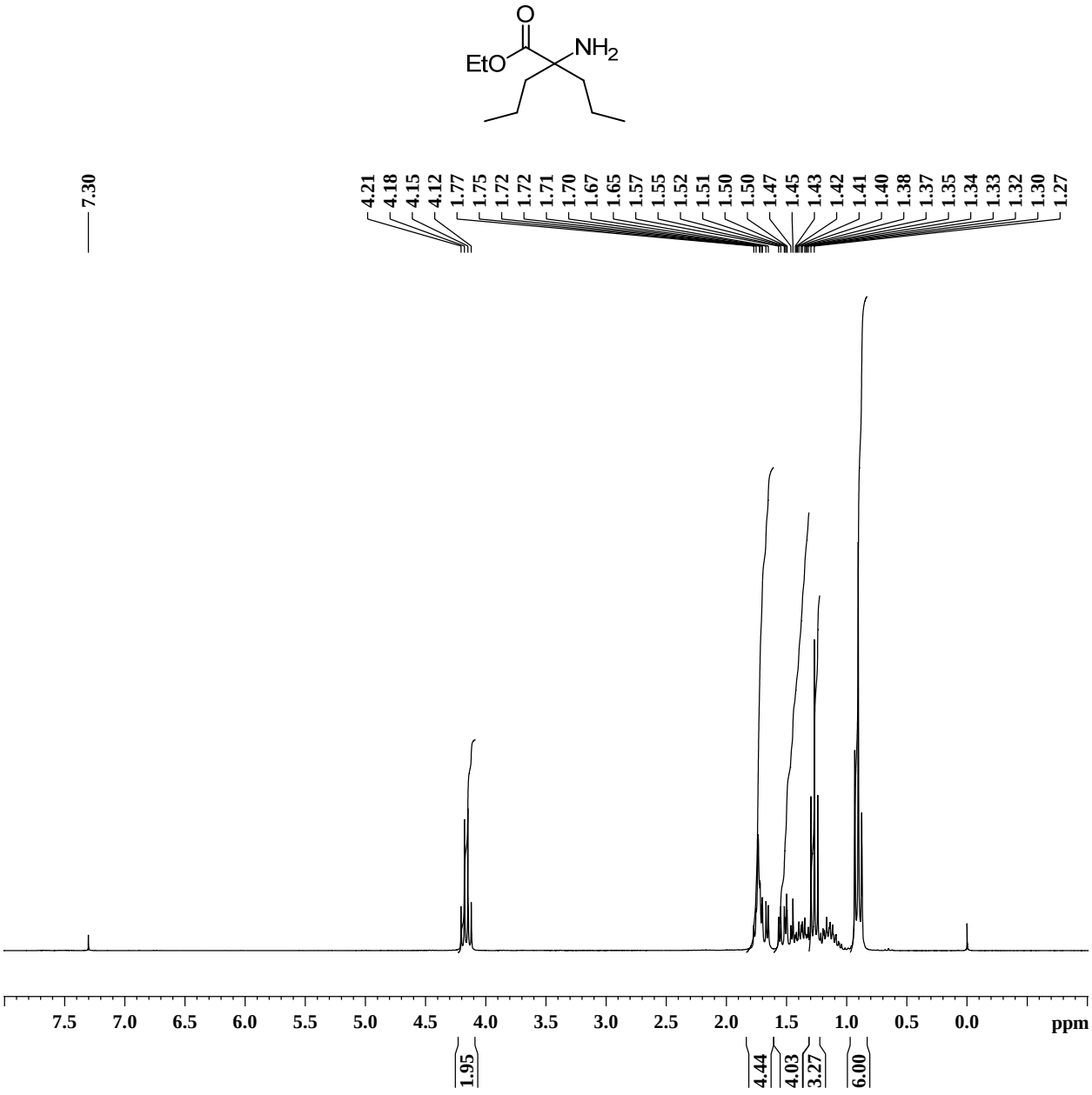

A.14 ^{13}C-NMR (250 MHz, $CDCl_3$)

Ethyl 2-amino-2,2-bis(propyl)acetate (**4.4.3**)

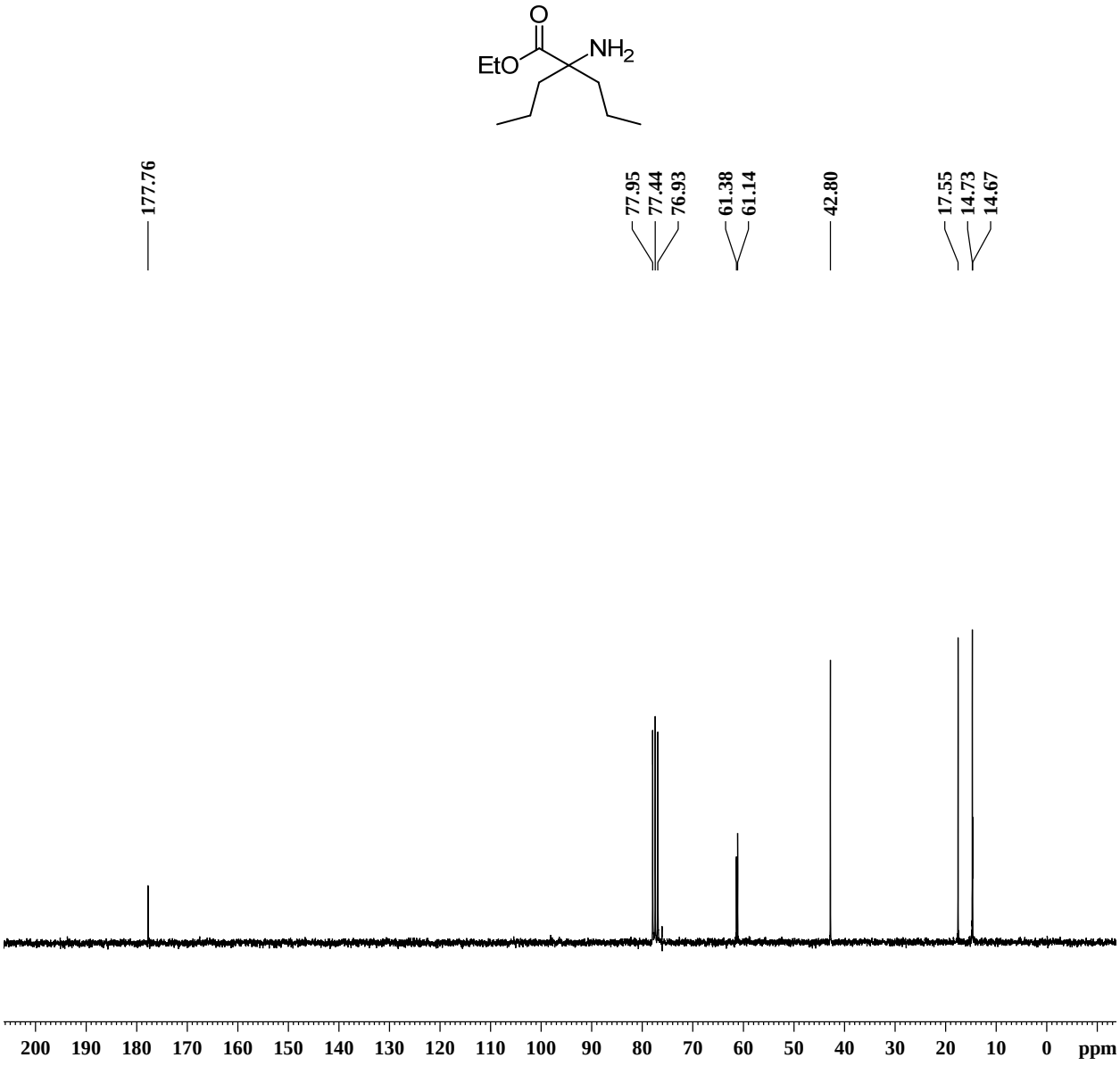

A.15 ^{1}H-NMR (250 MHz, DMSO-d_6)

2,2-Dipropylglycine (**4.4.4**)

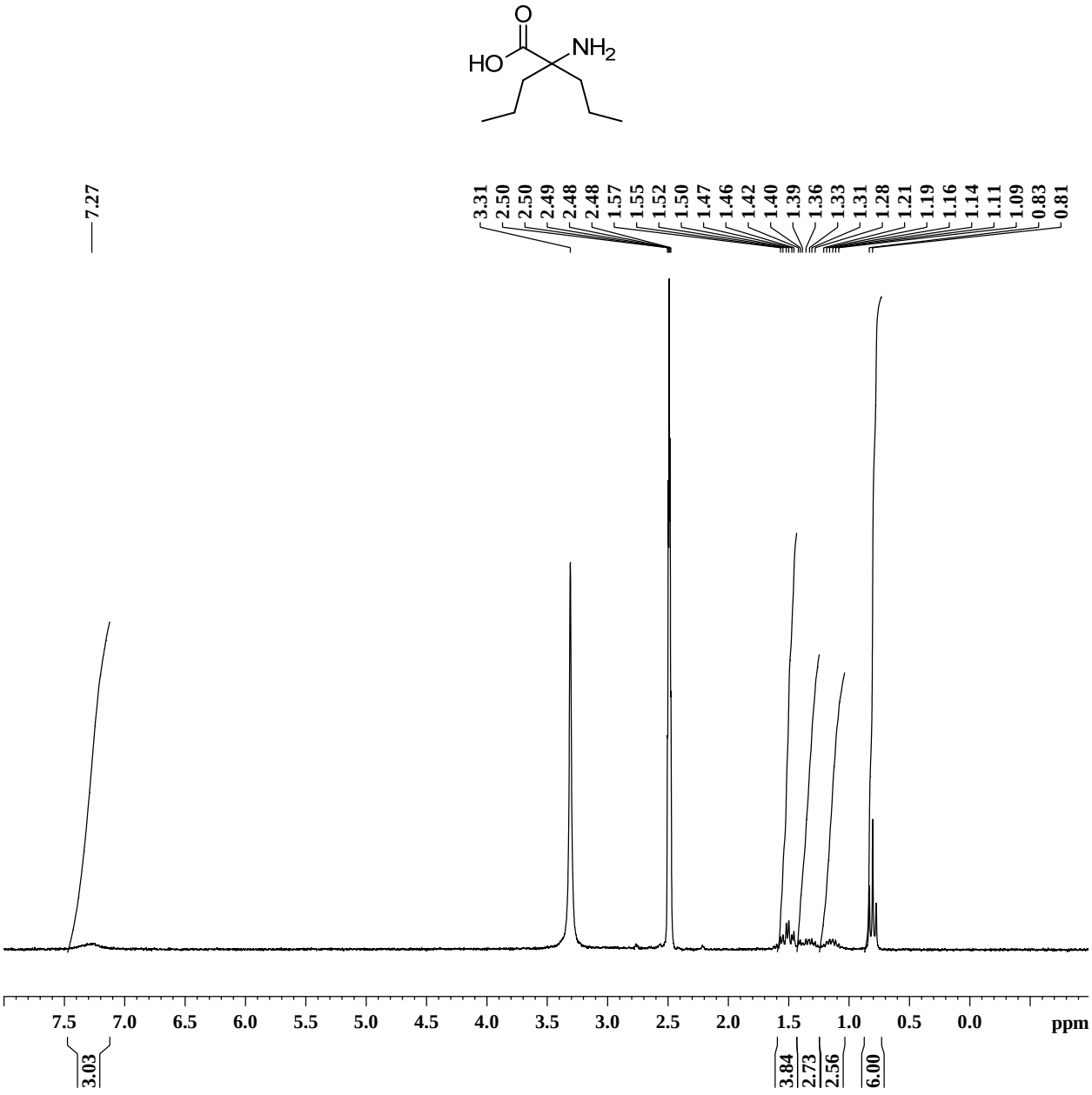

A.16 ^{1}H-NMR (250 MHz, DMSO-d_6)

N^{α}-(9-Fluorenylmethoxycarbonyl)-2,2-dipropylglycine (**4.4.5**)

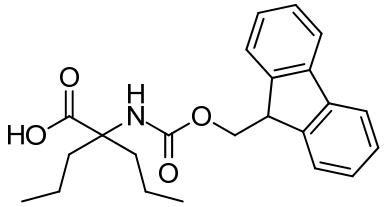

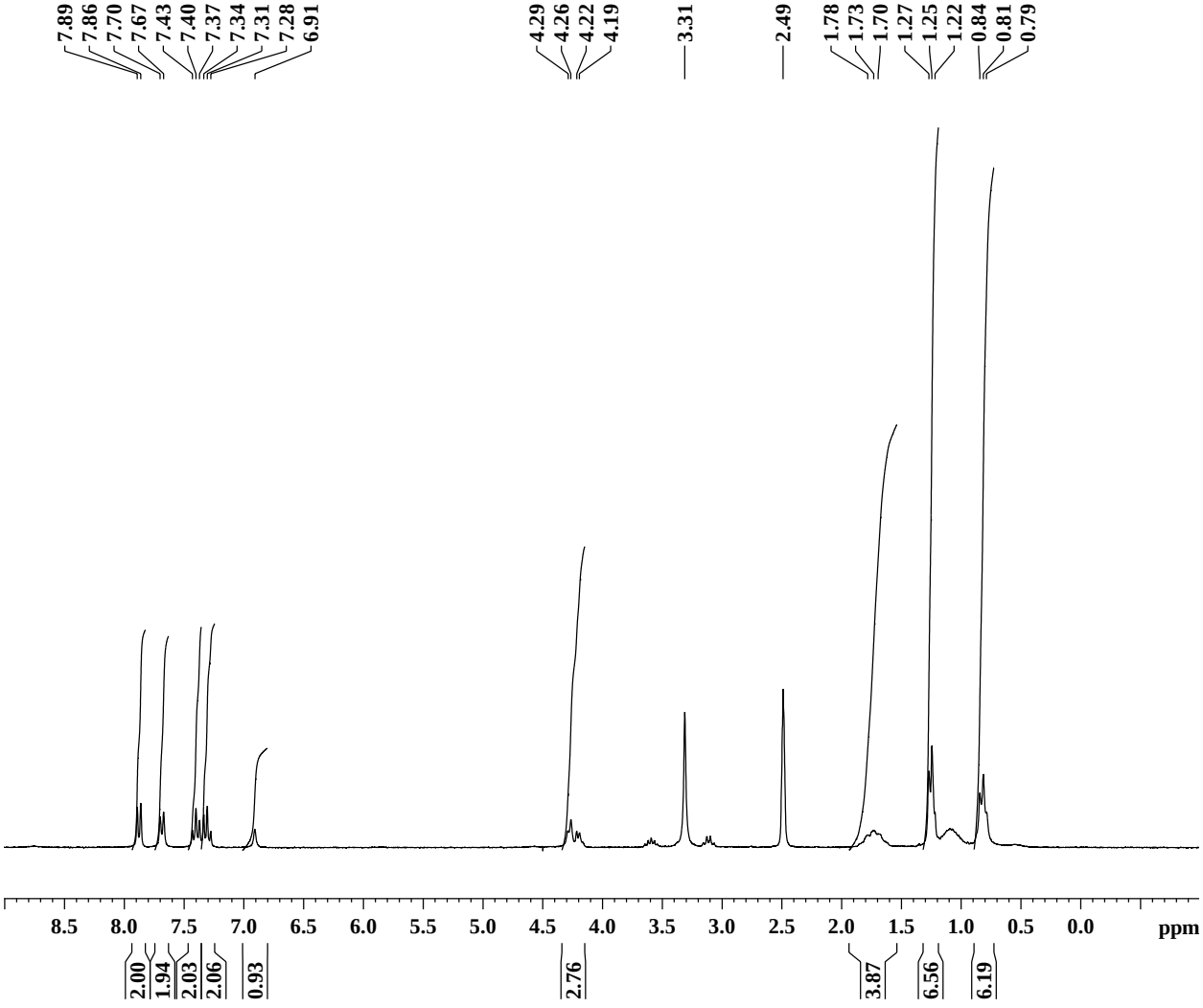

APPENDIX B - X-RAY DIFFRACTION DATA

B.1 Single Crystal X-ray Diffraction Data

Ethyl 2-(4-(methylthio)benzyl)-3-(4-(methylthio)phenyl)-2-nitropropanoate (**2.4.2**)

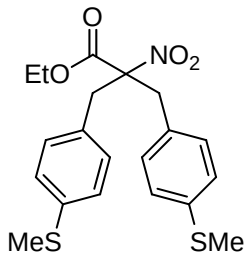

GregMc1.cif

Crystal data

$C_{20}H_{23}NO_4S_2$	D_x = 1.356 Mg m^{-3}
M_r = 405.51	
Monoclinic, $P2_1/n$	Mo $K\alpha$ radiation λ = 0.71073 Å
Hall symbol: -P 2yn	Cell parameters from 4532 reflections
a = 16.029 (2) Å	θ = 2.5–27.1°
b = 6.1465 (5) Å	μ = 0.29 mm^{-1}
c = 21.146 (3) Å	T = 170 K
β = 107.533 (6)°	
V = 1986.6 (4) Å^3	Lath, colorless
Z = 4	0.37 × 0.12 × 0.05 mm
F_{000} = 856	

Data collection

Nonius KappaCCD (with Oxford Cryostream) diffractometer	23907 measured reflections
Radiation source: fine-focus sealed tube	4393 independent reflections
Monochromator: graphite	2985 reflections with $I > 2\sigma(I)$
	R_{int} = 0.037
T = 170 K	θ_{max} = 27.2°
	θ_{min} = 2.8°
ω scans with κ offsets	h = −20→20
Absorption correction: multi-scan HKL Scalepack (Otwinowski & Minor 1997)	k = −7→7
T_{min} = 0.899, T_{max} = 0.986	l = −27→26

Refinement

Refinement on F^2

Least-squares matrix: full

$R[F^2 > 2\sigma(F^2)] = 0.048$

$wR(F^2) = 0.123$

$S = 1.04$

4393 reflections

247 parameters

Primary atom site location: structure-invariant direct methods

Secondary atom site location: difference Fourier map

Hydrogen site location: inferred from neighbouring sites

H-atom parameters constrained

$w = 1/[\sigma^2(F_o^2) + (0.0475P)^2 + 1.1258P]$ where $P = (F_o^2 + 2F_c^2)/3$

$(\Delta/\sigma)_{max} = 0.001$

$\Delta\rho_{max} = 0.50$ e Å^{-3}

$\Delta\rho_{min} = -0.44$ e Å^{-3}

Extinction correction: SHELXL, $Fc^* = kFc[1+0.001xFc^2\lambda^3/\sin(2\theta)]^{-1/4}$

Extinction coefficient: 0.0017 (5)

Special details

Geometry. All e.s.d.'s (except the e.s.d. in the dihedral angle between two l.s. planes) are estimated using the full covariance matrix. The cell e.s.d.'s are taken into account individually in the estimation of e.s.d.'s in distances, angles and torsion angles; correlations between e.s.d.'s in cell parameters are only used when they are defined by crystal symmetry. An approximate (isotropic) treatment of cell e.s.d.'s is used for estimating e.s.d.'s involving l.s. planes.

Refinement. Refinement of F^2 against ALL reflections. The weighted *R*-factor *wR* and goodness of fit *S* are based on F^2, conventional *R*-factors *R* are based on *F*, with *F* set to zero for negative F^2. The threshold expression of $F^2 > 2\sigma(F^2)$ is used only for calculating *R*-factors(gt) *etc.* and is not relevant to the choice of reflections for refinement. *R*-factors based on F^2 are statistically about twice as large as those based on *F*, and *R*- factors based on ALL data will be even larger.

Fractional atomic coordinates and isotropic or equivalent isotropic displacement parameters (Å^2)

	x	*y*	*z*	U_{iso}*/U_{eq}
S1	−0.00793 (4)	0.50965 (13)	0.74859 (3)	0.0486 (2)
S2	0.72810 (4)	0.41894 (12)	0.67240 (3)	0.0482 (2)
O1	0.31241 (12)	0.0526 (3)	0.61851 (9)	0.0461 (5)
O2	0.28667 (12)	0.0447 (3)	0.51272 (9)	0.0511 (5)
O3	0.16399 (11)	0.5994 (3)	0.49121 (10)	0.0528 (5)
O4	0.12729 (11)	0.2708 (3)	0.51829 (10)	0.0539 (5)
N1	0.29296 (12)	0.1403 (3)	0.56448 (11)	0.0328 (4)
C1	0.27736 (13)	0.3869 (3)	0.55935 (11)	0.0265 (5)
C2	0.29302 (13)	0.4885 (4)	0.62836 (11)	0.0283 (5)
H2A	0.3420	0.4094	0.6598	0.034*
H2B	0.3124	0.6406	0.6264	0.034*
C3	0.21656 (13)	0.4906 (3)	0.65682 (10)	0.0266 (5)

C4	0.16279 (14)	0.6716 (4)	0.64747 (12)	0.0330 (5)
H4	0.1733	0.7901	0.6220	0.040*
C5	0.09367 (15)	0.6841 (4)	0.67443 (12)	0.0356 (5)
H5	0.0578	0.8103	0.6675	0.043*
C6	0.07727 (13)	0.5124 (4)	0.71143 (10)	0.0309 (5)
C7	0.13106 (14)	0.3308 (4)	0.72110 (11)	0.0336 (5)
H7	0.1205	0.2121	0.7465	0.040*
C8	0.19977 (14)	0.3200 (4)	0.69436 (11)	0.0315 (5)
H8	0.2359	0.1943	0.7017	0.038*
C9	−0.06535 (17)	0.7573 (5)	0.72069 (15)	0.0522 (7)
H9A	−0.0259	0.8809	0.7363	0.078*
H9B	−0.1152	0.7686	0.7383	0.078*
H9C	−0.0865	0.7583	0.6721	0.078*
C10	0.33985 (14)	0.4805 (4)	0.52328 (11)	0.0301 (5)
H10A	0.3284	0.4063	0.4799	0.036*
H10B	0.3265	0.6368	0.5144	0.036*
C11	0.43538 (13)	0.4572 (3)	0.56086 (11)	0.0286 (5)
C12	0.48217 (14)	0.2709 (4)	0.55591 (11)	0.0330 (5)
H12	0.4528	0.1542	0.5288	0.040*
C13	0.57087 (14)	0.2508 (4)	0.58959 (11)	0.0348 (5)
H13	0.6011	0.1211	0.5856	0.042*
C14	0.61531 (14)	0.4204 (4)	0.62906 (11)	0.0331 (5)
C15	0.56904 (15)	0.6080 (4)	0.63469 (12)	0.0360 (5)
H15	0.5984	0.7244	0.6619	0.043*
C16	0.48080 (14)	0.6261 (4)	0.60097 (12)	0.0335 (5)
H16	0.4505	0.7556	0.6051	0.040*
C17	0.76385 (18)	0.1557 (5)	0.65550 (15)	0.0576 (8)
H17A	0.7312	0.0436	0.6711	0.086*
H17B	0.8265	0.1398	0.6785	0.086*
H17C	0.7534	0.1395	0.6076	0.086*
C18	0.18082 (15)	0.4077 (4)	0.51948 (12)	0.0353 (5)

C19	0.0705 (2)	0.6499 (7)	0.4592 (2)	0.1078 (17)
H19A	0.0441	0.5308	0.4281	0.129*
H19B	0.0404	0.6543	0.4937	0.129*
C20	0.0565 (2)	0.8404 (6)	0.4257 (2)	0.0812 (11)
H20A	0.0875	0.9575	0.4549	0.122*
H20B	−0.0063	0.8721	0.4108	0.122*
H20C	0.0781	0.8297	0.3871	0.122*

Atomic displacement parameters (Å^2)

	U^{11}	U^{22}	U^{33}	U^{12}	U^{13}	U^{23}
S1	0.0377 (4)	0.0676 (5)	0.0491 (4)	0.0088 (3)	0.0261 (3)	0.0136 (3)
S2	0.0311 (3)	0.0641 (5)	0.0480 (4)	0.0022 (3)	0.0100 (3)	−0.0052 (3)
O1	0.0600 (11)	0.0293 (9)	0.0560 (12)	0.0086 (8)	0.0279 (9)	0.0129 (8)
O2	0.0634 (12)	0.0378 (10)	0.0558 (12)	−0.0062 (9)	0.0235 (9)	−0.0196 (9)
O3	0.0304 (9)	0.0556 (12)	0.0677 (13)	0.0020 (8)	0.0076 (8)	0.0273 (10)
O4	0.0351 (9)	0.0511 (12)	0.0700 (13)	−0.0116 (9)	0.0075 (9)	0.0021 (10)
N1	0.0307 (10)	0.0239 (10)	0.0471 (13)	−0.0043 (8)	0.0169 (9)	−0.0043 (9)
C1	0.0262 (10)	0.0202 (11)	0.0344 (12)	−0.0006 (9)	0.0111 (9)	0.0008 (9)
C2	0.0262 (11)	0.0248 (11)	0.0358 (12)	−0.0035 (9)	0.0123 (9)	−0.0028 (9)
C3	0.0241 (10)	0.0274 (11)	0.0296 (11)	−0.0027 (9)	0.0101 (9)	−0.0033 (9)
C4	0.0370 (12)	0.0266 (12)	0.0406 (13)	0.0001 (10)	0.0197 (10)	0.0039 (10)
C5	0.0338 (12)	0.0321 (13)	0.0436 (14)	0.0051 (10)	0.0160 (11)	0.0033 (11)
C6	0.0252 (11)	0.0430 (13)	0.0259 (11)	−0.0009 (10)	0.0100 (9)	−0.0004 (10)
C7	0.0335 (12)	0.0360 (13)	0.0329 (13)	−0.0006 (10)	0.0127 (10)	0.0079 (10)
C8	0.0301 (11)	0.0308 (12)	0.0332 (13)	0.0042 (10)	0.0090 (10)	0.0040 (10)
C9	0.0388 (14)	0.0567 (17)	0.0695 (19)	0.0088 (13)	0.0288 (13)	−0.0043 (15)
C10	0.0320 (11)	0.0294 (12)	0.0323 (12)	0.0005 (9)	0.0150 (9)	0.0038 (10)
C11	0.0288 (11)	0.0295 (12)	0.0334 (12)	−0.0009 (9)	0.0180 (9)	0.0033 (10)
C12	0.0354 (12)	0.0307 (12)	0.0386 (14)	−0.0032 (10)	0.0196 (10)	−0.0033 (10)
C13	0.0355 (13)	0.0339 (13)	0.0405 (14)	0.0071 (10)	0.0200 (11)	0.0015 (11)
C14	0.0308 (11)	0.0412 (14)	0.0319 (12)	−0.0009 (10)	0.0164 (9)	0.0007 (10)

C15	0.0356 (12)	0.0337 (13)	0.0430 (14)	−0.0066 (10)	0.0186 (11)	−0.0061 (10)
C16	0.0352 (12)	0.0268 (12)	0.0442 (14)	0.0009 (10)	0.0206 (11)	−0.0009 (10)
C17	0.0408 (15)	0.073 (2)	0.0560 (18)	0.0224 (14)	0.0099 (13)	0.0002 (15)
C18	0.0333 (12)	0.0380 (14)	0.0353 (13)	−0.0022 (11)	0.0114 (10)	0.0009 (11)
C19	0.0322 (16)	0.117 (3)	0.150 (4)	0.0022 (19)	−0.0091 (19)	0.076 (3)
C20	0.0490 (18)	0.072 (2)	0.101 (3)	0.0110 (17)	−0.0108 (18)	0.005 (2)

Geometric parameters (Å, °)

S1—C6	1.769 (2)	C9—H9A	0.9800
S1—C9	1.785 (3)	C9—H9B	0.9800
S2—C14	1.764 (2)	C9—H9C	0.9800
S2—C17	1.788 (3)	C10—C11	1.505 (3)
O1—N1	1.216 (2)	C10—H10A	0.9900
O2—N1	1.220 (2)	C10—H10B	0.9900
O3—C18	1.312 (3)	C11—C12	1.390 (3)
O3—C19	1.479 (3)	C11—C16	1.398 (3)
O4—C18	1.197 (3)	C12—C13	1.391 (3)
N1—C1	1.535 (3)	C12—H12	0.9500
C1—C18	1.528 (3)	C13—C14	1.390 (3)
C1—C2	1.537 (3)	C13—H13	0.9500
C1—C10	1.541 (3)	C14—C15	1.395 (3)
C2—C3	1.519 (3)	C15—C16	1.383 (3)
C2—H2A	0.9900	C15—H15	0.9500
C2—H2B	0.9900	C16—H16	0.9500
C3—C4	1.384 (3)	C17—H17A	0.9800
C3—C8	1.390 (3)	C17—H17B	0.9800
C4—C5	1.393 (3)	C17—H17C	0.9800
C4—H4	0.9500	C19—C20	1.352 (5)
C5—C6	1.385 (3)	C19—H19A	0.9900
C5—H5	0.9500	C19—H19B	0.9900
C6—C7	1.388 (3)	C20—H20A	0.9800

C7—C8	1.383 (3)	C20—H20B	0.9800
C7—H7	0.9500	C20—H20C	0.9800
C8—H8	0.9500		
C6—S1—C9	103.61 (12)	C1—C10—H10A	108.7
C14—S2—C17	103.94 (13)	C11—C10—H10B	108.7
C18—O3—C19	115.9 (2)	C1—C10—H10B	108.7
O1—N1—O2	123.9 (2)	H10A—C10—H10B	107.6
O1—N1—C1	119.65 (19)	C12—C11—C16	117.6 (2)
O2—N1—C1	116.4 (2)	C12—C11—C10	121.7 (2)
C18—C1—N1	103.77 (17)	C16—C11—C10	120.7 (2)
C18—C1—C2	109.79 (18)	C11—C12—C13	121.8 (2)
N1—C1—C2	110.95 (18)	C11—C12—H12	119.1
C18—C1—C10	113.37 (18)	C13—C12—H12	119.1
N1—C1—C10	106.67 (17)	C14—C13—C12	120.0 (2)
C2—C1—C10	111.95 (17)	C14—C13—H13	120.0
C3—C2—C1	117.33 (18)	C12—C13—H13	120.0
C3—C2—H2A	108.0	C13—C14—C15	118.8 (2)
C1—C2—H2A	108.0	C13—C14—S2	124.59 (18)
C3—C2—H2B	108.0	C15—C14—S2	116.62 (18)
C1—C2—H2B	108.0	C16—C15—C14	120.7 (2)
H2A—C2—H2B	107.2	C16—C15—H15	119.7
C4—C3—C8	117.94 (19)	C14—C15—H15	119.7
C4—C3—C2	119.48 (19)	C15—C16—C11	121.2 (2)
C8—C3—C2	122.54 (19)	C15—C16—H16	119.4
C3—C4—C5	121.6 (2)	C11—C16—H16	119.4
C3—C4—H4	119.2	S2—C17—H17A	109.5
C5—C4—H4	119.2	S2—C17—H17B	109.5
C6—C5—C4	119.9 (2)	H17A—C17—H17B	109.5
C6—C5—H5	120.0	S2—C17—H17C	109.5
C4—C5—H5	120.0	H17A—C17—H17C	109.5
C5—C6—C7	118.76 (19)	H17B—C17—H17C	109.5

C5—C6—S1	124.15 (18)	O4—C18—O3	125.1 (2)
C7—C6—S1	117.08 (17)	O4—C18—C1	123.6 (2)
C8—C7—C6	121.0 (2)	O3—C18—C1	111.19 (19)
C8—C7—H7	119.5	C20—C19—O3	114.0 (3)
C6—C7—H7	119.5	C20—C19—H19A	108.7
C7—C8—C3	120.8 (2)	O3—C19—H19A	108.7
C7—C8—H8	119.6	C20—C19—H19B	108.7
C3—C8—H8	119.6	O3—C19—H19B	108.7
S1—C9—H9A	109.5	H19A—C19—H19B	107.6
S1—C9—H9B	109.5	C19—C20—H20A	109.5
H9A—C9—H9B	109.5	C19—C20—H20B	109.5
S1—C9—H9C	109.5	H20A—C20—H20B	109.5
H9A—C9—H9C	109.5	C19—C20—H20C	109.5
H9B—C9—H9C	109.5	H20A—C20—H20C	109.5
C11—C10—C1	114.39 (17)	H20B—C20—H20C	109.5
C11—C10—H10A	108.7		

O1—N1—C1—C18	−115.9 (2)	C2—C1—C10—C11	56.5 (2)
O2—N1—C1—C18	65.8 (2)	C1—C10—C11—C12	87.0 (2)
O1—N1—C1—C2	2.0 (3)	C1—C10—C11—C16	−94.6 (2)
O2—N1—C1—C2	−176.39 (17)	C16—C11—C12—C13	0.3 (3)
O1—N1—C1—C10	124.2 (2)	C10—C11—C12—C13	178.7 (2)
O2—N1—C1—C10	−54.2 (2)	C11—C12—C13—C14	−0.6 (3)
C18—C1—C2—C3	27.6 (3)	C12—C13—C14—C15	0.8 (3)
N1—C1—C2—C3	−86.5 (2)	C12—C13—C14—S2	−178.12 (17)
C10—C1—C2—C3	154.41 (18)	C17—S2—C14—C13	−2.5 (2)
C1—C2—C3—C4	−93.6 (2)	C17—S2—C14—C15	178.58 (19)
C1—C2—C3—C8	88.8 (3)	C13—C14—C15—C16	−0.8 (3)
C8—C3—C4—C5	−0.1 (3)	S2—C14—C15—C16	178.22 (17)
C2—C3—C4—C5	−177.9 (2)	C14—C15—C16—C11	0.5 (3)
C3—C4—C5—C6	−0.2 (4)	C12—C11—C16—C15	−0.3 (3)
C4—C5—C6—C7	0.4 (3)	C10—C11—C16—C15	−178.7 (2)

C4—C5—C6—S1	179.59 (18)	C19—O3—C18—O4	3.8 (4)
C9—S1—C6—C5	4.5 (2)	C19—O3—C18—C1	−171.6 (3)
C9—S1—C6—C7	−176.31 (19)	N1—C1—C18—O4	26.5 (3)
C5—C6—C7—C8	−0.1 (3)	C2—C1—C18—O4	−92.2 (3)
S1—C6—C7—C8	−179.40 (18)	C10—C1—C18—O4	141.8 (2)
C6—C7—C8—C3	−0.3 (3)	N1—C1—C18—O3	−158.0 (2)
C4—C3—C8—C7	0.4 (3)	C2—C1—C18—O3	83.3 (2)
C2—C3—C8—C7	178.0 (2)	C10—C1—C18—O3	−42.7 (3)
C18—C1—C10—C11	−178.64 (19)	C18—O3—C19—C20	−174.4 (4)
N1—C1—C10—C11	−65.1 (2)		

B.2 Single Crystal X-ray Diffraction Data

Ethyl 2-(4-methoxybenzyl)-3-(4-methoxyphenyl)-2-nitropropanoate (**2.4.3**)

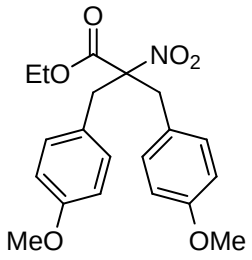

GregMc2.cif

Crystal data

$C_{20}H_{23}NO_6$	D_x = 1.332 Mg m^{-3}
M_r = 373.39	
Orthorhombic, *Pna*2$_1$	Cu *K*α radiation λ = 1.54178 Å
Hall symbol: P 2c -2n	Cell parameters from 9431 reflections
a = 18.0681 (9) Å	θ = 4.9–69.3°
b = 17.1151 (6) Å	μ = 0.82 mm^{-1}
c = 6.0216 (3) Å	*T* = 90 K
V = 1862.10 (15) Å^3	
Z = 4	Needle fragment, colorless
F_{000} = 792	0.25 × 0.19 × 0.15 mm

Data collection

Bruker Kappa Apex-II CCD area detector diffractometer	12499 measured reflections
Radiation source: fine-focus sealed tube	3188 independent reflections
Monochromator: graphite	3156 reflections with $I > 2\sigma(I)$
	R_{int} = 0.018
T = 90 K	θ_{max} = 69.9°
	θ_{min} = 3.5°
phi and ω scans	*h* = −19→21
Absorption correction: multi-scan SADABS (Sheldrick, 2002)	*k* = −19→20
T_{min} = 0.822, T_{max} = 0.887	*l* = −6→7

Refinement

Refinement on F^2

Least-squares matrix: full

$R[F^2 > 2\sigma(F^2)] = 0.022$

$wR(F^2) = 0.056$

$S = 1.06$

3188 reflections

249 parameters

1 restraint

Primary atom site location: structure-invariant direct methods

Secondary atom site location: difference Fourier map

Hydrogen site location: inferred from neighbouring sites

H-atom parameters constrained

$w = 1/[\sigma^2(F_o^2) + (0.0293P)^2 + 0.3528P]$ where $P = (F_o^2 + 2F_c^2)/3$

$(\Delta/\sigma)_{max} = 0.001$

$\Delta\rho_{max} = 0.19$ e Å^{-3}

$\Delta\rho_{min} = -0.10$ e Å^{-3}

Extinction correction: SHELXL, $Fc^* = kFc[1+0.001xFc^2\lambda^3/\sin(2\theta)]^{-1/4}$

Extinction coefficient: 0.0027 (2)

Absolute structure: Flack (1983)

Flack parameter: −0.11 (11)

Special details

Geometry. All e.s.d.'s (except the e.s.d. in the dihedral angle between two l.s. planes) are estimated using the full covariance matrix. The cell e.s.d.'s are taken into account individually in the estimation of e.s.d.'s in distances, angles and torsion angles; correlations between e.s.d.'s in cell parameters are only used when they are defined by crystal symmetry. An approximate (isotropic) treatment of cell e.s.d.'s is used for estimating e.s.d.'s involving l.s. planes.

Refinement. Refinement of F^2 against ALL reflections. The weighted *R*-factor *wR* and goodness of fit *S* are based on F^2, conventional *R*-factors *R* are based on *F*, with *F* set to zero for negative F^2. The threshold expression of $F^2 > 2\sigma(F^2)$ is used only for calculating *R*-factors(gt) *etc.* and is not relevant to the choice of reflections for refinement. *R*-factors based on F^2 are statistically about twice as large as those based on *F*, and *R*- factors based on ALL data will be even larger.

Fractional atomic coordinates and isotropic or equivalent isotropic displacement parameters (Å^2)

	x	*y*	*z*	U_{iso}*/U_{eq}
O1	0.81432 (5)	0.18357 (5)	0.15178 (15)	0.0216 (2)
O2	0.73974 (5)	0.08486 (5)	0.13668 (16)	0.0226 (2)
O3	0.73377 (5)	0.24610 (4)	0.73410 (15)	0.01741 (19)
O4	0.69771 (5)	0.26502 (5)	0.37989 (15)	0.01869 (19)
O5	0.39950 (5)	0.14728 (5)	0.42791 (16)	0.0239 (2)
O6	0.97920 (4)	−0.15767 (5)	0.49657 (15)	0.0192 (2)
N1	0.77133 (5)	0.13745 (6)	0.23703 (18)	0.0160 (2)
C1	0.75967 (6)	0.14492 (6)	0.4875 (2)	0.0142 (2)
C2	0.70475 (6)	0.08297 (7)	0.5752 (2)	0.0160 (3)
H2A	0.7182	0.0320	0.5090	0.019*

H2B	0.7118	0.0784	0.7377	0.019*
C3	0.62297 (6)	0.09715 (6)	0.5312 (2)	0.0164 (2)
C4	0.58630 (7)	0.06336 (7)	0.3526 (2)	0.0183 (3)
H4	0.6130	0.0303	0.2544	0.022*
C5	0.51116 (7)	0.07689 (7)	0.3138 (2)	0.0194 (3)
H5	0.4869	0.0525	0.1922	0.023*
C6	0.47225 (6)	0.12629 (7)	0.4548 (2)	0.0187 (3)
C7	0.50772 (7)	0.15894 (7)	0.6381 (2)	0.0210 (3)
H7	0.4810	0.1916	0.7373	0.025*
C8	0.58193 (7)	0.14373 (7)	0.6757 (2)	0.0188 (3)
H8	0.6054	0.1655	0.8027	0.023*
C9	0.36264 (7)	0.11869 (8)	0.2357 (3)	0.0268 (3)
H9A	0.3909	0.1332	0.1029	0.040*
H9B	0.3130	0.1415	0.2273	0.040*
H9C	0.3587	0.0617	0.2443	0.040*
C10	0.83718 (6)	0.13657 (6)	0.5959 (2)	0.0146 (2)
H10A	0.8707	0.1761	0.5304	0.018*
H10B	0.8329	0.1479	0.7565	0.018*
C11	0.87155 (6)	0.05644 (6)	0.5670 (2)	0.0142 (2)
C12	0.91199 (6)	0.03703 (7)	0.3770 (2)	0.0147 (2)
H12	0.9161	0.0738	0.2594	0.018*
C13	0.94616 (6)	−0.03508 (7)	0.3576 (2)	0.0155 (2)
H13	0.9735	−0.0474	0.2275	0.019*
C14	0.94054 (6)	−0.08946 (6)	0.5285 (2)	0.0150 (2)
C15	0.89882 (6)	−0.07247 (7)	0.7161 (2)	0.0156 (2)
H15	0.8933	−0.1101	0.8308	0.019*
C16	0.86507 (6)	0.00048 (7)	0.7341 (2)	0.0153 (2)
H16	0.8370	0.0123	0.8632	0.018*
C17	0.97914 (7)	−0.21297 (7)	0.6751 (2)	0.0218 (3)
H17A	0.9954	−0.1872	0.8119	0.033*
H17B	1.0129	−0.2560	0.6398	0.033*

H17C	0.9290	−0.2336	0.6957	0.033*
C18	0.72741 (6)	0.22691 (6)	0.5215 (2)	0.0146 (2)
C19	0.69671 (7)	0.31798 (7)	0.8043 (2)	0.0191 (3)
H19A	0.6902	0.3172	0.9676	0.023*
H19B	0.6470	0.3204	0.7357	0.023*
C20	0.74002 (7)	0.38986 (7)	0.7396 (3)	0.0226 (3)
H20A	0.7911	0.3848	0.7922	0.034*
H20B	0.7172	0.4361	0.8069	0.034*
H20C	0.7398	0.3953	0.5776	0.034*

Atomic displacement parameters (Å^2)

	U^{11}	U^{22}	U^{33}	U^{12}	U^{13}	U^{23}
O1	0.0241 (4)	0.0246 (4)	0.0160 (5)	0.0002 (3)	0.0029 (4)	0.0037 (4)
O2	0.0268 (4)	0.0250 (4)	0.0161 (5)	−0.0002 (4)	−0.0024 (4)	−0.0074 (4)
O3	0.0231 (4)	0.0149 (4)	0.0142 (4)	0.0059 (3)	−0.0001 (3)	−0.0027 (4)
O4	0.0209 (4)	0.0178 (4)	0.0173 (5)	0.0037 (3)	−0.0031 (3)	0.0014 (4)
O5	0.0157 (4)	0.0300 (5)	0.0260 (5)	0.0017 (3)	−0.0012 (4)	−0.0058 (4)
O6	0.0224 (4)	0.0130 (4)	0.0221 (5)	0.0039 (3)	0.0025 (4)	0.0005 (4)
N1	0.0175 (5)	0.0169 (5)	0.0137 (5)	0.0049 (4)	−0.0010 (4)	0.0003 (4)
C1	0.0180 (5)	0.0151 (5)	0.0096 (6)	0.0023 (4)	0.0003 (4)	−0.0009 (5)
C2	0.0178 (6)	0.0157 (5)	0.0145 (6)	0.0009 (4)	−0.0009 (5)	0.0006 (5)
C3	0.0164 (5)	0.0154 (5)	0.0174 (6)	−0.0010 (4)	0.0004 (5)	0.0026 (5)
C4	0.0190 (6)	0.0164 (5)	0.0193 (7)	0.0019 (4)	0.0013 (5)	−0.0014 (5)
C5	0.0204 (6)	0.0187 (6)	0.0191 (7)	−0.0027 (5)	−0.0027 (5)	−0.0022 (5)
C6	0.0156 (5)	0.0182 (6)	0.0222 (7)	−0.0008 (4)	0.0009 (5)	0.0032 (5)
C7	0.0193 (6)	0.0229 (6)	0.0208 (7)	0.0001 (5)	0.0042 (5)	−0.0040 (6)
C8	0.0206 (6)	0.0207 (6)	0.0150 (6)	−0.0025 (4)	−0.0006 (5)	−0.0014 (5)
C9	0.0170 (6)	0.0331 (7)	0.0305 (8)	−0.0001 (5)	−0.0050 (6)	−0.0075 (7)
C10	0.0157 (5)	0.0157 (5)	0.0124 (6)	0.0005 (4)	−0.0004 (4)	−0.0014 (5)
C11	0.0127 (5)	0.0150 (5)	0.0149 (6)	−0.0017 (4)	−0.0024 (4)	−0.0012 (5)
C12	0.0139 (5)	0.0154 (5)	0.0147 (6)	−0.0022 (4)	−0.0012 (5)	0.0012 (5)

C13	0.0133 (5)	0.0180 (5)	0.0151 (6)	−0.0009 (4)	0.0006 (4)	−0.0028 (5)
C14	0.0131 (5)	0.0131 (5)	0.0188 (6)	0.0002 (4)	−0.0022 (5)	−0.0027 (5)
C15	0.0157 (5)	0.0158 (5)	0.0154 (6)	−0.0013 (4)	−0.0023 (4)	0.0017 (5)
C16	0.0143 (5)	0.0189 (6)	0.0129 (6)	−0.0012 (4)	0.0005 (4)	−0.0018 (5)
C17	0.0247 (6)	0.0163 (6)	0.0246 (7)	0.0035 (5)	0.0015 (5)	0.0048 (5)
C18	0.0147 (5)	0.0151 (5)	0.0142 (6)	−0.0003 (4)	0.0004 (5)	0.0001 (5)
C19	0.0216 (6)	0.0168 (6)	0.0188 (7)	0.0069 (5)	0.0013 (5)	−0.0045 (5)
C20	0.0231 (6)	0.0178 (6)	0.0268 (7)	0.0020 (5)	−0.0011 (5)	−0.0058 (6)

Geometric parameters (Å, °)

O1—N1	1.2207 (13)	C9—H9A	0.9800
O2—N1	1.2251 (14)	C9—H9B	0.9800
O3—C18	1.3267 (16)	C9—H9C	0.9800
O3—C19	1.4632 (13)	C10—C11	1.5155 (15)
O4—C18	1.2002 (15)	C10—H10A	0.9900
O5—C6	1.3722 (14)	C10—H10B	0.9900
O5—C9	1.4224 (16)	C11—C16	1.3941 (17)
O6—C14	1.3739 (13)	C11—C12	1.3979 (17)
O6—C17	1.4322 (15)	C12—C13	1.3849 (16)
N1—C1	1.5284 (16)	C12—H12	0.9500
C1—C18	1.5331 (15)	C13—C14	1.3911 (17)
C1—C2	1.5452 (15)	C13—H13	0.9500
C1—C10	1.5514 (15)	C14—C15	1.3890 (18)
C2—C3	1.5206 (15)	C15—C16	1.3938 (16)
C2—H2A	0.9900	C15—H15	0.9500
C2—H2B	0.9900	C16—H16	0.9500
C3—C4	1.3894 (18)	C17—H17A	0.9800
C3—C8	1.3939 (17)	C17—H17B	0.9800
C4—C5	1.3969 (17)	C17—H17C	0.9800
C4—H4	0.9500	C19—C20	1.5093 (17)
C5—C6	1.3891 (18)	C19—H19A	0.9900

C5—H5	0.9500	C19—H19B	0.9900
C6—C7	1.3935 (19)	C20—H20A	0.9800
C7—C8	1.3846 (17)	C20—H20B	0.9800
C7—H7	0.9500	C20—H20C	0.9800
C8—H8	0.9500		

C18—O3—C19	116.59 (10)	C1—C10—H10A	108.8
C6—O5—C9	117.03 (10)	C11—C10—H10B	108.8
C14—O6—C17	117.14 (10)	C1—C10—H10B	108.8
O1—N1—O2	124.34 (11)	H10A—C10—H10B	107.7
O1—N1—C1	116.65 (10)	C16—C11—C12	118.14 (10)
O2—N1—C1	118.96 (10)	C16—C11—C10	120.30 (11)
N1—C1—C18	105.11 (9)	C12—C11—C10	121.54 (11)
N1—C1—C2	111.60 (9)	C13—C12—C11	120.91 (11)
C18—C1—C2	109.77 (9)	C13—C12—H12	119.5
N1—C1—C10	106.43 (9)	C11—C12—H12	119.5
C18—C1—C10	111.81 (9)	C12—C13—C14	120.10 (11)
C2—C1—C10	111.89 (9)	C12—C13—H13	120.0
C3—C2—C1	117.06 (9)	C14—C13—H13	120.0
C3—C2—H2A	108.0	O6—C14—C15	124.58 (11)
C1—C2—H2A	108.0	O6—C14—C13	115.33 (11)
C3—C2—H2B	108.0	C15—C14—C13	120.08 (10)
C1—C2—H2B	108.0	C14—C15—C16	119.23 (11)
H2A—C2—H2B	107.3	C14—C15—H15	120.4
C4—C3—C8	117.89 (11)	C16—C15—H15	120.4
C4—C3—C2	122.13 (11)	C15—C16—C11	121.50 (12)
C8—C3—C2	119.96 (11)	C15—C16—H16	119.3
C3—C4—C5	121.58 (12)	C11—C16—H16	119.3
C3—C4—H4	119.2	O6—C17—H17A	109.5
C5—C4—H4	119.2	O6—C17—H17B	109.5
C6—C5—C4	119.39 (12)	H17A—C17—H17B	109.5
C6—C5—H5	120.3	O6—C17—H17C	109.5

C4—C5—H5	120.3	H17A—C17—H17C	109.5
O5—C6—C5	124.89 (12)	H17B—C17—H17C	109.5
O5—C6—C7	115.40 (11)	O4—C18—O3	126.14 (11)
C5—C6—C7	119.70 (11)	O4—C18—C1	124.93 (11)
C8—C7—C6	119.96 (11)	O3—C18—C1	108.81 (10)
C8—C7—H7	120.0	O3—C19—C20	111.92 (10)
C6—C7—H7	120.0	O3—C19—H19A	109.2
C7—C8—C3	121.38 (12)	C20—C19—H19A	109.2
C7—C8—H8	119.3	O3—C19—H19B	109.2
C3—C8—H8	119.3	C20—C19—H19B	109.2
O5—C9—H9A	109.5	H19A—C19—H19B	107.9
O5—C9—H9B	109.5	C19—C20—H20A	109.5
H9A—C9—H9B	109.5	C19—C20—H20B	109.5
O5—C9—H9C	109.5	H20A—C20—H20B	109.5
H9A—C9—H9C	109.5	C19—C20—H20C	109.5
H9B—C9—H9C	109.5	H20A—C20—H20C	109.5
C11—C10—C1	113.90 (9)	H20B—C20—H20C	109.5
C11—C10—H10A	108.8		

O1—N1—C1—C18	61.58 (12)	C2—C1—C10—C11	56.38 (13)
O2—N1—C1—C18	−120.99 (10)	C1—C10—C11—C16	−96.30 (13)
O1—N1—C1—C2	−179.49 (9)	C1—C10—C11—C12	85.40 (13)
O2—N1—C1—C2	−2.06 (14)	C16—C11—C12—C13	−1.55 (16)
O1—N1—C1—C10	−57.16 (12)	C10—C11—C12—C13	176.79 (11)
O2—N1—C1—C10	120.27 (10)	C11—C12—C13—C14	0.04 (17)
N1—C1—C2—C3	−76.58 (13)	C17—O6—C14—C15	−3.35 (15)
C18—C1—C2—C3	39.54 (15)	C17—O6—C14—C13	175.75 (10)
C10—C1—C2—C3	164.28 (10)	C12—C13—C14—O6	−177.23 (10)
C1—C2—C3—C4	96.52 (13)	C12—C13—C14—C15	1.92 (17)
C1—C2—C3—C8	−85.19 (14)	O6—C14—C15—C16	176.78 (10)
C8—C3—C4—C5	1.71 (18)	C13—C14—C15—C16	−2.28 (16)
C2—C3—C4—C5	−179.96 (11)	C14—C15—C16—C11	0.74 (17)

C3—C4—C5—C6	1.06 (19)	C12—C11—C16—C15	1.17 (16)
C9—O5—C6—C5	−2.83 (18)	C10—C11—C16—C15	−177.20 (10)
C9—O5—C6—C7	176.51 (11)	C19—O3—C18—O4	4.38 (17)
C4—C5—C6—O5	176.54 (12)	C19—O3—C18—C1	−171.78 (9)
C4—C5—C6—C7	−2.78 (18)	N1—C1—C18—O4	20.09 (15)
O5—C6—C7—C8	−177.67 (11)	C2—C1—C18—O4	−100.06 (13)
C5—C6—C7—C8	1.71 (19)	C10—C1—C18—O4	135.16 (12)
C6—C7—C8—C3	1.15 (19)	N1—C1—C18—O3	−163.69 (9)
C4—C3—C8—C7	−2.83 (18)	C2—C1—C18—O3	76.16 (12)
C2—C3—C8—C7	178.81 (12)	C10—C1—C18—O3	−48.63 (13)
N1—C1—C10—C11	−65.77 (12)	C18—O3—C19—C20	−78.20 (13)
C18—C1—C10—C11	179.98 (10)		

B.3 Single Crystal X-ray Diffraction Data

4-(methylsulfonyl)benzaldehyde (**3.5**)

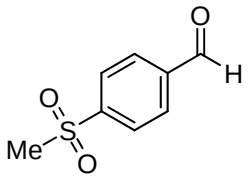

GregMc3.cif

Crystal data

$C_9H_{11}NO_2$	D_x = 1.303 Mg m^{-3}
M_r = 165.19	
Monoclinic, $P2_1/c$	Mo $K\alpha$ radiation λ = 0.71073 Å
Hall symbol: -P 2ybc	Cell parameters from 1901 reflections
a = 7.1823 (15) Å	θ = 2.5–27.8°
b = 4.6410 (10) Å	μ = 0.09 mm^{-1}
c = 25.425 (6) Å	T = 90 K
β = 96.583 (9)°	
V = 841.9 (3) Å^3	Needle, colorless
Z = 4	0.40 × 0.05 × 0.05 mm
F_{000} = 352	

Data collection

Nonius KappaCCD (with Oxford Cryostream) diffractometer	1951 independent reflections
Radiation source: fine-focus sealed tube	1514 reflections with $I > 2\sigma(I)$
Monochromator: graphite	R_{int} = 0.025
	θ_{max} = 27.8°
T = 90 K	θ_{min} = 2.8°
	h = −9→9
ω scans with κ offsets	k = −5→5
Absorption correction: none	l = −32→32
9151 measured reflections	

Refinement

Refinement on F^2

Least-squares matrix: full

$R[F^2 > 2\sigma(F^2)] = 0.039$

$wR(F^2) = 0.095$

$S = 1.06$

1951 reflections

114 parameters

Primary atom site location: structure-invariant direct methods

Secondary atom site location: difference Fourier map

Hydrogen site location: inferred from neighbouring sites

H atoms treated by a mixture of independent and constrained refinement

$w = 1/[\sigma^2(F_o^2) + (0.0375P)^2 + 0.2775P]$ where $P = (F_o^2 + 2F_c^2)/3$

$(\Delta/\sigma)_{max} = 0.001$

$\Delta\rho_{max} = 0.25$ e Å^{-3}

$\Delta\rho_{min} = -0.18$ e Å^{-3}

Extinction correction: SHELXL, $Fc^* = kFc[1+0.001xFc^2\lambda^3/\sin(2\theta)]^{-1/4}$

Extinction coefficient: 0.015 (3)

Special details

Geometry. All e.s.d.'s (except the e.s.d. in the dihedral angle between two l.s. planes) are estimated using the full covariance matrix. The cell e.s.d.'s are taken into account individually in the estimation of e.s.d.'s in distances, angles and torsion angles; correlations between e.s.d.'s in cell parameters are only used when they are defined by crystal symmetry. An approximate (isotropic) treatment of cell e.s.d.'s is used for estimating e.s.d.'s involving l.s. planes.

Refinement. Refinement of F^2 against ALL reflections. The weighted *R*-factor *wR* and goodness of fit *S* are based on F^2, conventional *R*-factors *R* are based on *F*, with *F* set to zero for negative F^2. The threshold expression of $F^2 > 2\sigma(F^2)$ is used only for calculating *R*-factors(gt) *etc.* and is not relevant to the choice of reflections for refinement. *R*-factors based on F^2 are statistically about twice as large as those based on *F*, and *R*- factors based on ALL data will be even larger.

Fractional atomic coordinates and isotropic or equivalent isotropic displacement parameters (Å^2)

	x	*y*	*z*	U_{iso}*/U_{eq}
O1	0.81792 (13)	0.0643 (2)	0.79301 (4)	0.0206 (2)
O2	0.18744 (13)	1.1567 (2)	0.96729 (4)	0.0200 (2)
N1	0.30768 (15)	0.7295 (3)	0.94386 (4)	0.0168 (3)
H1N	0.297 (2)	0.547 (4)	0.9459 (6)	0.020*
C1	0.55120 (18)	0.6417 (3)	0.88528 (5)	0.0169 (3)
C2	0.72556 (18)	0.5319 (3)	0.90460 (5)	0.0186 (3)
H2	0.7821	0.5912	0.9385	0.022*
C3	0.81961 (18)	0.3365 (3)	0.87540 (5)	0.0183 (3)
H3	0.9389	0.2638	0.8892	0.022*
C4	0.73657 (18)	0.2495 (3)	0.82583 (5)	0.0162 (3)
C5	0.55973 (18)	0.3531 (3)	0.80618 (5)	0.0180 (3)

H5	0.5017	0.2899	0.7727	0.022*
C6	0.46938 (18)	0.5479 (3)	0.83565 (5)	0.0178 (3)
H6	0.3496	0.6193	0.8220	0.021*
C7	0.45527 (19)	0.8607 (3)	0.91653 (5)	0.0202 (3)
H7A	0.5491	0.9522	0.9429	0.024*
H7B	0.3999	1.0130	0.8923	0.024*
C8	0.18841 (18)	0.8891 (3)	0.96709 (5)	0.0169 (3)
H8	0.0972	0.7924	0.9849	0.020*
C9	1.00418 (19)	−0.0300 (3)	0.81032 (6)	0.0246 (3)
H9A	1.0868	0.1377	0.8163	0.037*
H9B	1.0488	−0.1539	0.7832	0.037*
H9C	1.0047	−0.1385	0.8434	0.037*

Atomic displacement parameters (Å^2)

	U^{11}	U^{22}	U^{33}	U^{12}	U^{13}	U^{23}
O1	0.0188 (5)	0.0216 (5)	0.0220 (5)	0.0044 (4)	0.0049 (4)	−0.0025 (4)
O2	0.0214 (5)	0.0146 (5)	0.0251 (5)	0.0007 (4)	0.0071 (4)	0.0004 (4)
N1	0.0183 (5)	0.0125 (6)	0.0207 (5)	−0.0012 (5)	0.0066 (4)	0.0001 (5)
C1	0.0188 (6)	0.0133 (6)	0.0198 (6)	−0.0029 (5)	0.0068 (5)	0.0008 (5)
C2	0.0202 (7)	0.0184 (7)	0.0172 (6)	−0.0034 (6)	0.0022 (5)	−0.0006 (5)
C3	0.0149 (6)	0.0193 (7)	0.0206 (6)	−0.0001 (5)	0.0014 (5)	0.0020 (5)
C4	0.0179 (6)	0.0130 (6)	0.0188 (6)	0.0001 (5)	0.0070 (5)	0.0013 (5)
C5	0.0188 (6)	0.0170 (7)	0.0182 (6)	−0.0014 (5)	0.0026 (5)	0.0005 (5)
C6	0.0147 (6)	0.0173 (7)	0.0215 (6)	0.0013 (5)	0.0032 (5)	0.0031 (5)
C7	0.0208 (7)	0.0172 (7)	0.0241 (7)	−0.0037 (6)	0.0094 (6)	−0.0009 (6)
C8	0.0162 (6)	0.0176 (7)	0.0172 (6)	−0.0018 (5)	0.0030 (5)	0.0008 (5)
C9	0.0196 (7)	0.0250 (8)	0.0301 (7)	0.0067 (6)	0.0068 (6)	0.0005 (6)

Geometric parameters (Å, °)

O1—C4	1.3744 (15)	C3—H3	0.9500
O1—C9	1.4282 (16)	C4—C5	1.3958 (18)
O2—C8	1.2423 (17)	C5—C6	1.3826 (18)

N1—C8	1.3218 (17)	C5—H5	0.9500
N1—C7	1.4648 (17)	C6—H6	0.9500
N1—H1N	0.853 (17)	C7—H7A	0.9900
C1—C2	1.3885 (19)	C7—H7B	0.9900
C1—C6	1.3989 (18)	C8—H8	0.9500
C1—C7	1.5048 (18)	C9—H9A	0.9800
C2—C3	1.3945 (19)	C9—H9B	0.9800
C2—H2	0.9500	C9—H9C	0.9800
C3—C4	1.3908 (18)		
C4—O1—C9	116.93 (11)	C5—C6—C1	121.17 (12)
C8—N1—C7	121.38 (12)	C5—C6—H6	119.4
C8—N1—H1N	117.4 (10)	C1—C6—H6	119.4
C7—N1—H1N	121.2 (10)	N1—C7—C1	111.71 (11)
C2—C1—C6	118.26 (12)	N1—C7—H7A	109.3
C2—C1—C7	120.67 (12)	C1—C7—H7A	109.3
C6—C1—C7	121.06 (12)	N1—C7—H7B	109.3
C1—C2—C3	121.50 (12)	C1—C7—H7B	109.3
C1—C2—H2	119.2	H7A—C7—H7B	107.9
C3—C2—H2	119.2	O2—C8—N1	124.48 (13)
C4—C3—C2	119.18 (12)	O2—C8—H8	117.8
C4—C3—H3	120.4	N1—C8—H8	117.8
C2—C3—H3	120.4	O1—C9—H9A	109.5
O1—C4—C3	124.32 (12)	O1—C9—H9B	109.5
O1—C4—C5	115.51 (11)	H9A—C9—H9B	109.5
C3—C4—C5	120.17 (12)	O1—C9—H9C	109.5
C6—C5—C4	119.70 (12)	H9A—C9—H9C	109.5
C6—C5—H5	120.2	H9B—C9—H9C	109.5
C4—C5—H5	120.2		

C6—C1—C2—C3	1.0 (2)	C3—C4—C5—C6	1.6 (2)
C7—C1—C2—C3	−177.71 (12)	C4—C5—C6—C1	−0.7 (2)
C1—C2—C3—C4	−0.1 (2)	C2—C1—C6—C5	−0.59 (19)

C9—O1—C4—C3	−3.66 (18)	C7—C1—C6—C5	178.08 (12)
C9—O1—C4—C5	175.81 (12)	C8—N1—C7—C1	−170.00 (12)
C2—C3—C4—O1	178.26 (12)	C2—C1—C7—N1	−101.81 (14)
C2—C3—C4—C5	−1.2 (2)	C6—C1—C7—N1	79.56 (15)
O1—C4—C5—C6	−177.93 (11)	C7—N1—C8—O2	1.3 (2)

Hydrogen-bond geometry (Å, °)

D—H···*A*	*D*—H	H···*A*	*D*···*A*	*D*—H···*A*
N1—H1N···O2^{i}	0.853 (17)	2.071 (16)	2.8785 (16)	157.6 (14)

Symmetry codes: (i) *x*, *y*−1, *z*.

B.4 Single Crystal X-ray Diffraction Data

4-nitrobenzyl chloride (**3.6**)

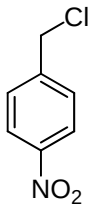

GregMc4.cif

Crystal data

$C_7H_6ClNO_2$	D_x = 1.553 Mg m^{-3}
M_r = 171.58	
Orthorhombic, $P2_12_12_1$	Cu $K\alpha$ radiation λ = 1.54178 Å
Hall symbol: P 2ac 2ab	Cell parameters from 2876 reflections
a = 4.6952 (2) Å	θ = 3.6–68.7°
b = 6.3691 (2) Å	μ = 4.17 mm^{-1}
c = 24.5393 (8) Å	T = 90 K
V = 733.83 (5) Å^3	
Z = 4	Lath fragment, colorless
F_{000} = 352	0.49 × 0.48 × 0.04 mm

Data collection

Bruker Kappa Apex-II CCD area detector diffractometer	2970 measured reflections
Radiation source: fine-focus sealed tube	1211 independent reflections
Monochromator: graphite	1192 reflections with $I > 2\sigma(I)$
	R_{int} = 0.040
T = 90 K	θ_{max} = 69.2°
	θ_{min} = 3.6°
phi and ω scans	$h = -5 \rightarrow 5$
Absorption correction: multi-scan SADABS (Sheldrick, 2002)	$k = -7 \rightarrow 7$
T_{min} = 0.234, T_{max} = 0.851	$l = -28 \rightarrow 27$

Refinement

Refinement on F^2

Least-squares matrix: full

$R[F^2 > 2\sigma(F^2)] = 0.041$

$wR(F^2) = 0.119$

$S = 1.16$

1211 reflections

101 parameters

Primary atom site location: structure-invariant direct methods

Secondary atom site location: difference Fourier map

Hydrogen site location: inferred from neighbouring sites

H-atom parameters constrained

$w = 1/[\sigma^2(F_o^2) + (0.0779P)^2 + 0.1713P]$ where $P = (F_o^2 + 2F_c^2)/3$

$(\Delta/\sigma)_{max} = 0.001$

$\Delta\rho_{max} = 0.58$ e Å^{-3}

$\Delta\rho_{min} = -0.55$ e Å^{-3}

Extinction correction: none

Absolute structure: Flack (1983)

Flack parameter: 0.15 (3)

Special details

Geometry. All e.s.d.'s (except the e.s.d. in the dihedral angle between two l.s. planes) are estimated using the full covariance matrix. The cell e.s.d.'s are taken into account individually in the estimation of e.s.d.'s in distances, angles and torsion angles; correlations between e.s.d.'s in cell parameters are only used when they are defined by crystal symmetry. An approximate (isotropic) treatment of cell e.s.d.'s is used for estimating e.s.d.'s involving l.s. planes.

Refinement. Refinement of F^2 against ALL reflections. The weighted *R*-factor *wR* and goodness of fit *S* are based on F^2, conventional *R*-factors *R* are based on *F*, with *F* set to zero for negative F^2. The threshold expression of $F^2 > 2\sigma(F^2)$ is used only for calculating *R*-factors(gt) *etc.* and is not relevant to the choice of reflections for refinement. *R*-factors based on F^2 are statistically about twice as large as those based on *F*, and *R*- factors based on ALL data will be even larger.

Fractional atomic coordinates and isotropic or equivalent isotropic displacement parameters (Å^2)

	x	*y*	*z*	U_{iso}*/U_{eq}
Cl1	0.25257 (14)	0.04947 (9)	0.77434 (2)	0.0244 (3)
N1	0.8797 (5)	0.6679 (3)	0.94692 (8)	0.0134 (5)
O1	0.9984 (4)	0.5876 (3)	0.98609 (8)	0.0179 (4)
O2	0.9324 (4)	0.8457 (3)	0.93026 (8)	0.0186 (5)
C1	0.6628 (5)	0.5443 (4)	0.91772 (10)	0.0124 (5)
C2	0.5988 (5)	0.3444 (4)	0.93669 (10)	0.0121 (5)
H2	0.6886	0.2897	0.9683	0.015*
C3	0.4005 (6)	0.2271 (4)	0.90822 (10)	0.0131 (5)
H3	0.3525	0.0901	0.9204	0.016*
C4	0.2700 (6)	0.3087 (4)	0.86158 (9)	0.0123 (5)
C5	0.3358 (5)	0.5108 (4)	0.84403 (10)	0.0149 (6)
H5	0.2440	0.5671	0.8128	0.018*

C6	0.5351 (5)	0.6303 (4)	0.87206 (10)	0.0146 (6)
H6	0.5826	0.7679	0.8602	0.018*
C7	0.0636 (5)	0.1777 (4)	0.82953 (10)	0.0158 (6)
H7A	−0.0895	0.2679	0.8146	0.019*
H7B	−0.0247	0.0711	0.8535	0.019*

Atomic displacement parameters (Å^2)

	U^{11}	U^{22}	U^{33}	U^{12}	U^{13}	U^{23}
Cl1	0.0304 (5)	0.0259 (4)	0.0170 (4)	−0.0019 (3)	−0.0002 (3)	−0.0089 (2)
N1	0.0157 (11)	0.0146 (10)	0.0100 (11)	−0.0005 (9)	0.0012 (9)	−0.0033 (9)
O1	0.0198 (9)	0.0200 (9)	0.0140 (10)	−0.0010 (8)	−0.0051 (7)	−0.0003 (7)
O2	0.0241 (10)	0.0137 (9)	0.0178 (10)	−0.0048 (8)	0.0020 (8)	0.0017 (7)
C1	0.0140 (11)	0.0141 (11)	0.0092 (12)	−0.0015 (9)	0.0002 (9)	−0.0006 (10)
C2	0.0141 (12)	0.0143 (12)	0.0079 (12)	0.0026 (10)	−0.0001 (9)	−0.0009 (10)
C3	0.0155 (12)	0.0131 (11)	0.0106 (13)	−0.0007 (10)	0.0032 (10)	0.0007 (9)
C4	0.0137 (12)	0.0147 (10)	0.0085 (12)	0.0014 (11)	−0.0003 (10)	−0.0020 (9)
C5	0.0188 (13)	0.0163 (11)	0.0094 (12)	0.0021 (10)	0.0001 (9)	0.0022 (10)
C6	0.0159 (12)	0.0149 (12)	0.0131 (13)	0.0008 (10)	0.0005 (10)	0.0015 (9)
C7	0.0165 (13)	0.0173 (11)	0.0135 (13)	−0.0026 (10)	0.0025 (10)	−0.0019 (10)

Geometric parameters (Å, °)

Cl1—C7	1.814 (3)	C3—H3	0.9500
N1—O1	1.223 (3)	C4—C5	1.392 (4)
N1—O2	1.229 (3)	C4—C7	1.501 (3)
N1—C1	1.473 (3)	C5—C6	1.389 (4)
C1—C6	1.384 (4)	C5—H5	0.9500
C1—C2	1.389 (3)	C6—H6	0.9500
C2—C3	1.383 (4)	C7—H7A	0.9900
C2—H2	0.9500	C7—H7B	0.9900
C3—C4	1.398 (3)		
O1—N1—O2	123.7 (2)	C3—C4—C7	120.3 (2)

O1—N1—C1	118.3 (2)	C6—C5—C4	120.2 (2)
O2—N1—C1	118.0 (2)	C6—C5—H5	119.9
C6—C1—C2	122.7 (2)	C4—C5—H5	119.9
C6—C1—N1	118.8 (2)	C1—C6—C5	118.4 (2)
C2—C1—N1	118.5 (2)	C1—C6—H6	120.8
C3—C2—C1	118.1 (2)	C5—C6—H6	120.8
C3—C2—H2	120.9	C4—C7—Cl1	109.01 (17)
C1—C2—H2	120.9	C4—C7—H7A	109.9
C2—C3—C4	120.5 (2)	Cl1—C7—H7A	109.9
C2—C3—H3	119.7	C4—C7—H7B	109.9
C4—C3—H3	119.7	Cl1—C7—H7B	109.9
C5—C4—C3	120.0 (2)	H7A—C7—H7B	108.3
C5—C4—C7	119.7 (2)		

O1—N1—C1—C6	−177.5 (2)	C2—C3—C4—C7	177.6 (2)
O2—N1—C1—C6	2.1 (3)	C3—C4—C5—C6	1.3 (4)
O1—N1—C1—C2	1.3 (3)	C7—C4—C5—C6	−177.4 (2)
O2—N1—C1—C2	−179.1 (2)	C2—C1—C6—C5	−0.3 (4)
C6—C1—C2—C3	0.5 (4)	N1—C1—C6—C5	178.5 (2)
N1—C1—C2—C3	−178.3 (2)	C4—C5—C6—C1	−0.6 (4)
C1—C2—C3—C4	0.2 (4)	C5—C4—C7—Cl1	84.1 (3)
C2—C3—C4—C5	−1.1 (4)	C3—C4—C7—Cl1	−94.6 (2)

B.5 Single Crystal X-ray Diffraction Data

N-(4-methoxybenzyl)formamide

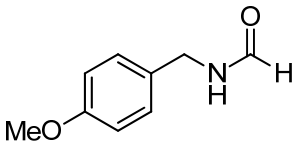

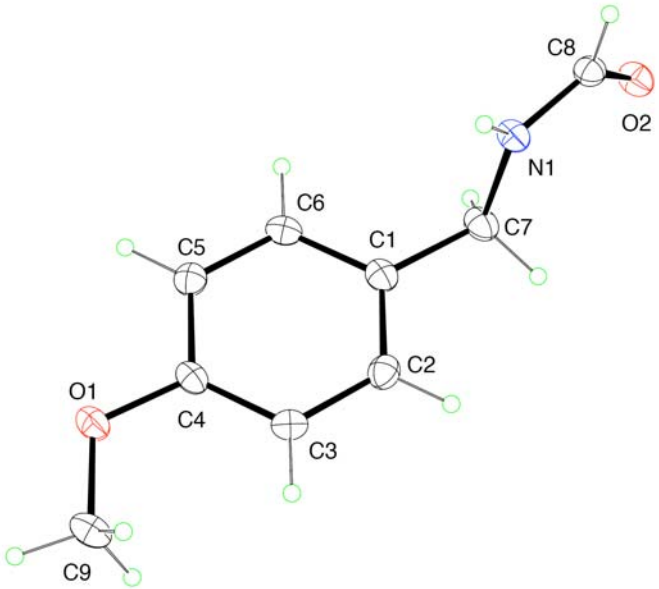

GregMc5.cif

Crystal data

$C_8H_8O_3S$	D_x = 1.527 Mg m^{-3}
M_r = 184.20	
Monoclinic, $P2_1/c$	Mo $K\alpha$ radiation λ = 0.71073 Å
Hall symbol: -P 2ybc	Cell parameters from 3791 reflections
a = 6.0820 (6) Å	θ = 2.5–36.3°
b = 7.9205 (9) Å	μ = 0.36 mm^{-1}
c = 16.639 (2) Å	T = 90 K
β = 90.547 (7)°	
V = 801.51 (15) Å^3	Needle fragment, colorless
Z = 4	0.25 × 0.17 × 0.12 mm
F_{000} = 384	

Data collection

Nonius KappaCCD (with Oxford Cryostream) diffractometer

Radiation source: fine-focus sealed tube

Monochromator: graphite

T = 90 K

ω scans with κ offsets

Absorption correction: multi-scan
HKL Scalepack (Otwinowski & Minor 1997)

T_{min} = 0.905, T_{max} = 0.958

18757 measured reflections

3774 independent reflections

3439 reflections with $I > 2\sigma(I)$

R_{int} = 0.016

θ_{max} = 36.3°

θ_{min} = 2.8°

$h = -9 \rightarrow 10$

$k = -13 \rightarrow 13$

$l = -27 \rightarrow 27$

Refinement

Refinement on F^2

Least-squares matrix: full

$R[F^2 > 2\sigma(F^2)]$ = 0.037

$wR(F^2)$ = 0.104

S = 1.08

3774 reflections

114 parameters

Primary atom site location: structure-invariant direct methods

Secondary atom site location: difference Fourier map

Hydrogen site location: inferred from neighbouring sites

H atoms treated by a mixture of independent and constrained refinement

$w = 1/[\sigma^2(F_o^2) + (0.0487P)^2 + 0.3939P]$
where $P = (F_o^2 + 2F_c^2)/3$

$(\Delta/\sigma)_{max} < 0.001$

$\Delta\rho_{max}$ = 0.70 e Å^{-3}

$\Delta\rho_{min}$ = −0.59 e Å^{-3}

Extinction correction: SHELXL,
$Fc^* = kFc[1+0.001xFc^2\lambda^3/\sin(2\theta)]^{-1/4}$

Extinction coefficient: 0.020 (4)

Special details

Geometry. All e.s.d.'s (except the e.s.d. in the dihedral angle between two l.s. planes) are estimated using the full covariance matrix. The cell e.s.d.'s are taken into account individually in the estimation of e.s.d.'s in distances, angles and torsion angles; correlations between e.s.d.'s in cell parameters are only used when they are defined by crystal symmetry. An approximate (isotropic) treatment of cell e.s.d.'s is used for estimating e.s.d.'s involving l.s. planes.

Refinement. Refinement of F^2 against ALL reflections. The weighted *R*-factor *wR* and goodness of fit *S* are based on F^2, conventional *R*-factors *R* are based on *F*, with *F* set to zero for negative F^2. The threshold expression of $F^2 > 2\sigma(F^2)$ is used only for calculating *R*-factors(gt) *etc.* and is not relevant to the choice of reflections for refinement. *R*-factors based on F^2 are statistically about twice as large as those based on *F*, and *R*- factors based on ALL data will be even larger.

Fractional atomic coordinates and isotropic or equivalent isotropic displacement parameters (Å^2)

	x	*y*	*z*	U_{iso}*/U_{eq}
S1	0.75956 (4)	0.55565 (3)	0.328970 (13)	0.01469 (7)
O1	0.60022 (15)	0.46206 (11)	0.28158 (5)	0.02440 (17)
O2	0.94738 (14)	0.46614 (10)	0.36146 (5)	0.02142 (15)
O3	0.11445 (14)	0.95140 (10)	0.60157 (5)	0.02330 (16)
C1	0.40855 (15)	0.80778 (11)	0.53594 (6)	0.01526 (15)
C2	0.61667 (16)	0.73782 (13)	0.54798 (6)	0.01697 (16)
H2	0.6847	0.7431	0.5996	0.020*
C3	0.72500 (15)	0.66025 (12)	0.48451 (5)	0.01542 (15)
H3	0.8673	0.6130	0.4921	0.019*
C4	0.62101 (14)	0.65319 (11)	0.40982 (5)	0.01355 (14)
C5	0.41248 (15)	0.72340 (13)	0.39671 (6)	0.01715 (16)
H5	0.3444	0.7175	0.3452	0.021*
C6	0.30648 (15)	0.80199 (13)	0.46026 (6)	0.01682 (16)
H6	0.1656	0.8514	0.4523	0.020*
C7	0.29828 (17)	0.89007 (13)	0.60491 (6)	0.01929 (17)
H7	0.382 (3)	0.894 (2)	0.6550 (10)	0.023*
C8	0.85351 (17)	0.72538 (13)	0.27034 (6)	0.01864 (17)
H8A	0.9507	0.7971	0.3030	0.028*
H8B	0.7276	0.7918	0.2512	0.028*
H8C	0.9347	0.6817	0.2242	0.028*

Atomic displacement parameters (Å^2)

	U^{11}	U^{22}	U^{33}	U^{12}	U^{13}	U^{23}
S1	0.01545 (11)	0.01553 (10)	0.01311 (10)	0.00019 (7)	0.00093 (7)	−0.00131 (6)
O1	0.0247 (4)	0.0279 (4)	0.0207 (3)	−0.0078 (3)	0.0006 (3)	−0.0090 (3)
O2	0.0226 (3)	0.0216 (3)	0.0201 (3)	0.0091 (3)	0.0019 (3)	0.0010 (3)
O3	0.0241 (4)	0.0226 (3)	0.0234 (4)	0.0058 (3)	0.0053 (3)	−0.0015 (3)
C1	0.0159 (3)	0.0143 (3)	0.0156 (3)	0.0004 (3)	0.0018 (3)	0.0007 (3)
C2	0.0173 (4)	0.0201 (4)	0.0135 (3)	0.0025 (3)	−0.0009 (3)	0.0000 (3)
C3	0.0139 (3)	0.0182 (4)	0.0141 (3)	0.0025 (3)	−0.0006 (3)	0.0009 (3)

C4	0.0127 (3)	0.0150 (3)	0.0129 (3)	0.0001 (3)	0.0004 (2)	0.0005 (3)
C5	0.0134 (3)	0.0227 (4)	0.0153 (4)	0.0016 (3)	−0.0019 (3)	−0.0006 (3)
C6	0.0135 (3)	0.0197 (4)	0.0173 (4)	0.0019 (3)	0.0001 (3)	0.0000 (3)
C7	0.0229 (4)	0.0180 (4)	0.0171 (4)	0.0021 (3)	0.0037 (3)	−0.0010 (3)
C8	0.0201 (4)	0.0210 (4)	0.0149 (4)	−0.0003 (3)	0.0028 (3)	0.0020 (3)

Geometric parameters (Å, °)

S1—O2	1.4450 (8)	C3—C4	1.3901 (13)
S1—O1	1.4477 (8)	C3—H3	0.9500
S1—C8	1.7596 (10)	C4—C5	1.4001 (13)
S1—C4	1.7716 (9)	C5—C6	1.3907 (13)
O3—C7	1.2198 (13)	C5—H5	0.9500
C1—C2	1.3944 (13)	C6—H6	0.9500
C1—C6	1.3994 (13)	C7—H7	0.972 (17)
C1—C7	1.4854 (13)	C8—H8A	0.9800
C2—C3	1.3929 (13)	C8—H8B	0.9800
C2—H2	0.9500	C8—H8C	0.9800
O2—S1—O1	118.38 (6)	C5—C4—S1	119.44 (7)
O2—S1—C8	108.81 (5)	C6—C5—C4	119.02 (8)
O1—S1—C8	107.96 (5)	C6—C5—H5	120.5
O2—S1—C4	108.05 (4)	C4—C5—H5	120.5
O1—S1—C4	108.43 (5)	C5—C6—C1	119.60 (8)
C8—S1—C4	104.31 (5)	C5—C6—H6	120.2
C2—C1—C6	120.70 (8)	C1—C6—H6	120.2
C2—C1—C7	118.64 (9)	O3—C7—C1	124.05 (10)
C6—C1—C7	120.66 (8)	O3—C7—H7	120.0 (10)
C3—C2—C1	120.11 (8)	C1—C7—H7	116.0 (10)
C3—C2—H2	119.9	S1—C8—H8A	109.5
C1—C2—H2	119.9	S1—C8—H8B	109.5
C4—C3—C2	118.75 (8)	H8A—C8—H8B	109.5
C4—C3—H3	120.6	S1—C8—H8C	109.5

C2—C3—H3	120.6	H8A—C8—H8C	109.5
C3—C4—C5	121.81 (8)	H8B—C8—H8C	109.5
C3—C4—S1	118.73 (7)		

C6—C1—C2—C3	−0.36 (15)	O1—S1—C4—C5	−39.48 (9)
C7—C1—C2—C3	−179.77 (9)	C8—S1—C4—C5	75.39 (8)
C1—C2—C3—C4	−0.48 (14)	C3—C4—C5—C6	−0.15 (15)
C2—C3—C4—C5	0.74 (14)	S1—C4—C5—C6	−179.02 (7)
C2—C3—C4—S1	179.62 (7)	C4—C5—C6—C1	−0.70 (14)
O2—S1—C4—C3	12.15 (9)	C2—C1—C6—C5	0.96 (14)
O1—S1—C4—C3	141.61 (8)	C7—C1—C6—C5	−179.64 (9)
C8—S1—C4—C3	−103.52 (8)	C2—C1—C7—O3	−178.10 (10)
O2—S1—C4—C5	−168.94 (8)	C6—C1—C7—O3	2.48 (16)

VITA

Gregory T. McCandless received his Bachelor of Science in Industrial Engineering degree from Louisiana State University in December of 1999. After graduation, he went into industry to work on piping systems for chemical plants, refineries and paper mills. His duties over the years ranged from performing mechanical stress analysis calculations to detailing pipe fabrication drawings needed to bring an engineered design to life.

He returned to Louisiana State University in January of 2005 to explore a new career path. That exploration continued the following summer in Professor Robin McCarley's laboratory where he assisted Dr. Guofang Chen, a postdoctoral fellow, in the fabrication of microfluidic devices with high aspect ratio nanopillars. Gregory went on to pursue graduate studies in chemistry in January of 2006. After joining Professor Robert Hammer's research group, he worked on the synthesis of sterically bulky amino acids and inhibitors of peptide aggregation. He also had the privilege to help mentor two outstanding undergraduate students, Sarah Curtis and Amber Scroggs, on their research projects. He will graduate with a master of science in chemistry from Louisiana State University in December of 2008.